

N O T I C E

THIS DOCUMENT HAS BEEN REPRODUCED FROM
MICROFICHE. ALTHOUGH IT IS RECOGNIZED THAT
CERTAIN PORTIONS ARE ILLEGIBLE, IT IS BEING RELEASED
IN THE INTEREST OF MAKING AVAILABLE AS MUCH
INFORMATION AS POSSIBLE

NY

NASA Contractor Report 159324

(NASA-CR-159324) INVESTIGATION OF
MULTILAYER MAGNETIC DOMAIN LATTICE FILE
Interim Report (Sperry Univac, St. Paul,
Minnesota) 125 P HC A06/MF A01 CSCL 09B

N81-12745

Unclas
29436

G3/60

Investigation of Multilayer Magnetic Domain Lattice File

E. J. Torok, M. Kamin, C. H. Tolman

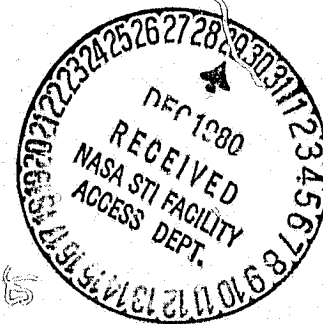
SPERRY UNIVAC CORPORATION
St. Paul, MN 55165

CONTRACT NAS1-15007
NOVEMBER 1980

NASA

National Aeronautics and
Space Administration

Langley Research Center
Hampton, Virginia 23665



CONTENTS

Section	Page
1. Introduction	1
1.1 Justification and Requirements	1
1.2 Multilayer Structures	1
1.3 Purpose of Report	1
2. Multilayer Self-Structured Lattice File	2
2.1 Definition	2
2.2 Current Access Design Selection Rationale	2
2.3 Matrix of Possible Multilayer Structures	2
2.4 Device Selection	6
3. Theoretical Investigations	7
3.1 Objectives	7
3.2 Coupling Between Multiple Layers of Bubble Domains	7
3.2.1 Interaction Between Bubbles in Adjacent Layers	7
3.2.2 Material Parameters for Multiple Layers of Bubbles	11
3.3 Coupling Between Stripe and Bubble Layers	16
3.3.1 Exchange Coupling	16
3.3.2 Mismatch Between Stripe Width and Bubble Diameter	17
3.3.3 Magnetostatic Coupling	19
3.3.4 Stripe and Bubble Interaction	23
3.3.5 Stripe and Bubble Material Selection	23
3.4 Stripe Domain and Material Parameters	25
3.4.1 Run-Out Threshold	26
3.4.2 Layer Thickness	27
3.4.3 Magnetization	28
3.4.4 Characteristic Length	31
3.4.5 Uniaxial Anisotropy and Exchange Constant	31
3.4.6 Stripe Domain Curvature	34
3.5 Stripe Domain and Magnetic Feature Coupling	38
3.5.1 Symmetric Stripe Domains	42
3.5.2 Asymmetric Stripe Domains	42

Section	Page
3.6 Field Calculations for Current Accessed Propagation Structures	44
3.6.1 Average Field Gradient from a Stripline	44
3.6.2 Nested Serpentine Conductors	48
3.6.3 Non-Nested Serpentine Conductors	48
3.7 Summary and Conclusions of Theoretical Studies	53
4. Experimental Investigations	58
4.1 Objectives	58
4.2 Experimental Equipment and Methods	58
4.3 Experimental Circuits	59
4.3.1 Early Current Accessed Circuits	59
4.3.2 Offset Serpentine Array	63
4.3.3 Magnetically Assisted Serpentine Circuits	72
4.3.4 Segmented Chevron Circuit	77
4.3.5 Stripe Domain Curvature	84
4.4 Magnetic Features and In-Plane Fields	86
4.5 Garnet Materials	89
4.5.1 Objectives	89
4.5.2 Garnet Survey	89
4.5.3 Multiple Layer Garnets	92
4.5.4 Magnetostatic Coupling in Multilayer Garnets	100
5. Test Vehicles	105
5.1 Introduction	105
5.2 Test Vehicle Evaluation	107
5.3 Test Vehicle Summary	115
6. Recommended Memory Storage Area Configuration	116
7. Conclusions	121
8. Acknowledgements	122
9. References	123

1. Introduction

1.1 Justification and Requirements

Magnetic bubble technology is essentially capable of higher bit densities than is currently available. The resolution of lithography employed for circuit fabrication limits the devices presently in use. A variety of modified technologies have been studied which would relax the lithographic resolution requirements, such as semi-disks, contiguous disks, and bubble lattices. In a multilayer self-structured bubble design, domain structures in one layer replace all or part of the control circuitry for the data bubbles in a second layer. This design reduces the technology restrictions imposed by the lithographic process, thereby allowing the full capability of the magnetic material to be utilized.

1.2 Multilayer Structures

Multilayered garnet structures offer a new degree of freedom, which promises to eliminate many problems associated with present-day devices. These structures, by allowing tailoring of the material properties of two or more layers, can optimize the parameters of each layer to serve a specific function. A periodic domain configuration can be generated in one layer and used to structure the data in a second layer. This implies that all structuring circuitry can conceivably be removed from the storage area. As the memory chip becomes larger, the reduction of circuit complexity becomes dramatic if the storage area circuitry is eliminated. Stable periodic domain configurations can be made to propagate coherently, thereby propagating bubbles in a data layer. This use of periodic domain configurations allow bubbles to move in a potential well of nearly constant depth, thereby improving device operating margins and upper frequency limitations. The use of natural garnet magnetic domain phenomena in place of lithographically configured features for structuring and propagating implies higher yields and lower costs for these devices.

1.3 Purpose of Report

This report describes the research leading to a practical multilayer self-structured memory device concept. Initially, the reasoning is presented leading to device selection. The theory of various concepts is described next, followed by experimental investigations of several current accessed circuits. Subsequently, the test vehicle design and evaluation are reported, in addition to a recommended memory storage area configuration.

2. Multilayer Self-Structured Lattice File

2.1 Definition

Multilayered self-structured lattice files have two or more coupled magnetic garnets grown on a common substrate. One layer, referred to as the data layer, supports data bubbles. One or more garnet layers, the carrier layers, contain arrays of stripe domains or bubble domains, and also determine the position of bubbles in the data layer. Propagation of the data is accomplished by moving the domain arrays in the carrier layers. Structuring can be accomplished by employing confinement rails or channels in the garnet, and/or a lattice of carrier bubbles.

Through incorporation of self-structured multilayer designs, the goals are to greatly reduce the total number of propagating elements, and to make the minimum feature size of the propagating elements consistent with conventional photolithography, while maintaining high bit density.

2.2 Matrix of Possible Multilayer Structures

A list of self-structured multilayer bubble file designs was prepared for device consideration. This list is most easily represented in a five dimensional matrix, figure 2.1, because there are five different independent characteristics for classification. These are (1) the type of carrier used to convey the data bubbles (e.g., stripe carrier, wavy wall carrier, or bubble carrier), (2) the means by which the carrier is propelled (e.g., T-bars, etc.), (3) the type of fences or guidance channels, (4) the type of coupling between carrier film and the data film (e.g., exchange, etc.) and (5) the type of bias field used. The total number of combinations is 540. This is too large to be represented in a two dimensional matrix. A reduced two dimensional matrix has been constructed, figure 2.2, and contains only 120 items. The different methods of bias are not represented on this list for simplicity, because for most structures the bias type will be determined by the requirements of bubble stability and stripe stability, and therefore, there will be little freedom of choice.

2.3 Design Feature Evaluation

The two dimensional matrix of figure 2.2 still contains too many candidates to be experimentally evaluated for a self-structured multilayer memory system. The candidates in each of the sections for carrier type, means of propulsion, and coupling type must be individually evaluated, and objective decisions made whether they are a viable technology for device application.

CARRIER	PROPULSION	FENCES OR GUIDANCE CHANNELS	COUPLING	BIAS
BUBBLE	ANGEL-FISH AUTOMOTION	PERMALLOY ION IMPLANTED	EXCHANGE	EXTERNAL
STRIPE CARRIER	ROTATING IN-PLANE FIELD (T-BARS etc.)	ETCHED GROOVE	EXCHANGE TYPE II	SELF-BIASED
WAVY WALL-CARRIER	CONDUCTOR PROPELLED	MAGNETIC DOMAIN FENCE NO FENCE	MAGNETO-STATIC	MIXED

FIGURE 2.1. MATRIX OF POSSIBLE MULTILAYER STRUCTURES

MEANS OF
PROPULSION

		Bubble Carrier				Stripe Carrier			Wavy Wall Carrier			
		Angelfish Type	Rotating In-Plane Field (T-bars etc.)	Automotion	Conductor Accessed	Angelfish Type	Rotating In-Plane Field (T-bars etc.)	Automotion	Conductor Accessed	Angelfish Type	Rotating In-Plane Field	Automotion
Exchange Coupling Type I or Type II	NiFe Fence											
	Ion Implanted Fence											
	Etched Groove											
	Magnetic Domain Fence											
	No Fence											
Magneto-Static Coupling	NiFe Fence											
	Ion Implanted Fence											
	Etched Groove											
	Magnetic Domain Fence											
	No Fence											

FIGURE 2.2. REDUCED MATRIX OF POSSIBLE MULTILAYER STRUCTURES

The wavy wall application for carrier propagation does not appear to be a serious candidate. Since its description in the literature, there has been very little interest or work throughout the industry associated with its development or application. The bubble carrier and the stripe carrier remain as excellent candidates.

Angelfish and T-bar type propagators place stringent requirements on the photo-lightography processing of devices. Since successful propagation of bubbles requires a complete array of propagation features, this limits both the element density and device yield. Control of stripe or bubble propagation by automation proved to be most difficult because of irregular displacement.

Conventional bubble memories employ a rotating magnetic field for access purposes, generated by externally mounted field coils. Field access requires the excitation of a large volume of the memory, requiring high voltage at the coils, and results in a system penalty for power. The memory operating frequency is limited by the inductance of the coils, which require excessive power at high drive frequencies. These coils also represent a significant fraction of the total weight and total cost of the memory. Through incorporation of current accessed techniques, the coils can be eliminated.

Table 2.1 lists the advantages and disadvantages of a current accessed bubble memory, as compared to a field accessed memory. For these reasons, an effort has been placed in investigating current accessed techniques for domain propagation.

Exchange coupling between multiple layers of magnetic material generally requires intimate contact of these layers for adequate interaction. Variation of the coupling strength can be accomplished with very thin non-magnetic intermediate layers, but the results are very difficult to control accurately. Magnetostatic coupling between layers appears as a suitable candidate, since its magnitude can be controlled quite easily by geometrical considerations.

Structuring of the memory design can be accomplished in one of the two directions by providing an energy barrier to the bubble or stripe domains. Barriers such as a magnetic rail on the garnet surface, an ion implanted region of the garnet, or a groove etched in the garnet will provide an energy well to restrict domain location. All three of these barriers appear to be acceptable candidates, and their specific application will depend on the individual circuit requirements and physical layout. A magnetic domain fence is less desirable, since it is not a permanent feature of the device, and can contribute to device failure if eradicated.

TABLE 2.1 CURRENT ACCESSED BUBBLE MEMORY FEATURES

	<u>Advantage</u>	<u>Disadvantage</u>
1. current access	x	
2. large propagation features	x	
3. multilayer construction		x
4. self-structured	x	
5. coherent propagation	x	
6. high density	x	
7. high frequency operation	x	
8. propagation circuitry connections		x
9. no wall state storage	x	
10. medium Q materials	x	
11. heat generated by current lines		x
12. low access time	x	

The number of combinations that are serious candidates for the multilayer self-structured memory design has, therefore, been reduced to six. Current access; bubble or stripe carrier propagation; and barriers of magnetic rails, ion implanted areas, or an etched groove are the salient design features.

2.4 Device Design

Based on the above reasoning, a theoretical and experimental effort was initiated on a self-structured memory device. The design consisted of a multiple layer garnet with the magnetic layers coupled by magnetostatic interaction, magnetically-assisted current accessed stripe domain propagators, current accessed bubble and stripe domain generators, and magnetic bars for stripe domain end pinning. Propagation of bubbles in the data layer is controlled by current accessed domain propagation in the carrier layer. Detection and readout of data were not necessarily included in the device design.

3. Theoretical Investigations

3.1 Objectives

The behavior of bubble domains and stripe domains in single layer garnet materials, and their interaction in multiple layer garnet materials, depends upon many geometrical and material properties. It is the object of the following theoretical investigations to describe these interactions and couplings, and to employ the results in selecting device designs for development of a multi-layer lattice file. These calculations, and the resultant formulas, allow prediction of bubble and stripe behavior before fabrication of test circuits.

3.2 Coupling Between Multiple Layers of Bubble Domains

3.2.1 Interaction Between Bubbles in Adjacent Layers

Bubbles in different layers exert forces on each other. These forces are exerted by the stray field emanating from a bubble which affects the bubbles in the adjacent layer in two ways; 1) it exerts a force tending to move the bubble directly over the center of the first bubble; and 2) it opposes the bias field and tends to increase the size of the bubble. To evaluate the interactions between bubbles, it is necessary to calculate this stray field. This can be done exactly¹ for both the radial component $H_r(r, z)$ and the normal component, $H_z(r, z)$. See Table 3.1 for symbol definition.

$$\begin{aligned} H_r(r, z) &= \left\{ \frac{2}{\pi} \left(\frac{r_0}{r} \right)^{\frac{1}{2}} \left(\frac{(1 - \frac{1}{2}K_1^2) K(K_1) - E(K_1)}{K_1} \right) \right. \\ &\quad \left. - \frac{(1 - \frac{1}{2}K_2^2) K(K_2) - E(K_2)}{K_2} \right\} 4\pi M \quad (3.1) \\ \\ \frac{H_z(r, z)}{4\pi M} &= - \frac{1}{2\pi r_0 (rr_0)^{\frac{1}{2}}} [zK_1K(K_1) - (h+z)K_2K(K_2)] \\ &\quad - \frac{\Lambda_0(\alpha_1, \beta_1) - \Lambda_0(\alpha_2, \beta_2)}{2r_0} \quad \text{for } r < r_0 \\ &= - \frac{1}{2\pi r_0 (rr_0)^{\frac{1}{2}}} [zK_1K(K_1) - (h+z)K_2K(K_2)] \\ &\quad + \frac{\Lambda_0(\alpha_1, \beta_1) - \Lambda_0(\alpha_2, \beta_2)}{2r_0} \quad \text{for } r > r_0 \end{aligned}$$

$$= -\frac{1}{2\pi r_0^2} [zK_1K(K_1) - (h+z)E_2K(K_2)] \text{ for } r = r_0$$

where $K(K)$, $E(K)$, and $\Lambda_0(\alpha, \beta)$ are the complete elliptic integrals of the first, second, and third kinds, respectively, with

$$K_1^2 = 4rr_0 [z^2 + (r + r_0)^2]^{-1} \quad (3.2)$$

$$K_2^2 = 4rr_0 [(h+z)^2 + (r + r_0)^2]^{-1}$$

$$\alpha_1 = \sin^{-1} K_1,$$

$$\alpha_2 = \sin^{-1} K_2,$$

$$\beta_1 = \sin^{-1} \left\{ z [(h+z)^2 + (r - r_0)^2]^{-\frac{1}{2}} \right\}, \text{ and}$$

$$\beta_2 = \sin^{-1} \left\{ (h+z) [(h+z)^2 + (r - r_0)^2]^{-\frac{1}{2}} \right\}$$

Equations 3.1 and 3.2 are plotted in Figures 3.1 and 3.2. Note that the field is a large fraction of $4\pi M$; the coupling field is more than enough to trap and move bubbles, which has been observed experimentally. Note also that the coupling field extends beyond the radius of the bubble when the spacing between layers is significant, so that the cluster of trapped bubbles can even extend somewhat beyond the outside a bubble. The coupling field is (1) larger for thicker bubbles, (2) larger for larger diameter bubbles, and (3) large when the distance from the bubble is small compared to the radius of the bubble. These three observations show that while the large bubble in the bottom layer has a large effect on the small bubbles in the upper layer, the bubbles in the upper layer have almost no effect on the large bubble. This simplifies the investigation considerably.

Table 3.1 presents a list of definition of symbols used in this section.

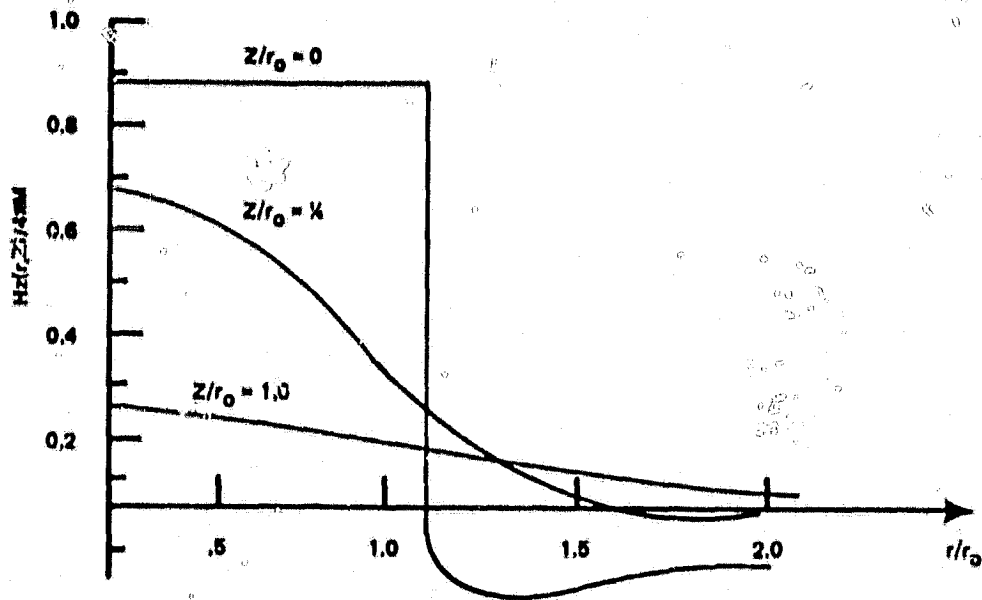


Figure 3.1 Radial Dependence of the Normal Field from a Bubble of Radius r_0 and Thickness $2 r_0$ at Various Heights.

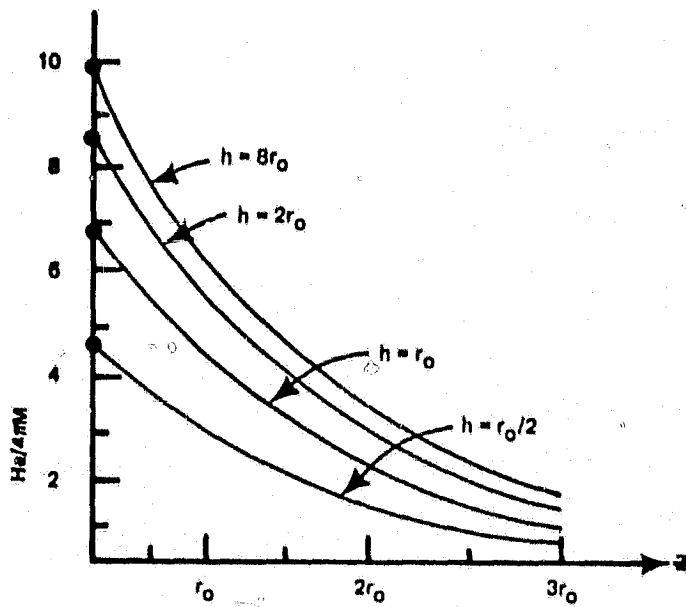


Figure 3.2 Normal Field from a Bubble as a Function of Height for Various Thicknesses.

TABLE 3.1. DEFINITIONS OF SYMBOLS

A	Exchange constant, ERG/CM
D	Width of an isolated stripe domain, m
H	Magnetic field normal to film surface, OE
\bar{H}	Normalized normal magnetic field, $H/4\pi M$
H_c	Coercive force, OE
H_K	Anisotropy field, $2K/M$, OE
H_0	Bubble collapse field threshold, OE
\bar{H}_0	Normalized collapse field, $H_0/4\pi M$
H_{RO}	Run-out field threshold, or strip-out field threshold, OE
\bar{H}_{RO}	Normalized run-out field, $H_{RO}/4\pi M$
H_D	Stray field on the wall of an infinitely long isolated stripe, averaged over film thickness, OE
\bar{H}_D	Stray field on the wall of an infinitely long isolated stripe, averaged over film thickness and strip width, OE
\bar{H}_{TIP}	Stray field at the tip of a rectangular isolated stripe, averaged over film thickness and stripe width, OE
h	Film thickness, m
K	Uniaxial anisotropy constant, $\frac{1}{2}MH_K$, ERG/CM ³
L	Length of an isolated stripe domain, m
l	Characteristic length of garnet, $T_w/4\pi M^2$, m
λ	Normalized characteristic length, l/h
M	Magnetic moment, EMU, GAUSS
r	Bubble domain radius, m
X	Normalized bubble domain radius, r/h
r_0	Bubble domain radius at collapse threshold, m
X_0	Normalized Bubble domain radius at collapse threshold, r_0/h
Q	Normalized anisotropy field, $H_K/4\pi M = K/2\pi M^2$
T_w	Wall energy per unit length and thickness $2\sqrt{AK}$, ERG/CM ²

3.2.2 Material Parameters for Multiple Layers of Bubbles

Multiple layers of bubble supporting materials provide increased flexibility in design considerations for self-structured applications. Listed below is a set of equations which relate the material parameters, bubble size, and various magnetic fields to each other.

$$X = \frac{1 - 3\lambda/4 - H}{3H} + \left[\frac{(1 - 3\lambda/4 - H)^2 - \frac{\lambda}{3H}}{3H} \right]^{1/2} \quad \begin{matrix} \text{(reference number)} \\ (2) \\ \downarrow \\ (2) \\ \downarrow \\ (2) \end{matrix} \quad (3.3)$$

$$H_0 = 1 + 3\lambda/4 - (3\lambda)^{1/2} \quad (2) \quad (3.4)$$

$$X_0 = \left((3\lambda)^{1/2} - 3/2 \right)^{-1} \quad (2) \quad (3.5)$$

$$\lambda = (4/3) (1 - 2H_0^{1/2} + H_0) \quad (3.6)$$

(Inversion of equation 3.4)

$$H_{RO} = \exp - (1 + \pi\lambda - H_{RO}) \quad (3) \quad (3.7)$$

$$\lambda = (H_{RO} - \ln H_{RO} - 1) / \pi \quad (3.8)$$

(Inversion of equation 3.7)

$$l = \left(\frac{106.7}{4\pi M} \right)^{1.231} = 313.8 (4\pi M)^{-1.231} \quad (3.9)$$

Equation 3.9 is an empirical relation found to hold true for large and small bubble garnets, both Ga and CaGe garnets (see section 4.5.2). There may be garnets for which equation 3.9 is not true, but garnets can be found that fit equation 3.9 over the full range of l and M .

In one type of multilayer self-structured bubble memory, a large diameter carrier bubble domain in one layer carries along with itself a number of small data bubbles in a second layer. Both the large bubbles and the small bubbles, in their own layer, must have wide operating regions that overlap. The run-out, or strip-out, field of one layer must not be higher than the collapse field of the other, and vice-versa. The following calculation

generates the proper parameters of the two layers so that the bubble sizes are different, yet the collapse field is the same.

As an example, consider the application of two magnetic layers with $4\pi M = 125$ Oe and 300 Oe, with a bubble collapse threshold $H_0 = 83$ Oe for both layers.

To convert Oersteds into ampere turns per meter, multiply by $1000/4\pi$, which equals 79.5775. What is the proper thickness, h , for each layer, and what are the values of λ , λ , X_0 , r_0 , H_{r0} ?

From equation 3.9, the characteristic length λ is $0.823\mu\text{m}$ for $4\pi M = 125$ Oe, and $.2804\mu\text{m}$ for $4\pi M = 300$ Oe. From the definition $H_0 = H_0/4\pi M$, $H_0 = 0.6639$ for $4\pi M = 125$ Oe, and 0.2767 for $4\pi M = 300$ Oe. From equation 3.6, $\lambda = 0.04572$ and 0.2996 for $4\pi M = 125$ Oe and 300 Oe, respectively. From the definition $\lambda = \lambda/h$, the thickness of the layer with $4\pi M = 125$ Oe must be $18\mu\text{m}$, and the thickness of the other layer must be $0.9359\mu\text{m}$. From equation 3.5, X_0 is 0.1515 and 0.6008 , respectively. From the definition $X_0 = r_0/h$, r_0 is 2.727 m and $0.5623\mu\text{m}$, respectively. From equation 3.7, the normalized run-out field is 0.5552 and 0.5623 , respectively, so that $H_{r0} = 69.4$ Oe and 51 Oe, respectively. If the operating bias field $H = 76$ Oe, from equation 3.3, X is 0.2118 and 0.9651 , which corresponds to a bubble radius of $5.61\mu\text{m}$ for the large bubble film and $0.903\mu\text{m}$ for the small bubble film. This procedure illustrates how such calculations can be performed, for a variety of values of $4\pi M$ and H_0 .

Figures 3.3, 3.4, and 3.5 are graphs of the proper film thickness as a function of $4\pi M$ for layers having a collapse threshold of 83 Oe, 57 Oe, and 198 Oe, respectively. The radius r_0 of the bubble at the collapse threshold is also plotted, as is the radius at a suitable operating bias.

To illustrate the use of figures 3.3, 3.4, and 3.5, assume a two layer bubble memory. The carrier bubbles have a chosen diameter of $7\mu\text{m}$ and operate at a bias field of 76 Oe. Figure 3.3 indicates that the $4\pi M$ of the carrier layer should be 150 Gauss, and that the thickness of the carrier layer should be $7.5\mu\text{m}$. If the diameter of the data bubbles is to be one fourth of the carrier bubbles, or $1.75\mu\text{m}$, then each carrier bubble may carry up to seven data bubbles. Figure 3.3 indicates that the $4\pi M$ of the data layer should be 315 Gauss, and the thickness of the data film should be $0.88\mu\text{m}$. In actual practice this data film would be made by gradually thinning a thicker layer, monitoring the bubble collapse threshold between thinnings until the operating regions of the two films coincide.

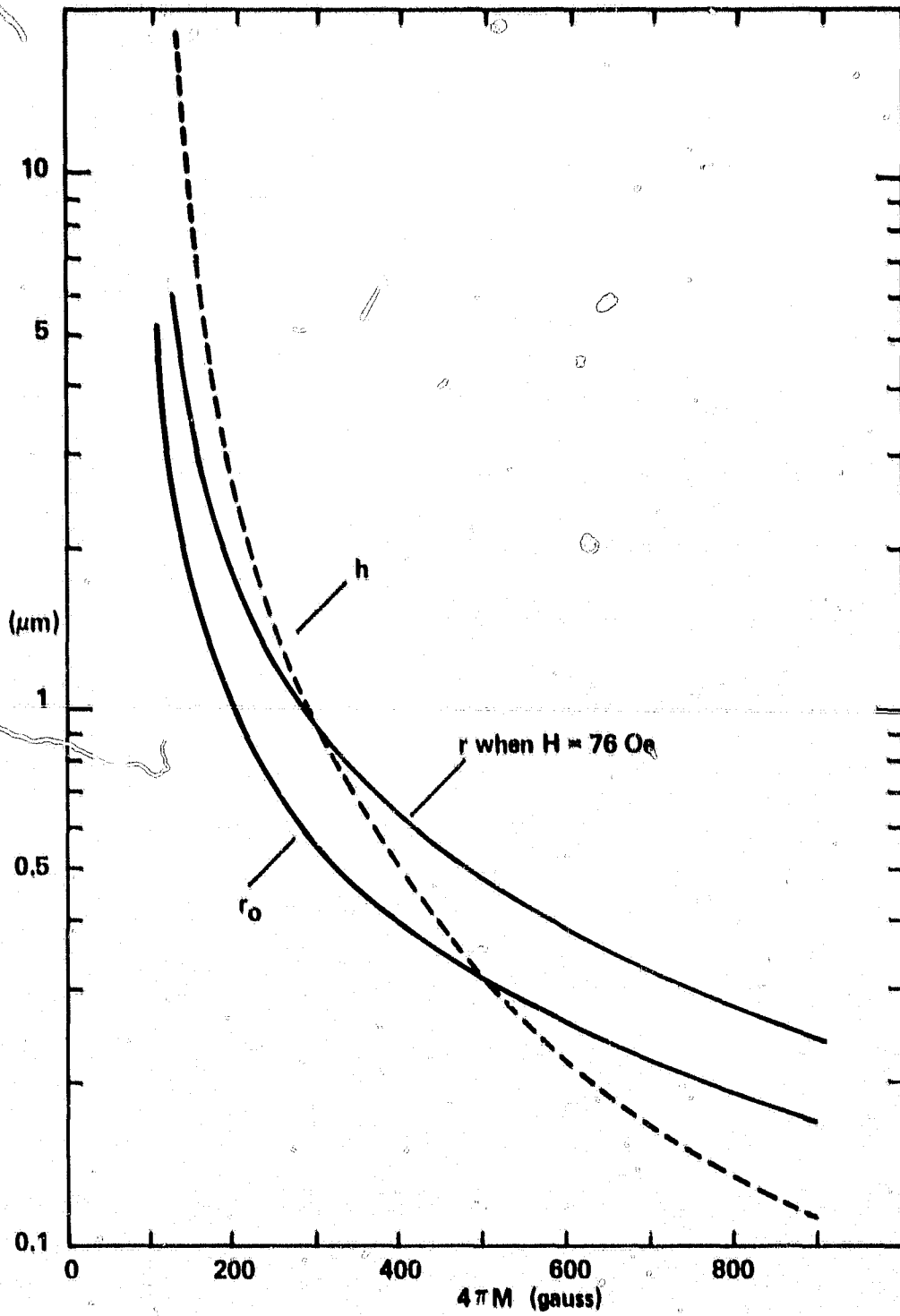


Figure 3.3 Bubble Radius r , and Film Thickness h vs. $4\pi M$, with Collapse Threshold $H_0 = 83 \text{ Oe}$.

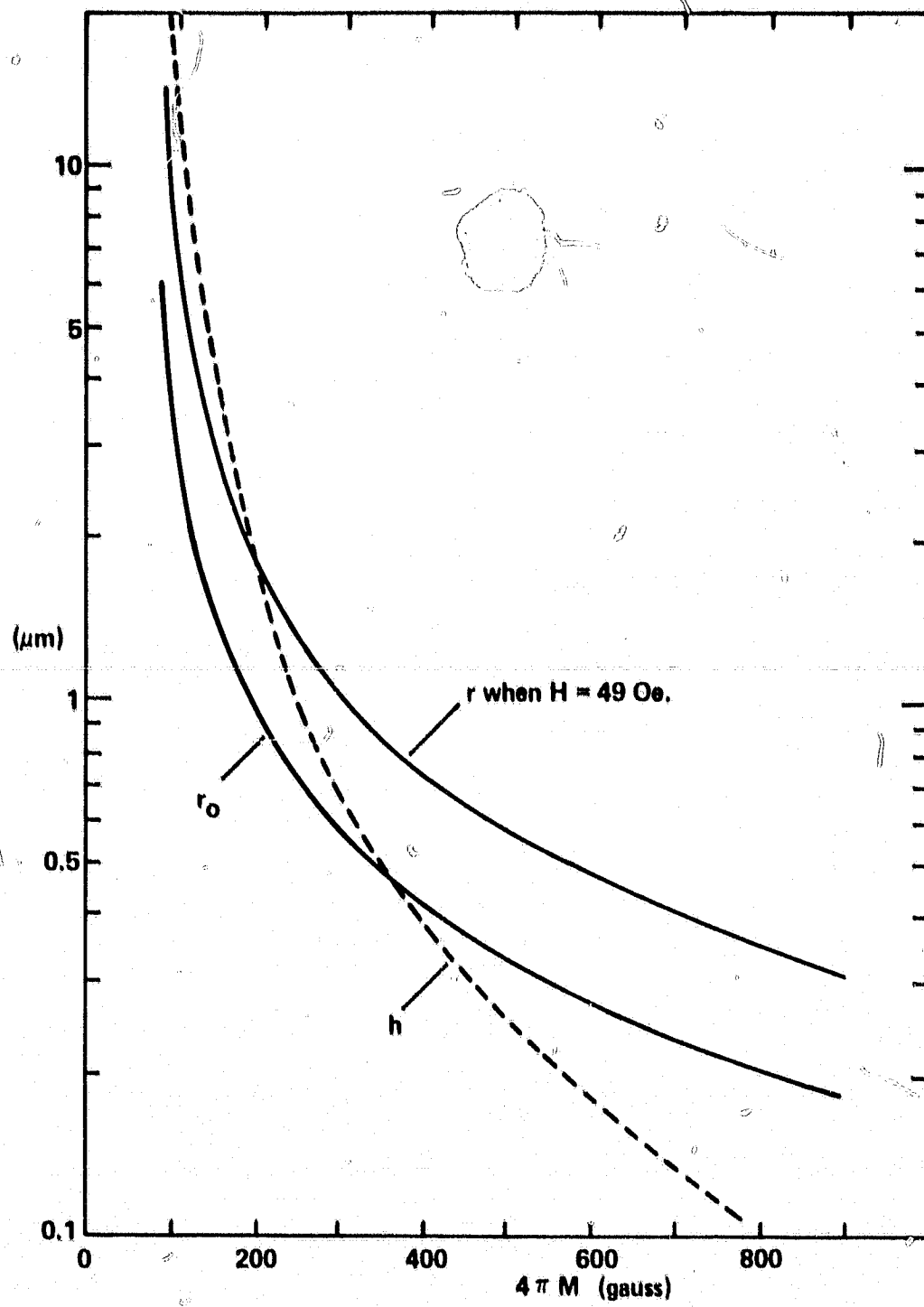


Figure 3.4 Bubble Radius r_0 and Film Thickness h vs. $4\pi M$, with Collapse Threshold $H_0 = 57$ Oe.

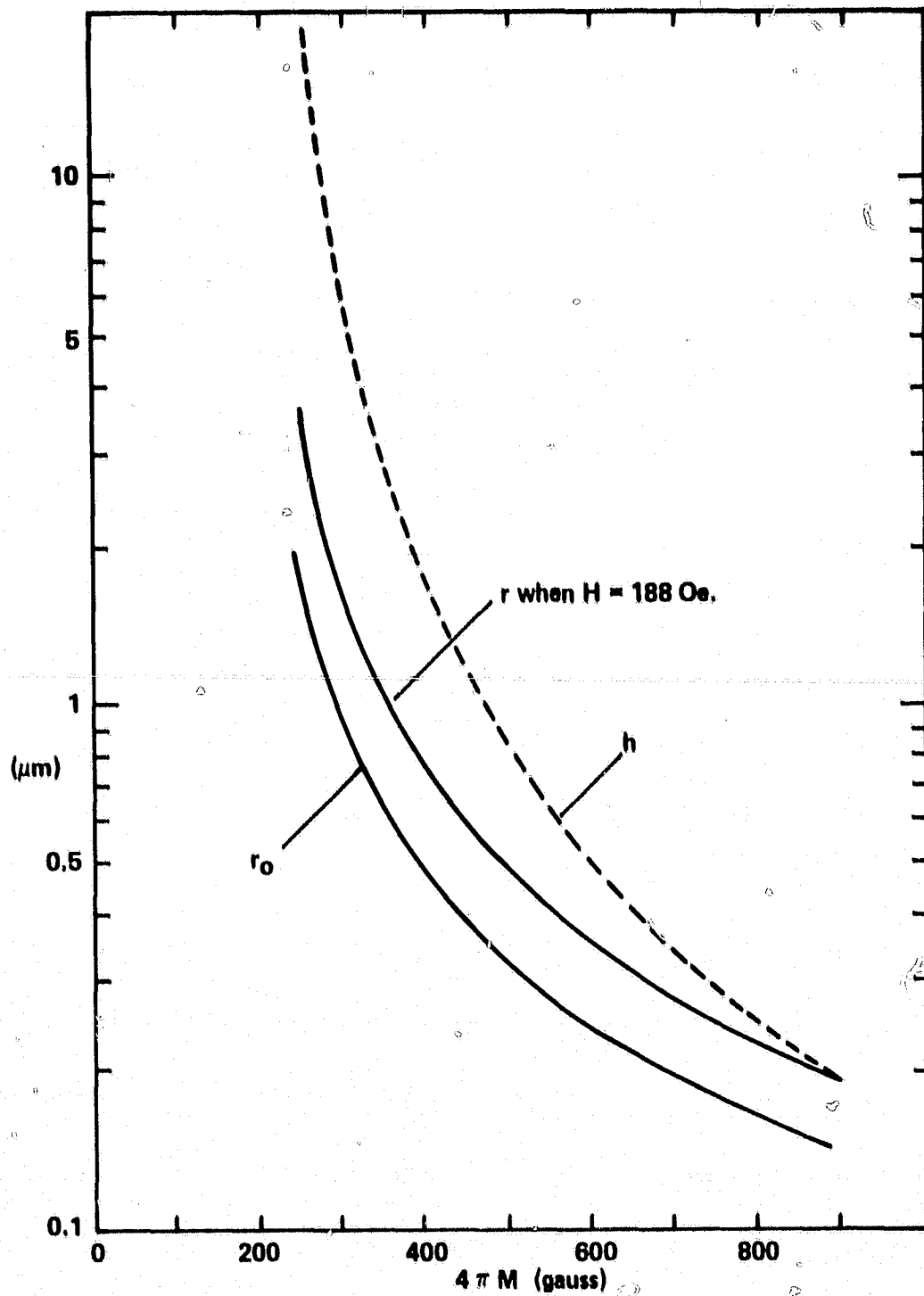


Figure 3.5 Bubble Radius r_0 and Film Thickness h vs. $4\pi M$, with Collapse Threshold $H_0 = 198$ Oe.

From these figures we see that large variations in bubble radius, a factor of 20 or more, can be obtained with compatible operating ranges. A practical difficulty is that the small bubbles require the films to be very thin. This, in turn, presents two problems which all small bubble memories have: a fabrication problem and a read-out problem. The fabrication problem is to grow thin enough layers. Using the usual lead oxide flux, initial growth rate is exceedingly fast, so that a one micron film grows when one just dips the film into the melt and pulls the film out. The problem can be solved either by using a lithium molybdate melt in which films have a very slow growth rate, or by thinning a film grown in the conventional lead melt by ion milling or chemical etching. The read-out problem is ameliorated somewhat by the fact that the small bubble films have higher $4\pi M$; however, read-out is still a problem for all small bubble memories and not just multilayer structures.

3.3 Coupling Between Stripe and Bubble Layers

One class of multilayer bubble lattice file uses stripe domains in one layer to propagate bubbles in a second layer. A calculation of the coupling strength due to both the exchange force and the magnetostatic field is presented herein.

Because the stripe films that respond best to in-plane fields have high $4\pi M$ values and very narrow stripes, a mismatch in size between bubbles and stripes is likely. The calculations show that the coupling strength decreases in a non-monotonic fashion as the stripe width decreases, relative to the bubble diameter. The coupling is never zero unless the stripe width is zero, and therefore, stripes can be used to propagate bubbles even though they are not matched in size.

Exchange coupling and magnetostatic coupling are roughly of equal importance if no separating layer is used. Magnetostatic coupling decreases as the thickness of the bubble layer increases, decreases as the width of stripes decreases, and, if a separating layer is used, decreases as the separation increases.

3.3.1 Exchange Coupling

Exchange coupled double layer garnet films are made by epitaxially growing a magnetic garnet layer directly on another magnetic garnet layer with different properties. There is no non-magnetic layer between them.

In the past, such double layer garnet films have been grown for the purpose of having one layer replace the external normal bias field required to sustain bubbles. For this application, one

layer is always saturated, while the other layer contains bubbles. Exchange energy causes the saturated layer to exert a torque on the spins of the bubble layer that tends to saturate the second layer, and thereby emulate a bias field. The magnetostatic field from the saturated film is negligible for the same reason that the electrostatic field of a parallel plate capacitor is negligible outside the capacitor.

The strength of the exchange coupling is experimentally measured by measuring the difference in the bubble collapse field in one layer with the other layer saturated in two opposite states. Half of the difference between the two collapse fields is the coupling strength in Oersteds. It is conventional to report the strength of the exchange coupling in Oersteds for that reason, although the exchange coupling is not a magnetic field. The experimental value obtained will depend strongly on the thickness and aspect ratio of the bubble. An exchange bias of 31 Oersteds on a 1.6 μ m thick bubble film of (YSm)₃GaIG exerted by a bias layer of (EuEr)₃GaIG has been reported.⁴ Therefore, for the theoretical calculations, an exchange coupling of 31 Oersteds is assumed. It is also assumed that there is no domain closure structure.

3.3.2 Mismatch Between Stripe Width and Bubble Diameter

When the diameter of a bubble is equal to or less than the width of a stripe in a double layer structure, the bubble will be held by the exchange force over the area of the surface of the bubble that is in contact with the stripe. When the bubble diameter is larger than the stripe width, the bubble will intersect two or more stripes. Those stripes in which the spins in the iron sublattice are parallel to those in the bubble will attract the bubble; those with oppositely oriented spins in the iron sublattice, repel. The net exchange attraction is proportional to the difference in area of those portions of attracting and repelling stripes enclosed by the bubble.

The bubble will position itself in order to maximize the area of contact with attracting stripes and minimize the area of contact with repelling stripes. Figure 3.6.a shows the equilibrium position when the diameter of the bubble is only slightly larger than the width of the stripe. Figure 3.6.b shows the equilibrium position when the width of the stripes is decreased further. Note that the bubble is non-symmetrically arranged with respect to the stripes. Equilibrium occurs when the condition

$$h_1 - h_2 + h_3 = 0$$

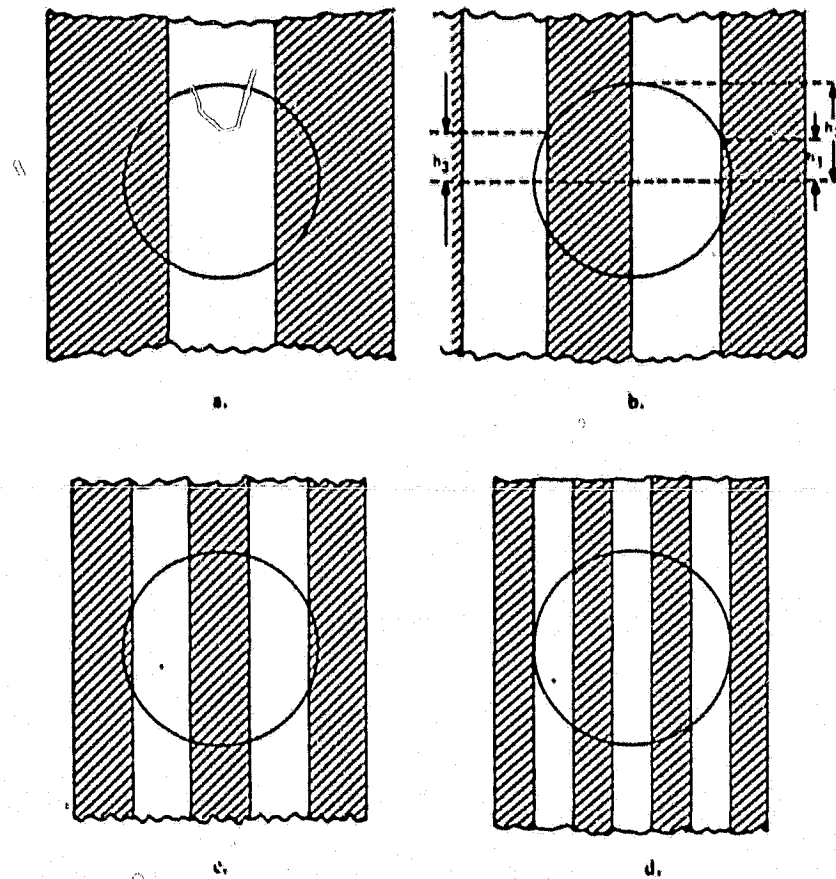


Figure 3.6 Equilibrium Configurations of Stripe and Bubble Domains.

is fulfilled, with h_1 , h_2 , and h_3 defined as in figure 3.6.b. Regardless of the width of the stripe, there is always some position where the bubble has lower energy; that is, there is always a positive coupling. Figures 3.6.c and d show stable configurations in which the stripe width is decreased further.

The strength of the coupling is easily determined by calculating the difference in area of those portions of attracting and repelling stripes enclosed by the bubble. The result is shown in figure 3.7. Coupling strength decreases in a non-monotonic fashion as the stripe width decreases, and is zero only when the stripe width is zero.

It is necessary to determine how much coupling is required for propagation. Conventional garnet bubble films for memories have coercivity of approximately one tenth of one Oersted. Thus, a coupling field greater than one tenth of one Oersted should be sufficient to propagate a bubble.

3.3.3 Magnetostatic Coupling

Coupling between stripes and bubbles also occurs by magnetostatic interaction. If stripes are of equal width, the dependence of magnetostatic coupling upon the relative stripe/bubble size is similar to that of exchange coupling, as shown in figure 3.7. The "full scale" magnitude of the magnetostatic coupling, the magnitude of coupling when the width of the stripe is larger than the bubble diameter, depends strongly on the thickness of the bubble film and on the intensity of magnetization $4\pi M$ of the stripe field.

The field from a stripe domain is calculated by considering a stripe domain layer of thickness h . Let the wavelength of the stripes be λ , let the distance parallel to the film surface and perpendicular to the stripes be x , let the point $x = 0$ be in the middle of a stripe, and let the distance above the top surface of the film be z . Starting with $\text{div } \vec{B} = 0$ and $\vec{B} = \vec{H} + 4\pi\vec{M}$,

$$\text{div } (\vec{H} + 4\pi\vec{M}) = 0 \quad (3.10)$$

$$\text{div } H = -4\pi(\nabla \cdot M) \equiv 4\pi p_m \quad (3.11)$$

where $p_m = \nabla \cdot M$ is the magnetic charge per unit volume. Consider a narrow strip, running along a stripe at the film surface, uniformly charged. Surrounding this with a Gaussian surface, the result is

$$H = \frac{2\lambda_m \hat{S}}{S} \quad (3.12)$$

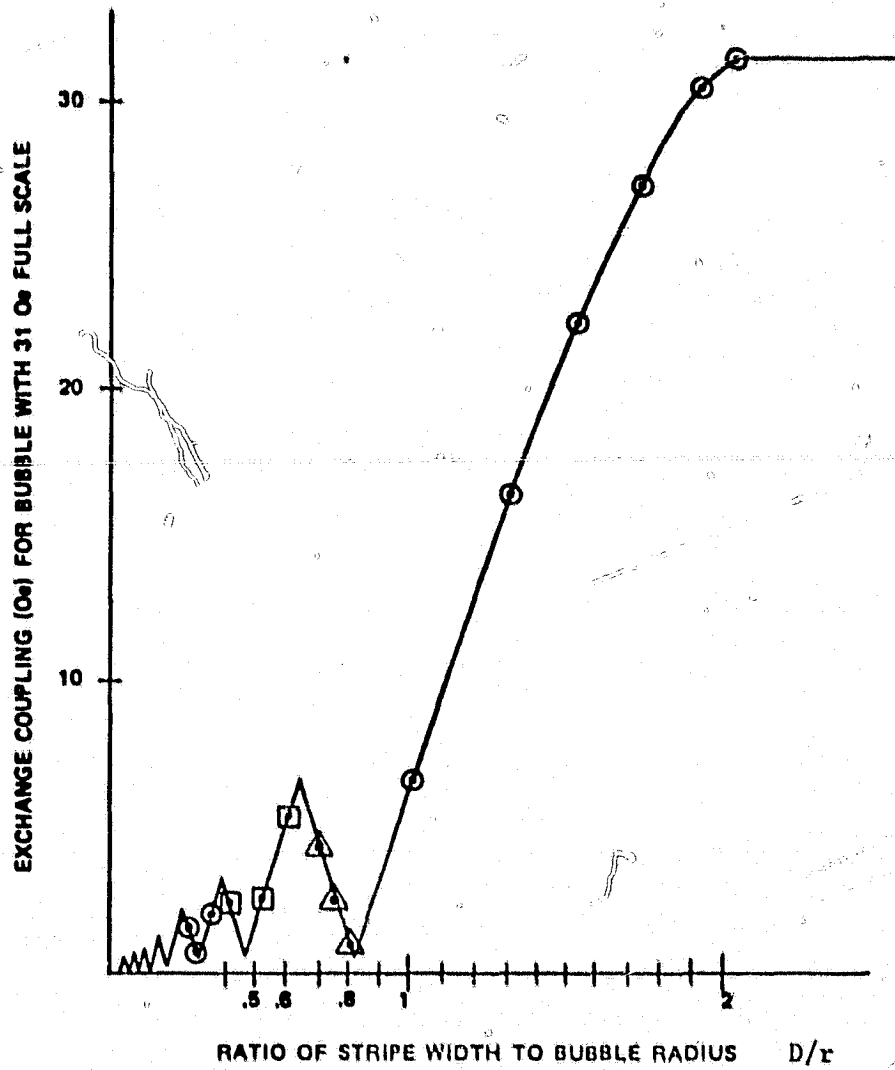


Figure 3.7 Exchange Coupling vs. Ratio of Stripe Width to Bubble Radius.

where s is the distance from the narrow strip, λ_m is the magnetic charge per unit length, and \hat{s} is a unit vector. The stripe domain garnets under consideration have a low anisotropy field H_k so that they may be aligned with a magnetic field. If the average z component of magnetization in the stripe film is assumed to be given by

$$M_z = M \cos \frac{2\pi x}{\lambda} \quad (3.13)$$

then the z component of the stray field is given by

$$H_z = 2M \cos \frac{2\pi x}{\lambda} \int_{-\infty}^{\infty} \left\{ \frac{\cos \frac{2\pi x}{\lambda} z}{z^2 + x^2} - \frac{\cos \frac{2\pi x}{\lambda} (z + h)}{(z + h)^2 + x^2} \right\} dx \quad (3.14)$$

This equation yields

$$H_z = 2\pi M \left[\exp\left(\frac{-2\pi z}{\lambda}\right) - \exp\left(\frac{-2\pi(z + h)}{\lambda}\right) \right] \cos \frac{2\pi x}{\lambda} \quad (3.15)$$

Let the thickness of the bubble film be h_B and let the spacing between the bubble film and the stripe film be h_G . The full scale magnetostatic coupling field, H_{FS} , from the stripe film to the bubble film is found by averaging equation 3.15 between the limits h_G and $h_G + h_B$:

$$H_{FS} = \frac{M\lambda}{h_B} \left[\exp\left(\frac{-2\pi h_G}{\lambda}\right) - \exp\left(\frac{-2\pi(h_G + h_B)}{\lambda}\right) + \exp\left(\frac{-2\pi(h_G + h_B + h)}{\lambda}\right) - \exp\left(\frac{-2\pi(h_G + h)}{\lambda}\right) \right] \quad (3.16)$$

When the thickness of the spacer layer is zero and when the thickness of the stripe film is greater than the stripe wavelength λ , equation 3.16 reduces to

$$H_{FS} = \frac{M\lambda}{h_B} \left[1 - \exp\left(\frac{-2\pi h_B}{\lambda}\right) \right] \quad (3.17)$$

Figures 3.8 and 3.9 show how this full scale coupling depends on the thickness of the bubble film, the wavelength of the stripes, and the thickness of the Gadolinium Gallium Garnet (GGG) layer

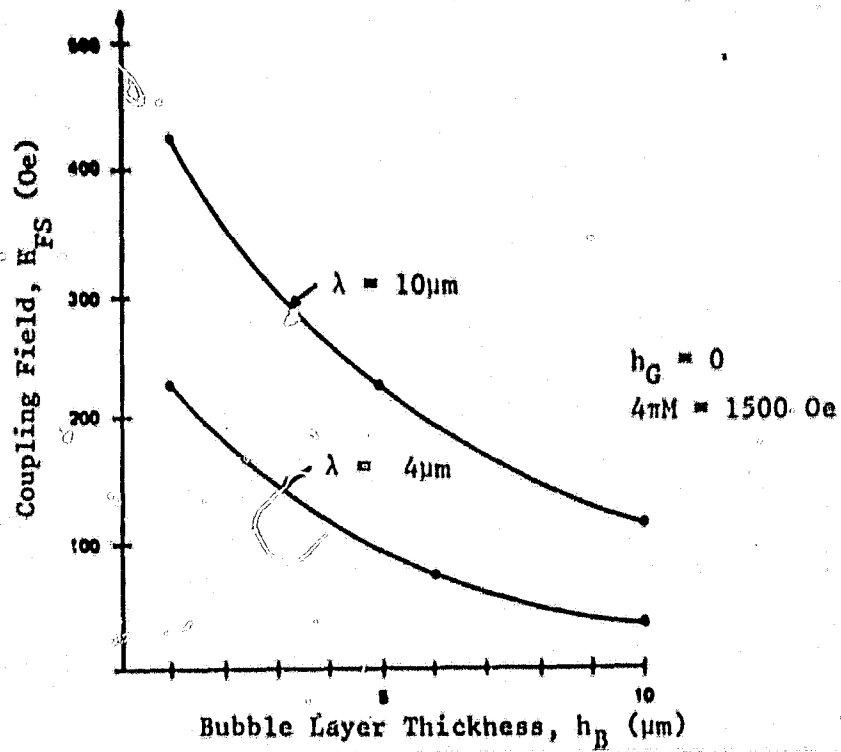


Figure 3.8 Magnetostatic Coupling vs. Bubble Layer Thickness with Zero Separation for Two Stripe Wavelengths.

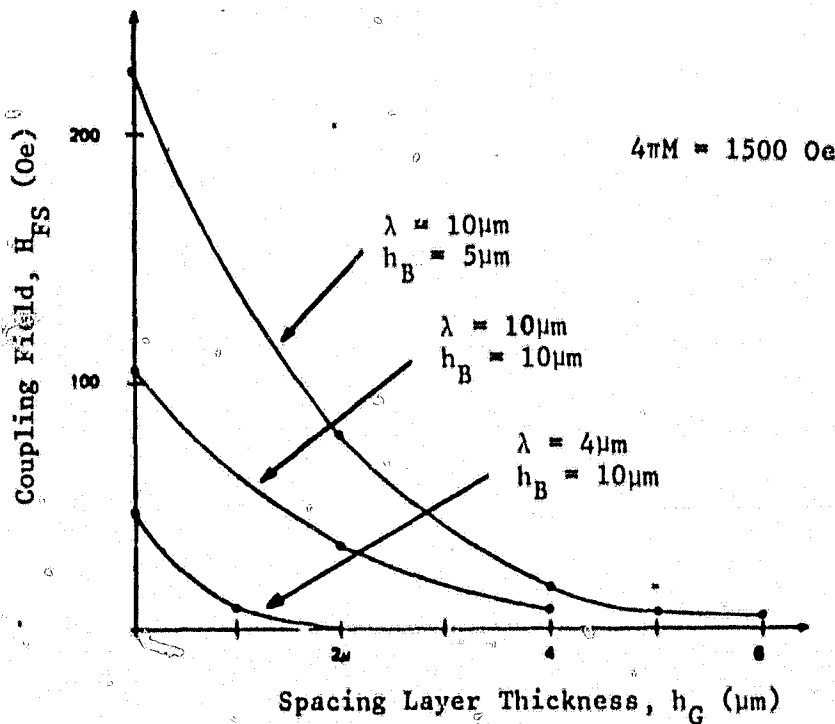


Figure 3.9 Magnetostatic Coupling vs. Gap Thickness Between Bubble Layer and Stripe Layer.

separating the stripe and bubble films. As thickness of the bubble layer increases, the coupling decreases; as the width of the stripes increases, the coupling increases; and, as the thickness of the separation layer increases, the coupling decreases. A $4\pi M$ value of 1500 Oe was assumed for the stripe film; if gallium is used to substitute for some of the iron, the $4\pi M$ will be less and the coupling proportionately reduced.

3.3.4 Stripe-Bubble Interaction

Stripe domains in one layer can trap bubbles in another layer, so that when the stripes are moved they move the bubbles along with them. The interaction is due to the magnetic stray field from the stripes. Therefore, knowledge of the strength and spatial dependence of that field is of importance for design considerations.

Equation 3.15 is plotted in figure 3.10 as a function of distance above the garnet layer. Note that the interaction can be made as strong as $2\pi M$, which is far more than needed for strong coupling. Also, the stray-field value can be adjusted to whatever value desired simply by choosing the proper spacer thickness. Note that the thickness of the stripe domain film is immaterial for thicknesses greater than the stripe wavelength, λ .

3.3.5 Stripe and Bubble Material Selection

In this section theoretical relationships are derived that provide the crystal grower with knowledge of the proper film parameters for a coupled strip-bubble multilayer.

The stripe layer in a multilayer self-structured bubble memory should have wide, rather than narrow, stripes if chevrons or current conductors are used to move the stripes. The properties of the stripe film and the bubble film should be similar, but since both must operate in the same external bias field, their characteristics must be different enough so that one is above the run-out threshold and the other is below. Explicit relationships are derived for the % change in run-out threshold due to a % change in: (1) thickness, (2) magnetization, (3) characteristic length, (4) anisotropy constant, and (5) exchange constant. Various stray field formulas for isolated stripes are also given.

Consider a double layer film in which one layer supports stripes and the other supports bubbles. The purpose of such a structure is to move the bubbles by moving the stripes. Since most stripe propagation schemes being investigated require small structures (conductors, chevrons, etc.), the stripes must be wide. Such wide stripes are found in high Q_c low $4\pi M$ films of the type used

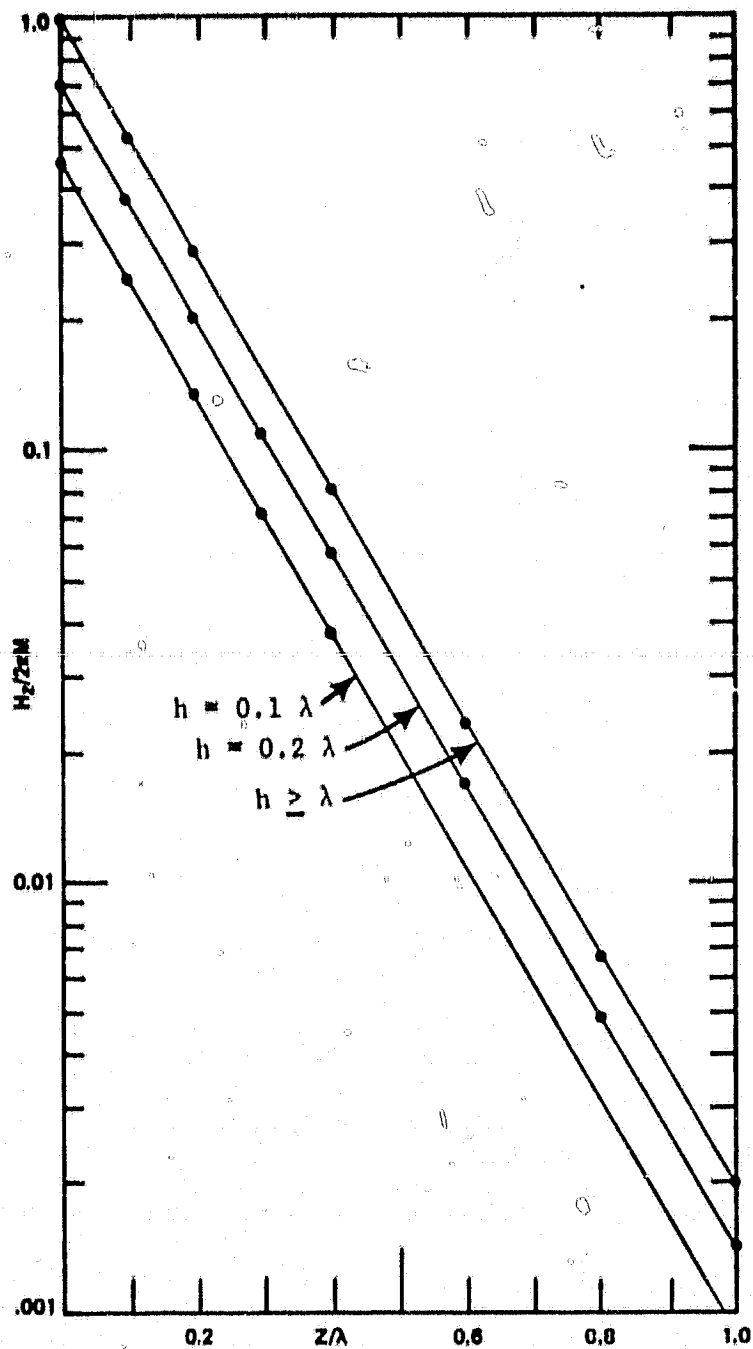


Figure 3.10 Normal Component of Stray Field vs. Height Above a Stripe Domain of Thickness h and Wavelength λ .

for bubbles rather than in the low Q, high $4\pi M$ films used for light deflectors. Therefore, the stripe and bubble films should be not too dissimilar.

3.4 Stripe Domain and Material Parameters

At the edge of an infinitely long stripe, the normal component of the stray field averaged over thickness was first derived by Kooy and Enz:⁵

$$\frac{H_W}{M} = \frac{2}{\pi} \left[\tan^{-1} \left(\frac{h}{w} \right) - \frac{w}{2h} \ln \left(1 + \frac{h^2}{w^2} \right) \right] \quad (3.18)$$

where w is the width of a stripe.

A useful approximation to equation 3.18 is given by O'Dell:⁶

$$\frac{H_W}{M} = \frac{4\pi}{1 + \pi W/h} \quad (3.19)$$

Let the x-axis lie in the film plane and let the walls of the stripe domain be at $x = 0$ and $x = W$. The z component of the stray field, $H(x)$ at the point x , can be calculated from H_W by considering the field to be due to two stripe domains, one of width x and the other of width $W - x$:

$$H(x) = H_W(x) + H_W(W - x) - 4\pi M.$$

Note that $4\pi M$ has been subtracted so as not to add twice the field from the saturated film in which the stripe is superposed. The average field over the whole domain is

$$\bar{H}_W = \frac{1}{W} \int_0^W H(x) dx. \quad (3.20)$$

When the O'Dell approximation, equation 3.19, is used, the result is:

$$\frac{\bar{H}_W}{M} = -4\pi + \frac{8h}{W} \ln \left(1 + \frac{\pi W}{h} \right) \quad (3.21)$$

Derivation of the field at the tip of an isolated rectangular stripe, averaged over both x and thickness, is similar to the derivation of equation 3.20, except that two rectangular strips joined end to end are considered:

$$\bar{H}_{\text{tip}} = \frac{1}{2}(\bar{H}_W + 4\pi M). \quad (3.22)$$

If the O'Dell approximation, equation 3.19, is used, then

$$\bar{H}_{\text{tip}} = \frac{4h}{W} \ln \left(1 + \frac{\pi W}{h} \right) \quad (3.23)$$

Note that from equations 3.19 and 3.21 the following relationship holds:

$$\frac{1}{2} \left[\bar{H}_W + W \frac{\partial \bar{H}_W}{\partial W} + 4\pi M \right] = H_W \quad (3.24)$$

3.4.1 Run-Out Threshold

Consider an isolated stripe domain of width W and length L in a film of thickness h. The total energy is the sum of the applied field energy, the stray field energy, and the wall energy:

$$\begin{aligned} E &= E_A + E_O + E_W \\ &= 2WhLMH + WhL(\bar{H}_W - 4\pi M) + 2(L + W) \sigma_W h. \end{aligned}$$

Assuming that $L \gg W$, and requiring that at the run-out threshold the domain neither shrinks or grows, so that $\partial E / \partial L = 0$, leads to

$$0 = H - \frac{1}{2} (\bar{H}_W + 4\pi M) + \sigma_W M^{-1} W^{-1}. \quad (3.25)$$

The condition $\partial E / \partial W = 0$ results in a second equation:

$$0 = 2H - \bar{H} - W \frac{\partial \bar{H}_D}{\partial W} - 4\pi M. \quad (3.26)$$

From equation 3.24, equation 3.26 becomes:

$$0 = H - H_W \quad (3.27)$$

and with equation 3.19 this becomes:

$$H = \frac{4\pi M}{1 + \pi W/h}, \text{ or } 1 + \frac{\pi W}{h} = \frac{4\pi M}{H} \quad (3.28)$$

Substituting equation 3.21 into equation 3.25 gives:

$$0 = H - \frac{4h}{W} \ln \left(1 + \frac{\pi W}{h} \right) + \frac{\sigma_W}{MW} \quad (3.29)$$

Using equation 3.28 to substitute for $(1 + \pi W/h)$ in equation 3.29 yields:

$$0 = H - \frac{4h}{W} \ln \left(\frac{4\pi M}{H} \right) - \frac{\sigma_W \pi}{Mh} \left[\frac{H}{4\pi M - H} \right] \quad (3.30)$$

Rewriting equation 3.30, using

$$\lambda = \frac{\sigma_W}{4\pi M^2 h} = \frac{\ell}{h} \quad (3.31)$$

and noting that, by definition, when $\partial E/\partial L = 0$, the applied bias field, H , is the run-out field, gives:

$$\frac{H_{RO}}{4\pi M} = 1 + \pi \lambda - \ln \left(\frac{4\pi M}{H_{RO}} \right) \quad (3.32)$$

3.4.2 Layer Thickness

The percent change in run-out threshold as a result of changing the thickness, h , by one percent is presented below. Taking the partial derivative of equation 3.32 with respect to h gives:

$$\frac{\delta H_{RO}}{4\pi M} = \frac{\pi \delta \lambda}{\delta h} \delta h + \frac{\delta H_{RO}}{H_{RO}} \quad (3.33)$$

Differentiation of equation 3.31 yields:

$$\frac{\delta \lambda}{\delta h} = - \frac{\lambda}{h} \quad (3.34)$$

Substituting equation 3.34 in equation 3.33 gives:

$$\frac{\partial H_{RO}}{H_{RO}} / \frac{\partial h}{h} = \frac{\pi \lambda}{1 - H_{RO}/4\pi M} \quad (3.35)$$

When equation 3.32 is used to remove λ from the equation 3.35, the result is:

$$\frac{\partial H_{RO}}{H_{RO}} / \frac{\partial h}{h} = \frac{\ln\left(\frac{4\pi M}{H_{RO}}\right)}{1 - H_{RO}/4\pi M} - 1 \quad (3.36)$$

Equation 3.36 is plotted in figures 3.11 and 3.12. Note that the right hand side of equation 3.36 is always positive, which means that as film thickness increases the run-out threshold increases.

3.4.3 Magnetization

The derivation of the ratio of the percent change in run-out field to the percent change in $4\pi M$ is similar to the derivation of the thickness dependence in the previous section. The assumption is made when $4\pi M$ is changed (for example, by the substitution of more iron oxide for gallium oxide), K , the anisotropy constant, remains unchanged. The result is:

$$\frac{\partial H_{RO}}{H_{RO}} / \frac{\partial M}{M} = \frac{2}{1 - H_{RO}/4\pi M} \ln\left(\frac{4\pi M}{H_{RO}}\right) \quad (3.37)$$

Equation 3.37 is always positive, so increasing $4\pi M$ always increases the run-out threshold. Moreover, the change is very large. Equation 3.37 is plotted in figures 3.13 and 3.14.

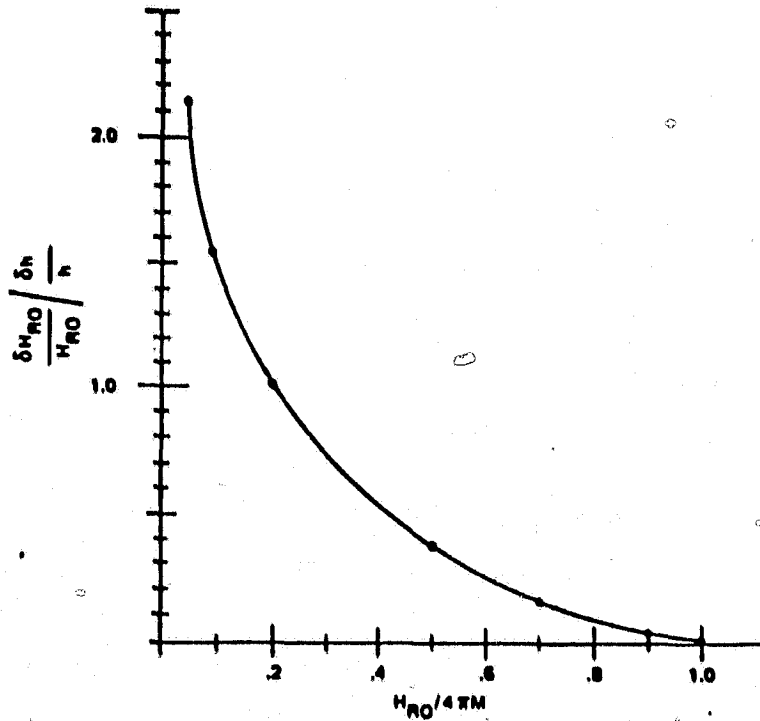


Figure 3.11 Ratio of the Percentage Change in Run-Out Field to the Percentage Change in Film Thickness vs. Run-Out Field.

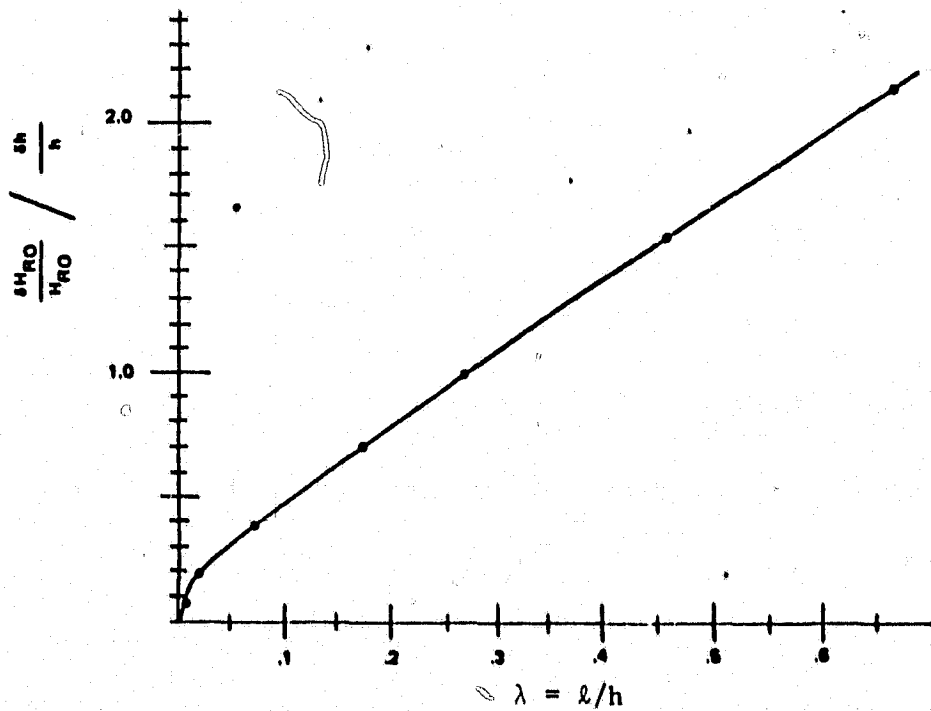


Figure 3.12 Ratio of the Percentage Change in Run-Out Field to the Percentage Change in Film Thickness vs. Characteristic Length.

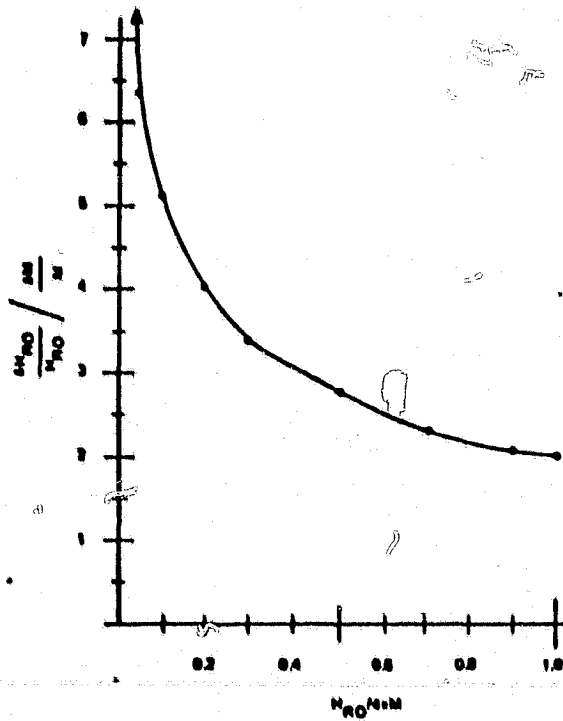


Figure 3.13 Ratio of the Percentage Change in Run-Out Field to the Percentage Change in Magnetization vs. Run-Out Field.

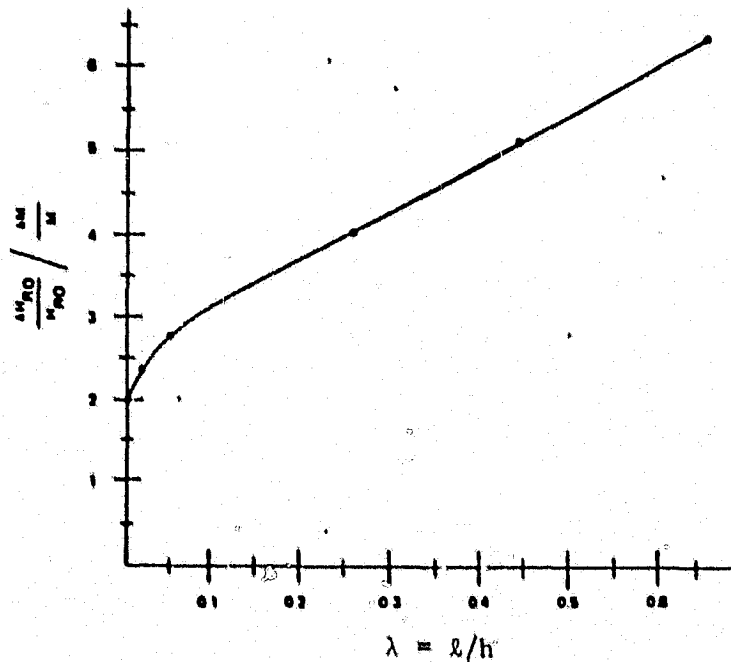


Figure 3.14 Ratio of the Percentage Change in Run-Out Field to the Percentage Change in Magnetization vs. Characteristic Length.

3.4.4 Characteristic Length

The characteristic length, ℓ , is one of the fundamental parameters measured in garnets, and is defined as $\sigma_w/4\pi M^2$. The percent change in run-out threshold due to a one percent change in characteristic length (for example, due to a change in wall energy) is given by:

$$\frac{\partial H_{RO}}{H_{RO}} \bigg/ \frac{\partial \ell}{\ell} = \frac{H_{RO}/4\pi M}{1 - H_{RO}/4\pi M} \ln \left(\frac{4\pi M}{H_{RO}} \right) \quad (3.38)$$

This is plotted in figures 3.15 and 3.16.

3.4.5 Uniaxial Anisotropy and Exchange Constant

The wall energy per unit length and thickness is $\sigma_w = 2A^{1/2}K^{1/2}$. The dependence of the run-out field on exchange constant and anisotropy constant can be calculated as in the preceding section knowing that

$$\frac{\partial \sigma_w}{\sigma} = \frac{1}{2} \frac{\partial K}{K} \quad \text{and} \quad \frac{\partial \sigma_w}{\sigma} = \frac{1}{2} \frac{\partial A}{A}$$

The resulting equations are:

$$\frac{\partial H_{RO}}{H_{RO}} \bigg/ \frac{\partial A}{A} = - \frac{1}{2} \frac{H_{RO}/4\pi M}{1 - H_{RO}/4\pi M} \ln \left(\frac{4\pi M}{H_{RO}} \right) \quad (3.39)$$

and

$$\frac{\partial H_{RO}}{H_{RO}} \bigg/ \frac{\partial K}{K} = - \frac{1}{2} \frac{H_{RO}/4\pi M}{1 - H_{RO}/4\pi M} \ln \left(\frac{4\pi M}{H_{RO}} \right) \quad (3.40)$$

These are plotted in figures 3.17 and 3.18.

The most important film parameter affecting the run-out threshold is magnetization, followed by film thickness, characteristic length, and exchange energy and anisotropy constant, in that order. For example, in a film with $H_{RO}/4\pi M = 0.2$, a 10% change in $4\pi M$ causes a 40% change in run-out threshold, a 10% change in

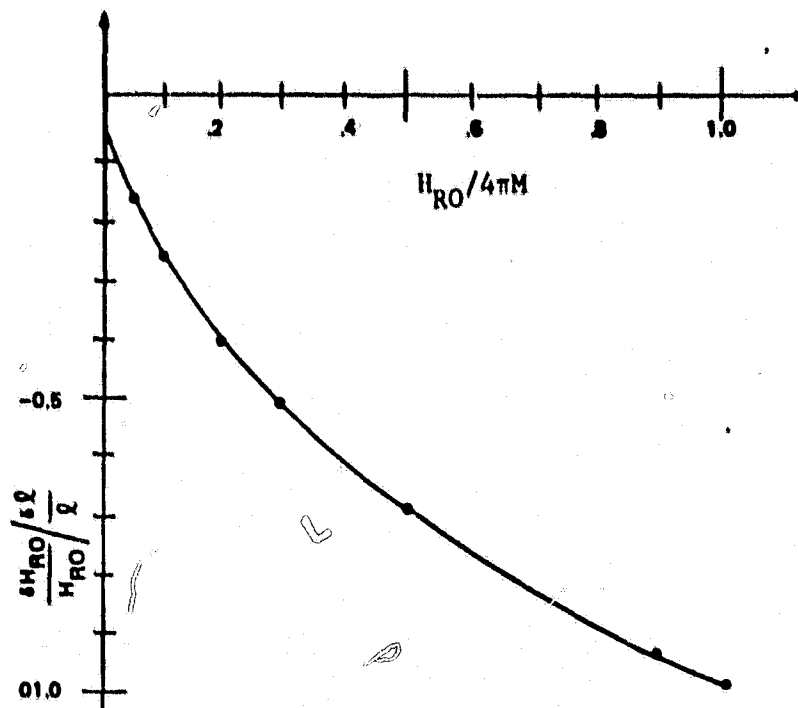


Figure 3.15 Ratio of the Percentage Change in Run-Out Field to the Percentage Change in Characteristic Length vs. Run-Out Field.

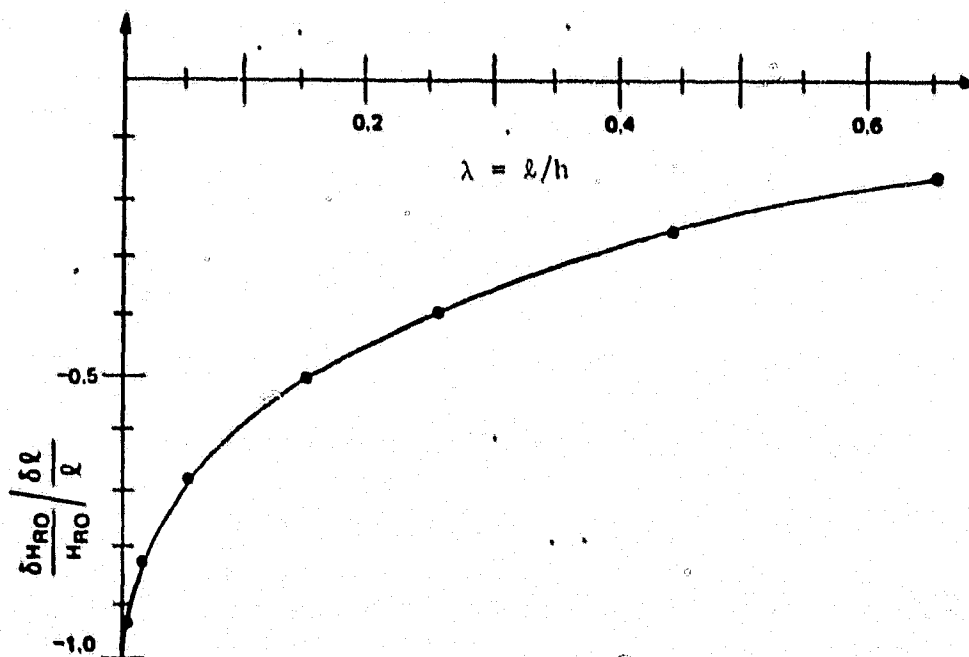


Figure 3.16 Ratio of the Percentage Change in Run-Out Field to the Percentage Change in Characteristic Length vs. Characteristic Length.

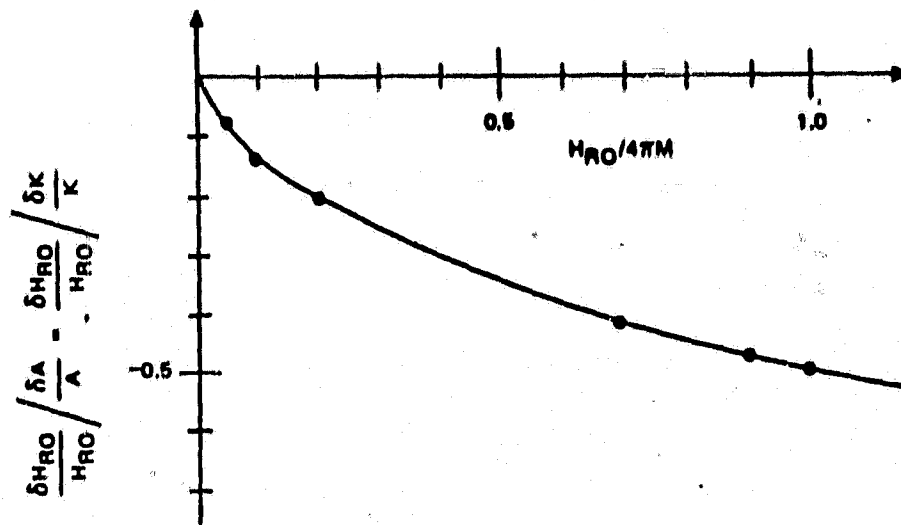


Figure 3.17 Ratio of the Percentage Change in Run-Out Field to the Percentage Change in Both the Anisotropy Constant and Exchange Constant vs. Run-Out Field.

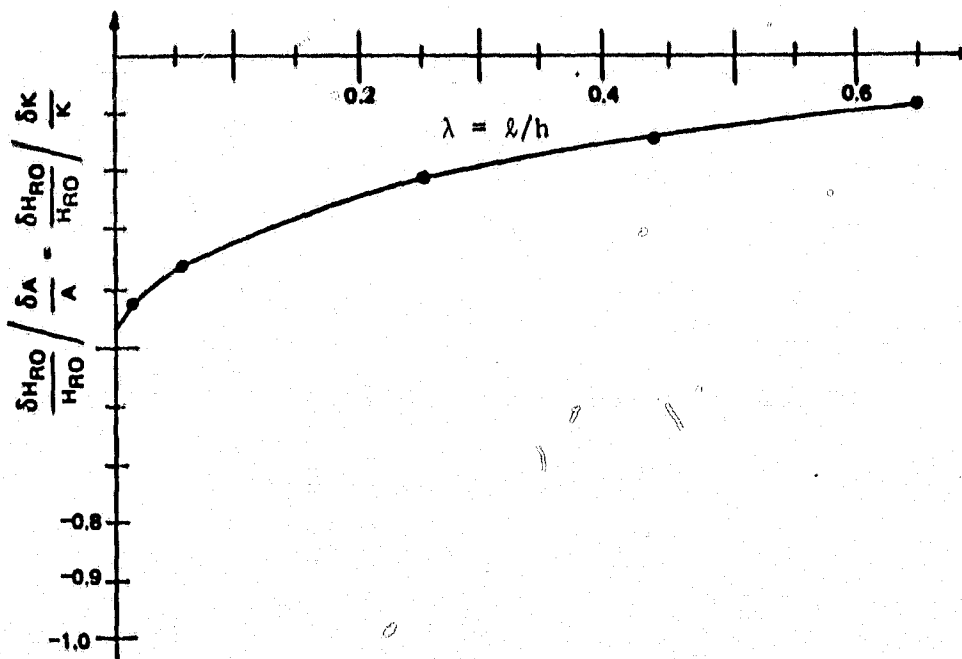


Figure 3.18 Ratio of the Percentage Change in Run-Out Field to the Percentage Change in Both the Anisotropy Constant and Exchange Constant vs. Characteristic Length.

thickness causes a 10% change in run-out threshold, a 10% change in characteristic length causes a -4% change in run-out field, and a 10% change in either anisotropy constant or exchange constant causes a -2% change in run-out threshold.

One of the intriguing possibilities emerging from this treatment is that a magnetostatically coupled stripe-bubble combination is possible in which the bubble and stripe films have the same composition but different thicknesses.

3.4.6 Stripe Domain Curvature

When a group of stripe domains are propagated between two rows of chevrons or other structures, they bow or curve backwards. Figure 3.19 displays the case of an isolated stripe. When an oscillating normal field commonly called a tickle field, is applied, the stripes straighten out. The bowing is caused by coercivity; the straightening out is caused by three factors: (1) The coercivity is effectively reduced because the oscillating normal field causes the width of each stripe domain to oscillate somewhat, helping that stripe to move past micro-defects, (2) The stripes repel each other magnetostatically, and (3) The oscillating field plus the bias field exceeds the strip-out threshold at least part of the time, causing the stripes to be in tension. If the ends of the stripes were not pinned to the chevrons, the stripes would contract to bubbles when the strip-out threshold is exceeded. However, when the ends are pinned, the stripes can only reduce their length, and therefore, lower their energy by straightening out. This third cause is the subject of this section. Note that a stripe near other stripes may see a local field higher than the strip-out field, although the external applied field is less than the strip-out threshold for an isolated strip, because of the stray field from nearby stripes. Therefore, this section will consider the case of an isolated stripe only.

Figure 3.19 shows an isolated stripe domain contracting under the influence of an applied field H that exceeds the strip-out or run-out threshold, H_{RO} . The stripe is in the form of an arc, with height Z and width Y . The question to be solved is the mathematical dependence of Z on H , H_{RO} , Y , and W , the width of the stripe.

Consider an isolated non-pinned stripe of length L . Let the applied normal field, H , be equal to the strip-out threshold, H_{RO} . At this field the stripe is free to contract or expand without loss of energy. However, when the bias field is raised so that it is higher than the strip-out field, the stripe contracts. When the stripe becomes shorter by a length ΔL , the energy per unit thickness changes by an amount ΔE_1 :

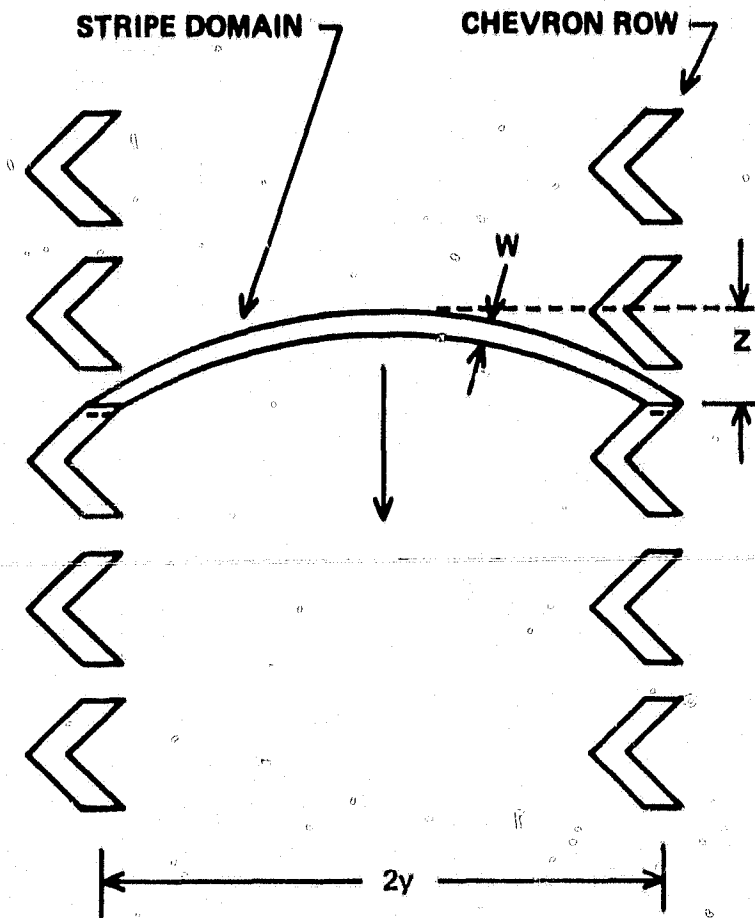


Figure 3.19 Isolated Pinned Stripe Domain Propagation by Chevron Rows.

$$\Delta E_1 = 2M (H - H_{RO}) W \cdot \Delta L \quad (3.41)$$

To determine the domain energy associated with a curved stripe, consider the case of a stripe that forms a circle, as shown in figure 3.20. When the applied normal field H exceeds the strip-out field, the radius of the circle becomes smaller. The change in energy is ΔE_2 , which in analogy to equation 3.41, is given by:

$$\Delta E_2 = 2M (H - H_{RO}) W \cdot (2\pi\delta R) \quad (3.42)$$

This change in radius is resisted by the coercivity. Each moving wall of a stripe domain has to overcome the coercive field, H_C . The corresponding change in energy is ΔE_3 :

$$\Delta E_3 = 2 M H_C (2\pi r) \delta R \cdot 2 \quad (3.43)$$

where the last factor of two is included because there are two walls that move. Set the two energies equal for the case of equilibrium:

$$\begin{aligned} \Delta E_2 &= \Delta E_3 \\ (H - H_{RO}) W (2\pi\delta R) &= H_C (2\pi r) \delta R \cdot 2 \\ \frac{H - H_{RO}}{H_C} &= \frac{2R}{W} \end{aligned} \quad (3.44)$$

The case of interest is that of figure 3.19, where the stripe forms an arc rather than a full circle. The radius of curvature, R , of the arc can be shown to be given by:

$$R = \frac{Y^2 + Z^2}{2Z} \quad (3.45)$$

When this is inserted into equation 3.44, the result is:

$$\frac{H - H_{RO}}{H_C} = \frac{Y^2 + Z^2}{ZW} \quad (3.46)$$

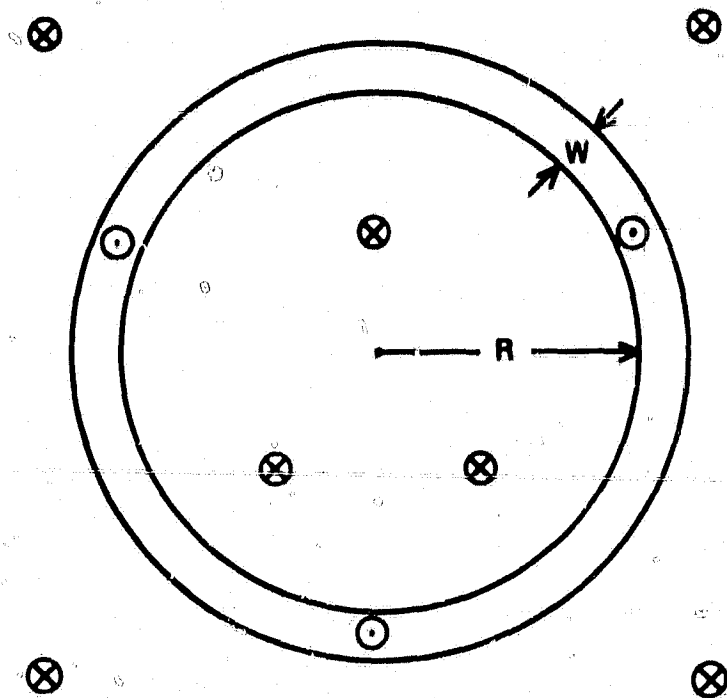


Figure 3.20 Circular Stripe Domain of Width W and Radius R , used as a Model to Calculate the Domain Energy Associated with Stripe Curvature.

Equation 3.44 or equation 3.46 relates the curvature of the stripe to the separation between chevron rows, the bias field, and the coercivity. These equations indicate that the higher the bias field, the smaller the curvature, or the larger the radius of curvature, R , or the smaller the ratio of Z to Y .

As an example, consider a garnet film with stripe width $W = 3\mu\text{m}$ and a coercivity of 0.1 Oe . Let the bias field exceed the strip-out field by 10 Oe . The radius of curvature according to equation 3.44 indicates that $R = 150\mu\text{m}$. Equation 3.46 indicates that when $Z = Y$, they both are equal to $150\mu\text{m}$.

As a second example, consider that the same garnet film with an applied normal rf tickle field that reduces the coercivity by a factor of 10. The radius of curvature is now $1500\mu\text{m}$ or 1.5 mm .

As a final example, suppose the chevron rows are placed 1 mm apart. In this case, $Y = 500\mu\text{m}$ and $Z = 86\mu\text{m}$.

Stripe domains with pinned ends can be made to reduce their curvature by application of a normal field higher than the strip-out field. The curvature becomes much less if a tickle field is used as well. Unless the coercivity is zero the curvature will not be zero; this means that the read out track in a multilayer memory will probably have to be similarly curved.

3.5 Stripe Domain and Magnetic Feature Coupling

In order for stripes in a high Q material to be straight in a multilayer self-structured memory, they must be biased above the run-out threshold. The ends of the stripes must be pinned in order to prevent the stripes from shrinking into bubbles. One method of keeping the ends of the stripe pinned is with a permalloy strip at each end of the stripe, as shown in figure 3.21. The permalloy must supply enough normal field so that the end of the stripe is below the run-out threshold, otherwise the stripe end will shrink. The purpose of the following calculation is to determine the pinning field from a permalloy strip with no applied horizontal bias field. This field is a function of the separation, Z , between the garnet and the permalloy, as shown in figure 3.22, as well as the thickness of the garnet film, h , and the stripe wavelength.

It is assumed that the permalloy has infinite permeability for horizontal in-plane fields. This implies that the permalloy has zero anisotropy and coercivity, and that when a stripe end extends under the permalloy strip, the magnetization configuration in the permalloy sets up a stray field that, inside the permalloy, exactly cancels the horizontal component of the field from the

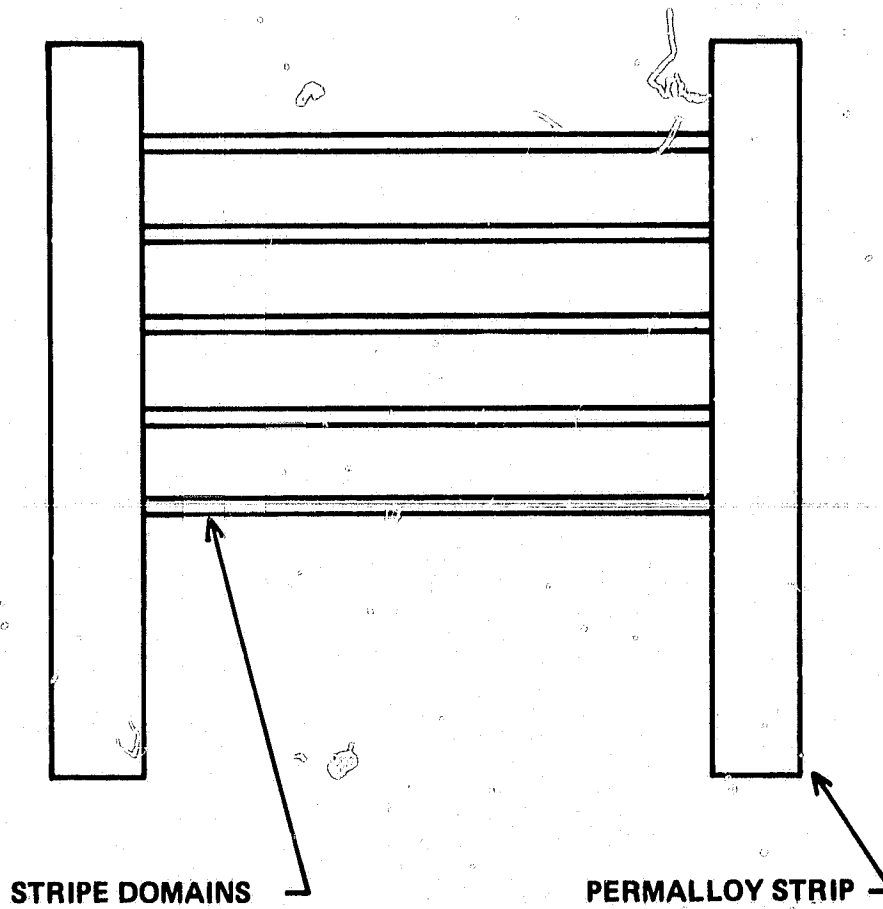


Figure 3.21 Stripe Domains with Ends Pinned by Permalloy Strips.

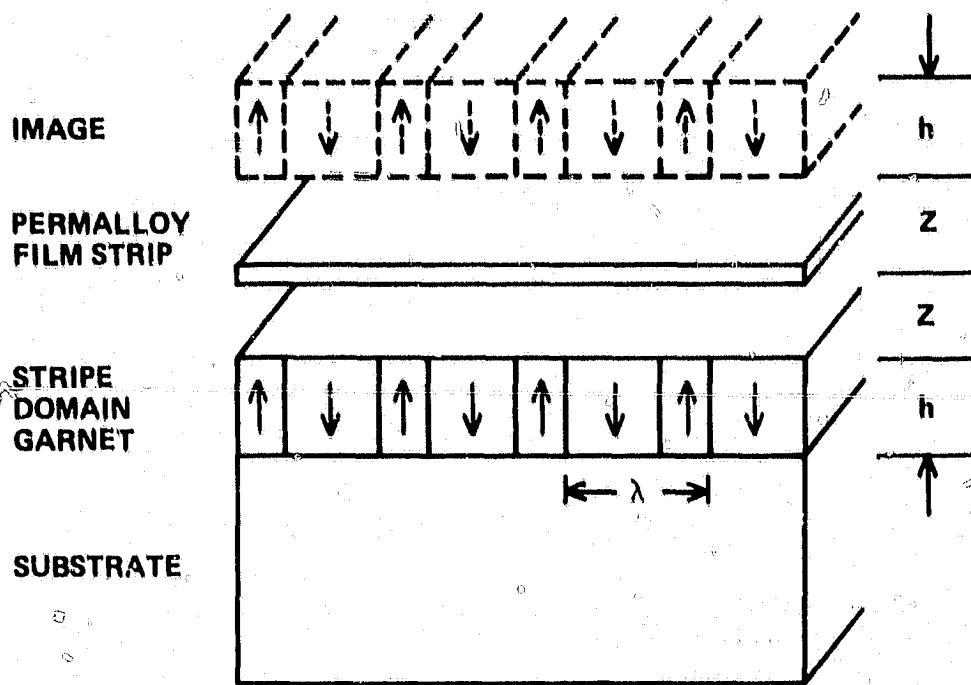


Figure 3.22 Stripe Domain Pattern and Image in a Permalloy Layer.

stripe. The normal field from the permalloy can then be calculated by the method of images. The image shown in figure 3.22 cancels out all stray fields in the plane of the permalloy film. The normal component of the stray field from the permalloy is then calculated by evaluating the normal field from the image.

The normal field from a stripe domain film having

$$M_z(x) = \sum_{n=0}^{\infty} a_n M \cos \frac{2nx}{\lambda} \quad (3.47)$$

was calculated in a Sperry Univac paper presented at the 1978 Conference on Magnetism and Magnetic Materials⁷.

The field H_z from this stripe is given in equation 5 of that paper as

$$H_z(x) = 2M \sum_{n=1}^{\infty} a_n \left\{ \exp \frac{-2\pi n Z}{\lambda} - \exp \frac{-2\pi n (Z+h)}{\lambda} \right\} \cos \frac{2\pi n x}{\lambda} \quad (3.48)$$

where, as shown in figure 3.22, λ is the wavelength of the stripes, and h is the thickness of the stripe film. The distance from the nearest surface of the stripe film is Z .

The normal field from the image is found from equation 3.48, and by noting that the separation between film and image is $2Z$. The quantity of interest is the average of the field from the image over the thickness of the stripe domain film, and provides the effective bias from the permalloy. The amplitude of this quantity, \bar{H}_z , is found by integrating equation 3.48 and suppressing the x dependence:

$$\bar{H}_z = \sum_{n=1}^{\infty} \frac{a_n \lambda M}{nh} \left\{ \exp \left(\frac{-4\pi n Z}{\lambda} \right) - 2 \exp \left(\frac{-4\pi n (Z+h/2)}{\lambda} \right) + \exp \left(\frac{-4\pi n (Z+h)}{\lambda} \right) \right\} \quad (3.49)$$

3.5.1 Symmetric Stripe Domains

Equation 3.49 is plotted in figure 3.23 for the case $a_1 = 1$ and $a_n = 0$ for $n > 1$. This is the case of symmetrical stripe domains in which the Z component of magnetization varies sinusoidally as a function of distance in the film plane: $M_z(X) = M \sin 2\pi x/\lambda$.

The physical meaning of \bar{H}_z is: when the normal bias field is raised above the run-out threshold, all unpinned stripes contract to bubbles. Stripes that are pinned at the ends by the two permalloy stripes do not pull loose and contract to bubbles until the bias field is raised by a value equal to H_z above the run-out threshold. At this point the total field under the stripe, the sum of the field from the permalloy and the bias field, equals the run-out threshold. This is how H_z is measured experimentally.

Figure 3.23 shows several interesting and important relationships:

- (1) The pinning field from a permalloy strip, with no in-plane bias, can be as large as $2.55M$, where M is the magnetization of the stripe containing garnet. For example, if $4\pi M$ is 200 Oe, then H_z can be as high as 41 Oe.
- (2) It is important that the space, A , between the permalloy and the top of the garnet be as small as possible. For example, if $\lambda = 10\mu\text{m}$, Z is $1\mu\text{m}$, and $h = 2\mu\text{m}$; then H_z is only 12 Oe instead of 41 Oe, as it would be if $Z = 0$.
- (3) The maximum value of \bar{H}_z occurs when $h/\lambda = 0.2$. If the film is thicker, \bar{H}_z is smaller because H_z is the average H_z over the whole film thickness. If the film is thinner, then H_z is smaller because H_z is smaller for the same reason as that the electric field outside a parallel plate capacitor is nearly zero.

3.5.2 Asymmetric Stripe Domains

When a normal field is applied to an array of stripes, they become asymmetric, i.e., the even numbered stripes have a different width than the odd numbered stripes. This case is treated mathematically by first finding the Fourier components of the asymmetric magnetization distribution to fit in equation 3.47. These are then inserted into equation 3.49 to yield H_z .

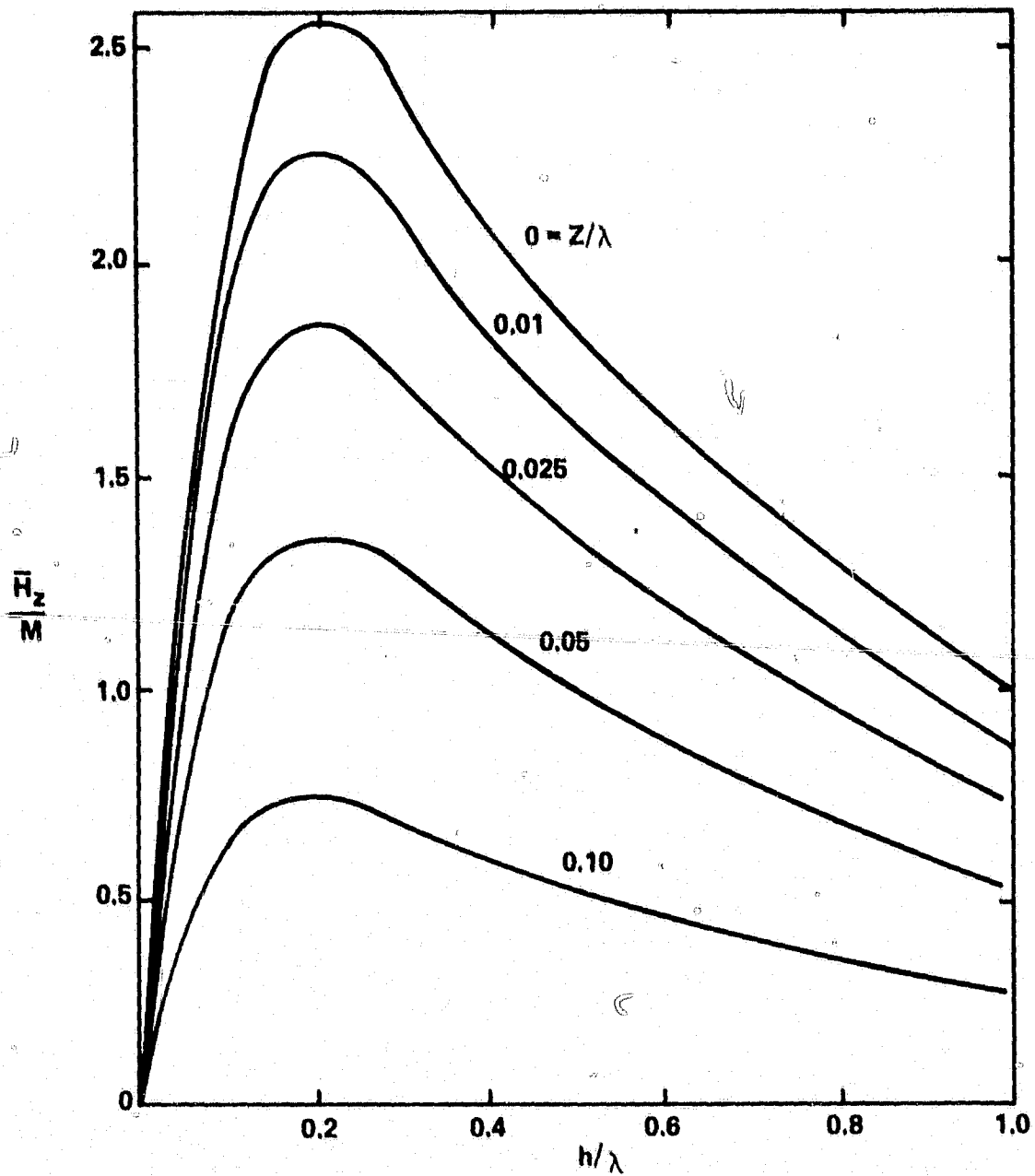


Figure 3.23 Field from a Permalloy Layer Covering an Array of Stripes, as a Function of Garnet Thickness h , Stripe Wavelength λ , and Permalloy to Garnet Spacing Z .

As an example, consider the case in which the stripes are biased so that the width of the odd numbered stripes is $\lambda/4$ and the width of the even numbered stripes is $3\lambda/4$. This is illustrated in figure 3.24. The Fourier components of the magnetization are:

$$a_n = \frac{2}{\pi n} \sin \frac{2\pi n x}{\lambda} \quad (n \geq 1) \quad (3.50)$$

The zeroth term does not contribute to \bar{H}_z . Equation 3.50 is inserted into equation 3.49 to yield \bar{H}_z . In the case that $Z = 0$ and $h/\lambda = 0.2$, yielding $\bar{H}_z = 1.88$ M. This is lower than the 2.55 M of the symmetric case. The following are numerical examples:

- (1) $\lambda = 16\mu\text{m}$, $4\pi M = 200$ Oe, $Z = 0$, $h = 3.2\mu\text{m}$, stripe width = $\lambda/4$. Then $\bar{H}_z = 30$ Oe. This is a case of zero separation between the garnet and permalloy.
- (2) $\lambda = 16\mu\text{m}$, $4\pi M = 200$ Oe, $Z = 0.16\mu\text{m}$, $h = 3.2\mu\text{m}$, stripe width = $\lambda/4$. Then $\bar{H}_z = 25.6$ Oe. This is a case of very small separation between the garnet and permalloy.
- (3) $\lambda = 16\mu\text{m}$, $4\pi M = 200$ Oe, $Z = 1.6\mu\text{m}$, $h = 3.2\mu\text{m}$, stripe width = $\lambda/4$. Then $\bar{H}_z = 6.15$ Oe. This is a case of large separation between the permalloy and garnet. Here the higher a_n terms in equation 3.50 do not contribute.
- (4) $\lambda = 16\mu\text{m}$, $4\pi M = 600$ Oe, $Z = 1.6\mu\text{m}$, $h = 3.2\mu\text{m}$, stripe width = $\lambda/4$. Then $\bar{H}_z = 18.4$ Oe. This is the same as case 3, except that $4\pi M$ has been increased by a factor of three.
- (5) $\lambda = 4\mu\text{m}$, $4\pi M = 200$ Oe, $Z = 0$, $h = 3.2\mu\text{m}$, stripe width = $1\mu\text{m}$, then $\bar{H}_z = 15$ Oe. This is a case of very high density stripes.

3.6 Field Calculations for Current Accessed Propagation Structures

3.6.1 Average Field Gradient From a Stripline

The force that a current accessed propagation circuit (stripline) exerts on a magnetic bubble or a stripe domain is proportional to the in-plane component of the gradient of the normal field from the stripline. The geometry is displayed in figure 3.25. The force in the x direction is proportional to:

$$F \equiv \frac{\partial \bar{H}_z}{\partial x} \quad (3.51)$$

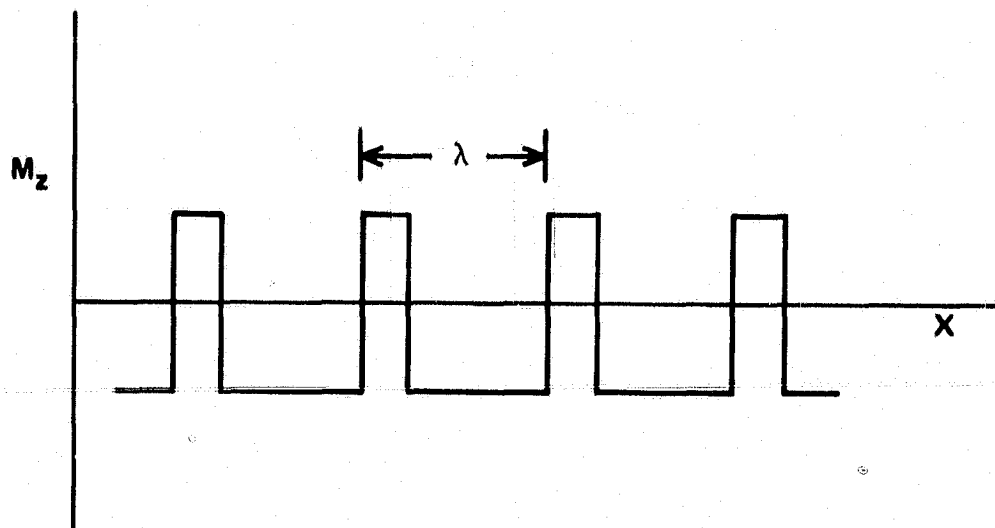


Figure 3.24 Asymmetric Magnetization Distribution in Strips with Stripe Width $\lambda/4$.

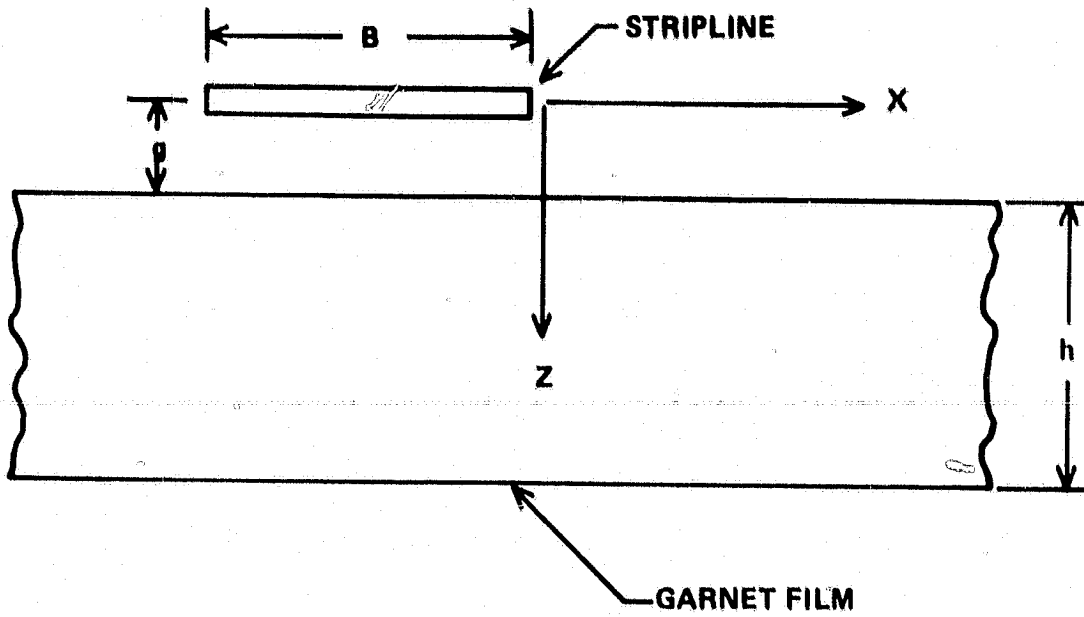


Figure 3.25 Coordinate System for a Field Gradient from a Stripline Conductor.

where \bar{H}_z is the normal component of field averaged over the film thickness. These quantities are calculated below.

Consider an infinitely small diameter wire carrying a current di . By Ampere's law, the field from that wire, dH , at a distance S is:

$$dH = 2 \frac{di}{S} \quad (3.52)$$

in electromagnetic units, and the normal component is:

$$dH_z = \frac{2x di}{S^2} = \frac{2x di}{x^2 + z^2} \quad (3.53)$$

If this infinitesimal wire is placed a distance g above a garnet film of thickness h , then the average field over the film thickness is:

$$\bar{dH}_z = \frac{1}{h} \int_g^{h+g} \left(\frac{2x di}{x^2 + z^2} \right) dz \quad (3.54)$$

$$\bar{dH}_z = \frac{2di}{h} \left\{ \tan^{-1} \left(\frac{h+g}{x} \right) - \tan^{-1} \left(\frac{g}{x} \right) \right\}.$$

For a stripline of width B as shown in figure 3.25, the field should be averaged over the width of the stripline as well:

$$\bar{H}_z = \frac{2i}{hB} \int_x^{x+B} \left\{ \tan^{-1} \left(\frac{h+g}{x} \right) - \tan^{-1} \left(\frac{g}{x} \right) \right\} dx \quad (3.55)$$

However, the gradient of that field is the item of interest:

$$\bar{F} = \frac{\partial \bar{H}_z}{\partial X}$$

$$\bar{F} = \frac{2i}{hB} \int_x^{x+B} \frac{\partial}{\partial x} \left\{ \tan^{-1} \left(\frac{h+g}{x} \right) - \tan^{-1} \left(\frac{g}{x} \right) \right\} dx \quad (3.56)$$

$$\bar{F} = \frac{2i}{hB} \left\{ \tan^{-1} \left(\frac{h+g}{B+X} \right) - \tan^{-1} \left(\frac{g}{B+X} \right) - \tan^{-1} \left(\frac{h+g}{x} \right) + \tan^{-1} \left(\frac{g}{x} \right) \right\}.$$

This is proportional to the force exerted by the stripline on a stripe domain or a bubble. The units in equation 3.56 are ab-amperes, centimeters and oersteds, where ten amperes equals one abampere.

3.6.2 Nested Serpentine Conductors

The single layer serpentine stripe propagation scheme discussed in section 4.3.2 has conventional serpentine circuits side by side and depends on the stripe stiffness in order that one circuit be able to move a stripe past a "dead-spot" in an adjacent circuit. An alternative method is to have the serpentine conductors nested, as shown in figure 3.26. This scheme does not depend on stripe stiffness and has the further advantage that it will propagate bubbles as well.

Figure 3.27 is the force, or gradient, in the normal field, $\frac{\delta H_z}{\delta X}$, exerted by one of the two serpentine conductors of figure 3.26. Note that there are four "dead spots" per period. Dead spots are regions in which the force (or field gradient) falls to zero, or below, the wall motion threshold for the allowable current. A circuit cannot propagate a domain past one of its own dead spots, and a second circuit is required for that. Likewise, it is absolutely essential that the two circuits not have dead spots that coincide. The dashed line in figure 3.27 shows the level corresponding to the maximum coercivity that we have experimentally observed in a garnet when 50 mA of current is used. The dead spot in the center ($X = 0$) is then slightly less than 4 microns wide, while the dead spots at $X = \pm 5.1 \mu\text{m}$ are a half micron wide. The dead spots at $X = \pm 11 \mu\text{m}$ have scarcely any width at all. Figure 3.28 shows where these dead spots are located in relation to the pair of nested serpentine circuits of figure 3.26. The dead spots of the upper circuit are on the top of the picture, while those of the bottom are shown below. As can be seen, the x-position of the dead spots do not coincide. Thus a stripe or bubble can be propagated by applying pulses of alternating polarity between the two serpentine conductors. Each pulse moves the stripe or bubble to the next dead spot.

This circuit can be used to propagate stripes by pulling on their ends, or it can be used to insert or remove a column of bubbles. The fact that only a single layer with only a single masking is required is of considerable economic interest.

3.6.3 Non-Nested Serpentine Conductors

Figure 3.29 illustrates the type of serpentine stripe propagators evaluated and reported in section 4.3.2. These have a low aspect ratio and thus a low tolerance for stripe bending and bowing.

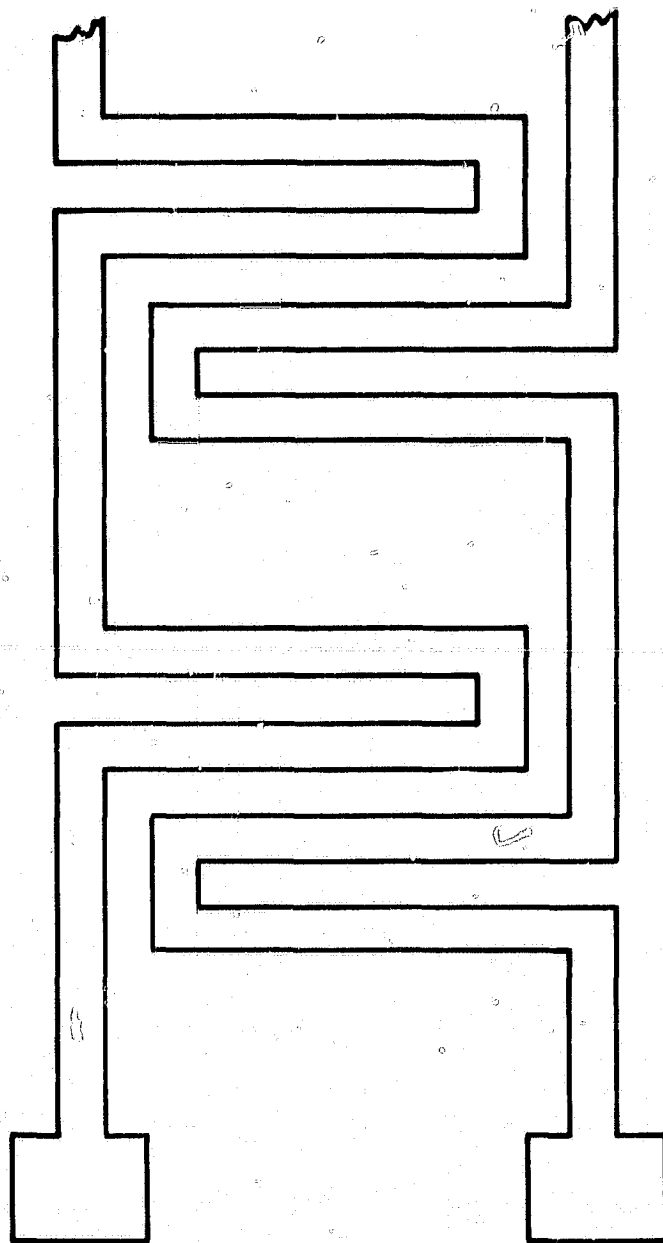


Figure 3.26 Nested Serpentine Conductors for Stripe or Bubble Domain Propagation.

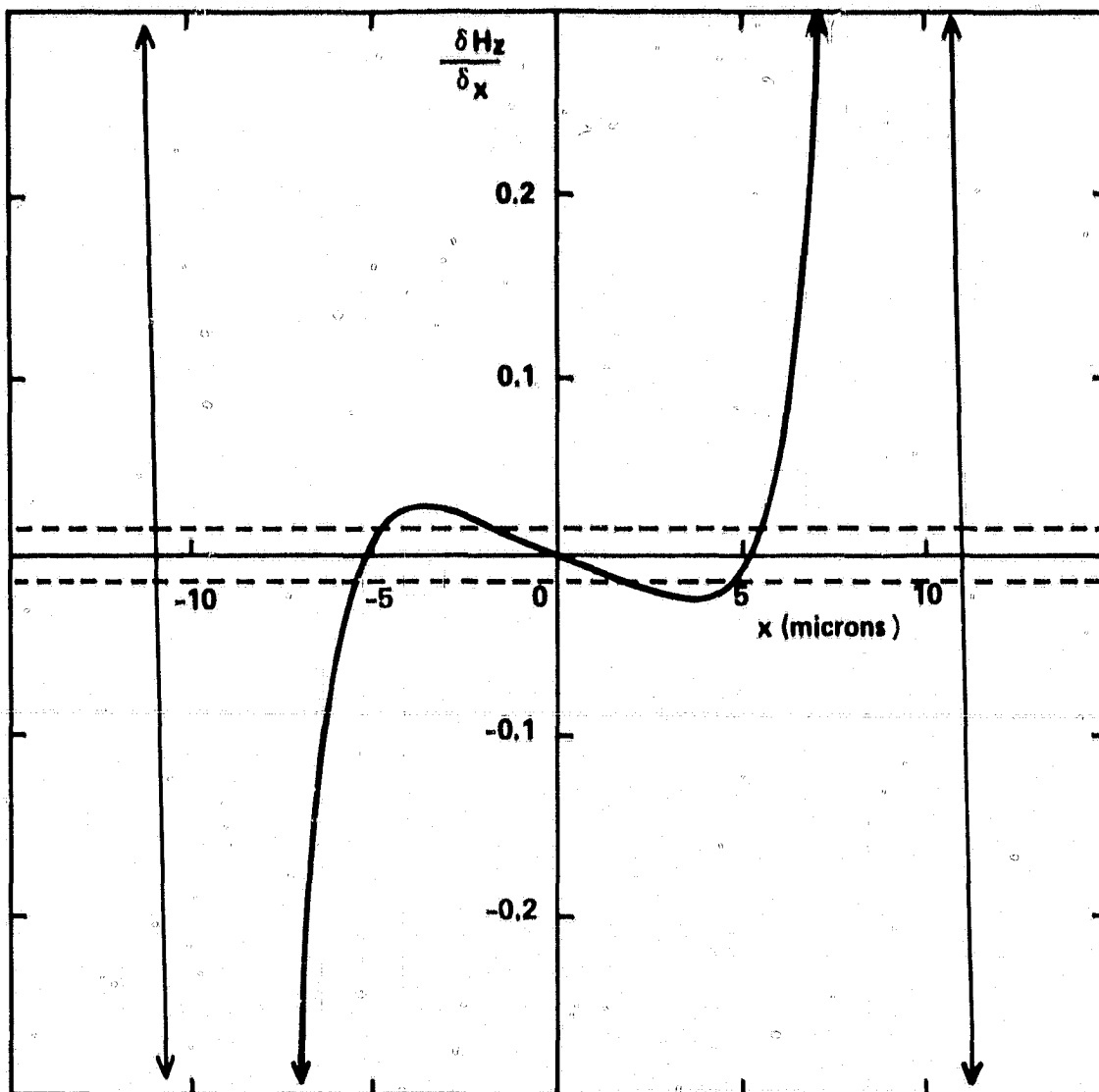


Figure 3. 27 Field Gradient from One Conductor of Fig. 3.26, with $h = 5\mu\text{m}$, $g = 1\mu\text{m}$, and $B = 3\mu\text{m}$.

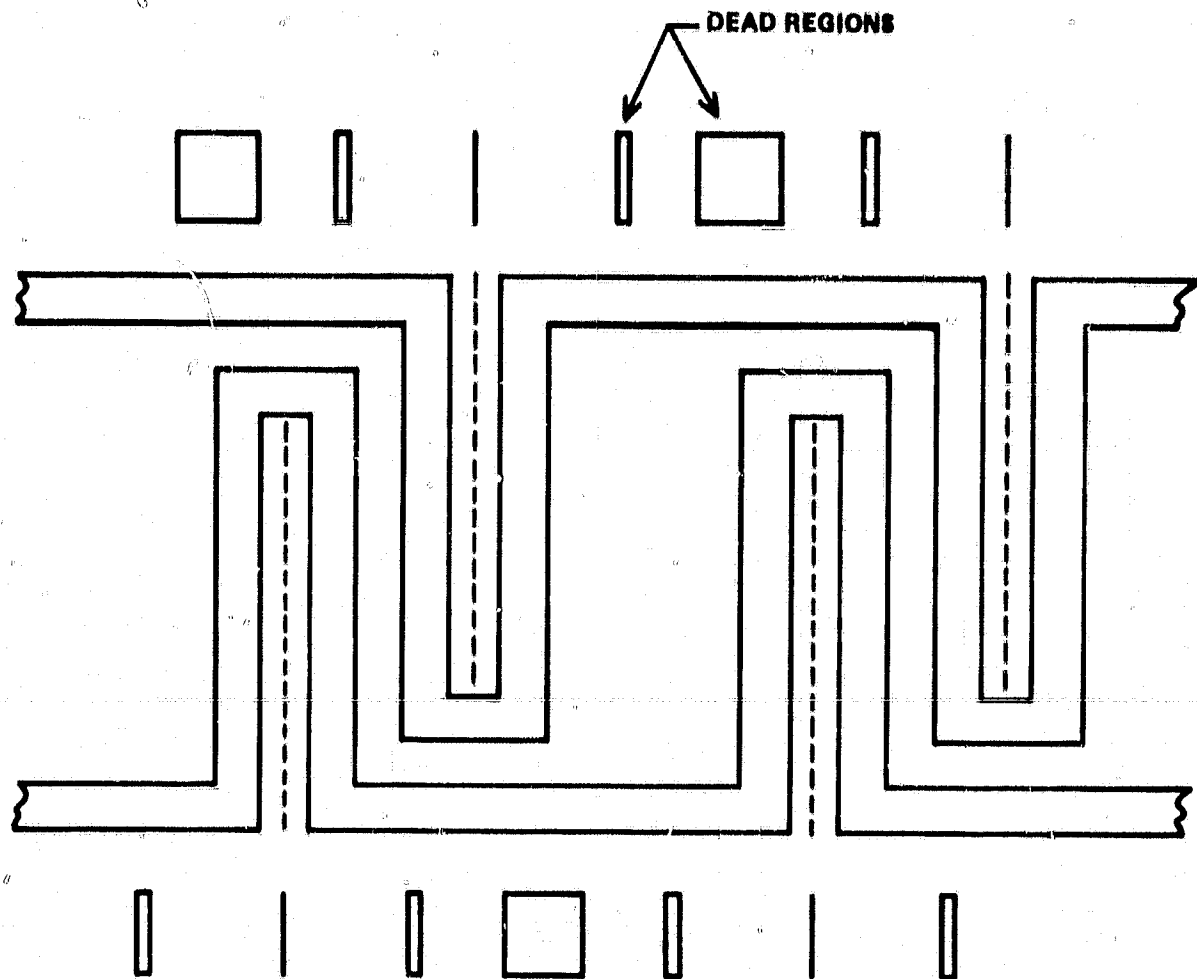


Figure 3.28 Nested Serpentine Conductors Showing Dead Regions for Upper and Lower Conductors.

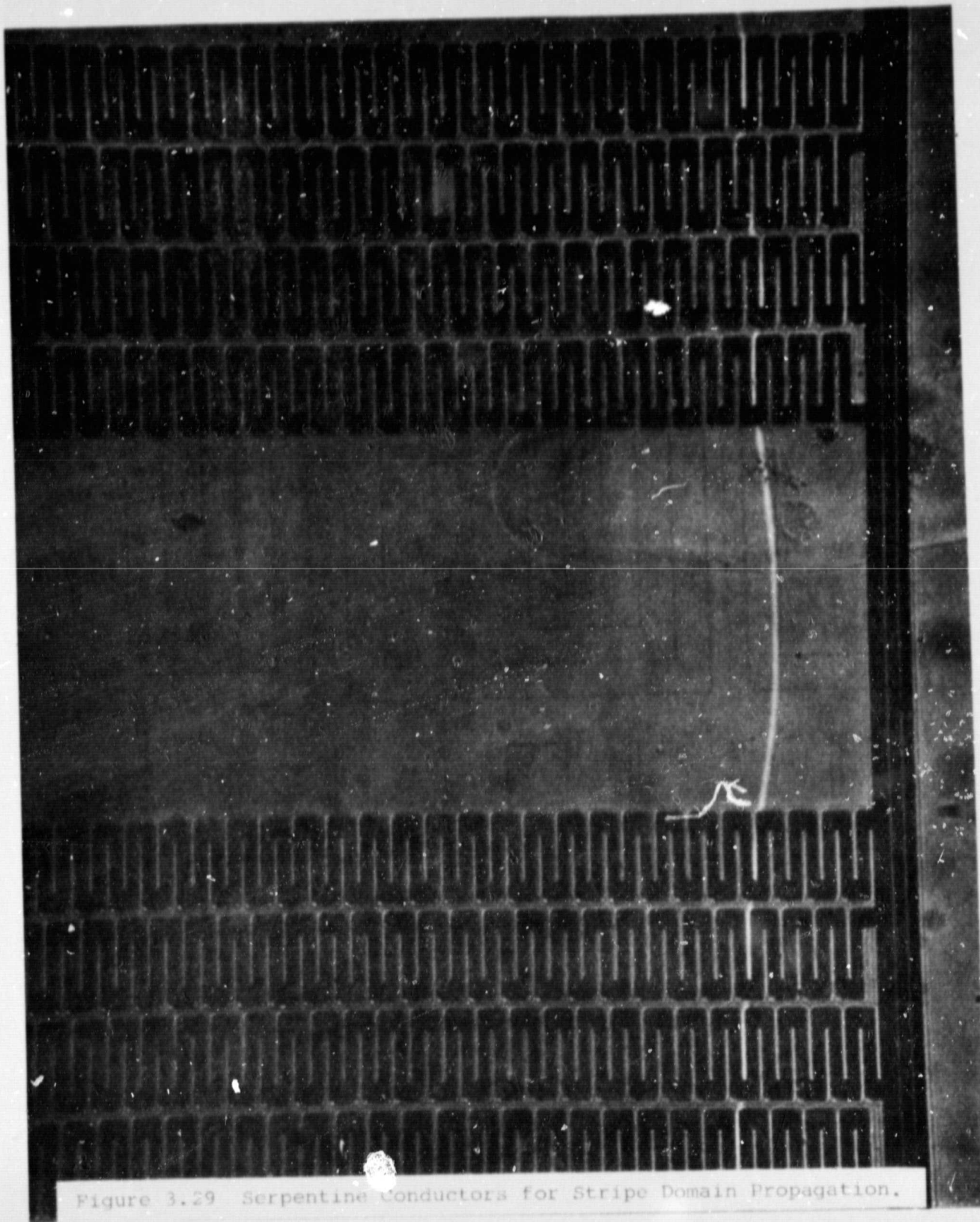


Figure 3.29 Serpentine conductors for Stripe Domain Propagation.

Figure 3.30a shows a pair of non-nested serpentine circuits with a large aspect ratio. These should be able to tolerate large amounts of stripe bowing, bending and tilting. The width of the conductor is made as wide as possible in order that each circuit have only two dead spots per cycle instead of four. As the aspect ratio increases, the deviation of the current direction from the desired direction increases. This can be corrected by incorporating slots in the serpentine conductors, as shown in figures 3.30b and c.

There are two adjustments to be made with the slots. One is to have equal current down each channel. The other is to ensure that the gradient of the normal field does not change sign under the slot, thereby creating a dead spot under each slot.

The problem of having equal current down each channel is one that is solved with an equivalent network of resistors, as shown in figure 3.31, for the case of a three slot configuration. The placement of the slots determines the resistance for each current path, and the placement that ensures equal current in each channel is shown in figures 3.30b and c.

The other problem is to eliminate the dead spots below the slots. This is done by using a spacing layer between the garnet and the conductors. Figure 3.32 shows the force on the stripe (the gradient of the average normal field) under the slot as a function of the separation between conductor and garnet for a $18\mu\text{m}$ wide line with a single $2\mu\text{m}$ slot in the center. The separating layer must be at least $1.5\mu\text{m}$ thick in order to eliminate the dead spot, and $3\mu\text{m}$ is optimum.

The use of slots thus permits the use of very high aspect non-nested serpentine stripe propagation conductors that are highly tolerant of stripe bending, bowing, and tilting.

3.7 Summary and Conclusions of Theoretical Studies

The preceding diverse theoretical studies in this section give information necessary for the design of test circuits and information about the behavior of various multilayer devices.

The interaction between bubbles in one layer and stripes or bubbles in another layer was calculated for various geometries. Coupling is found to be sufficient between stripes in one layer and bubbles in another so that moving stripes will cause the bubbles to move along with them. This is true for both magneto-static and exchange coupling, and even when the stripes are much narrower than the bubbles.

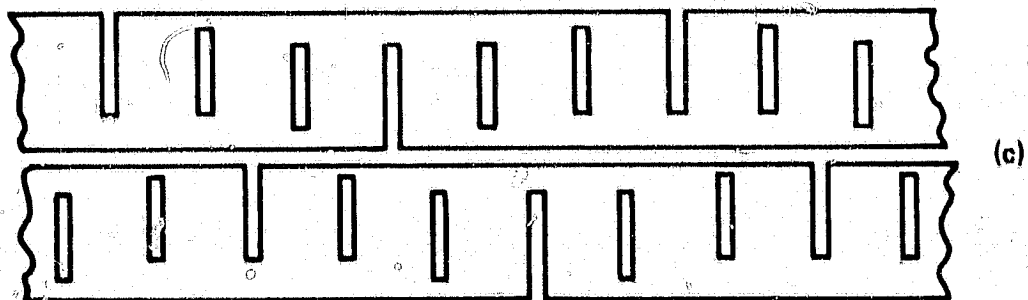
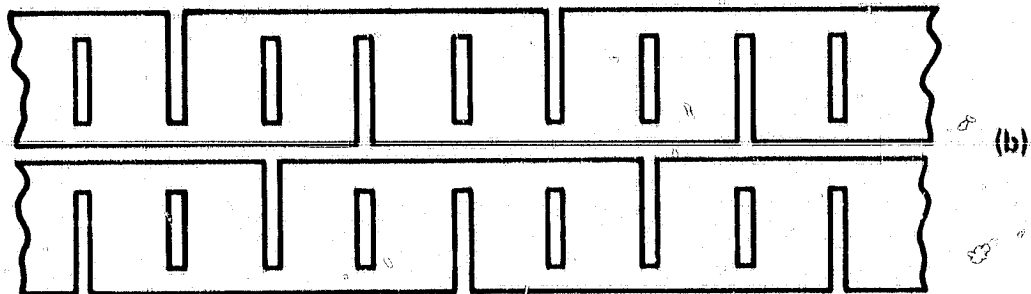
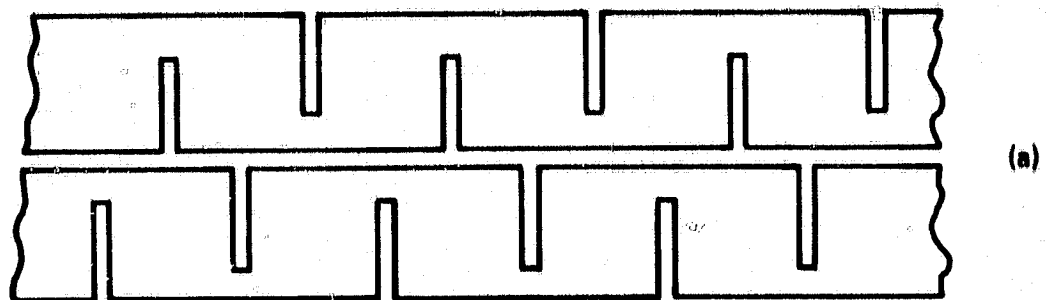


Figure 3.30 Non-nested, High Aspect Ratio, Serpentine Stripe Propagators.

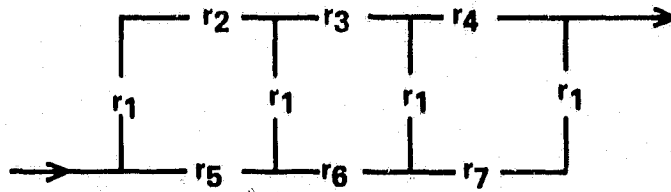
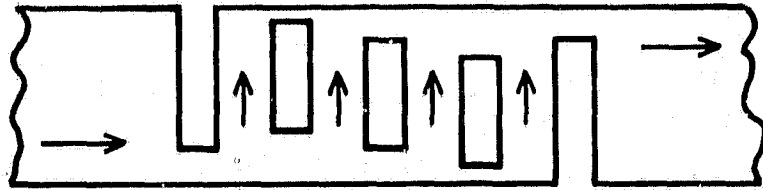


Figure 3.31 Three Slot Conductor Configuration and Equivalent Resistor Network.

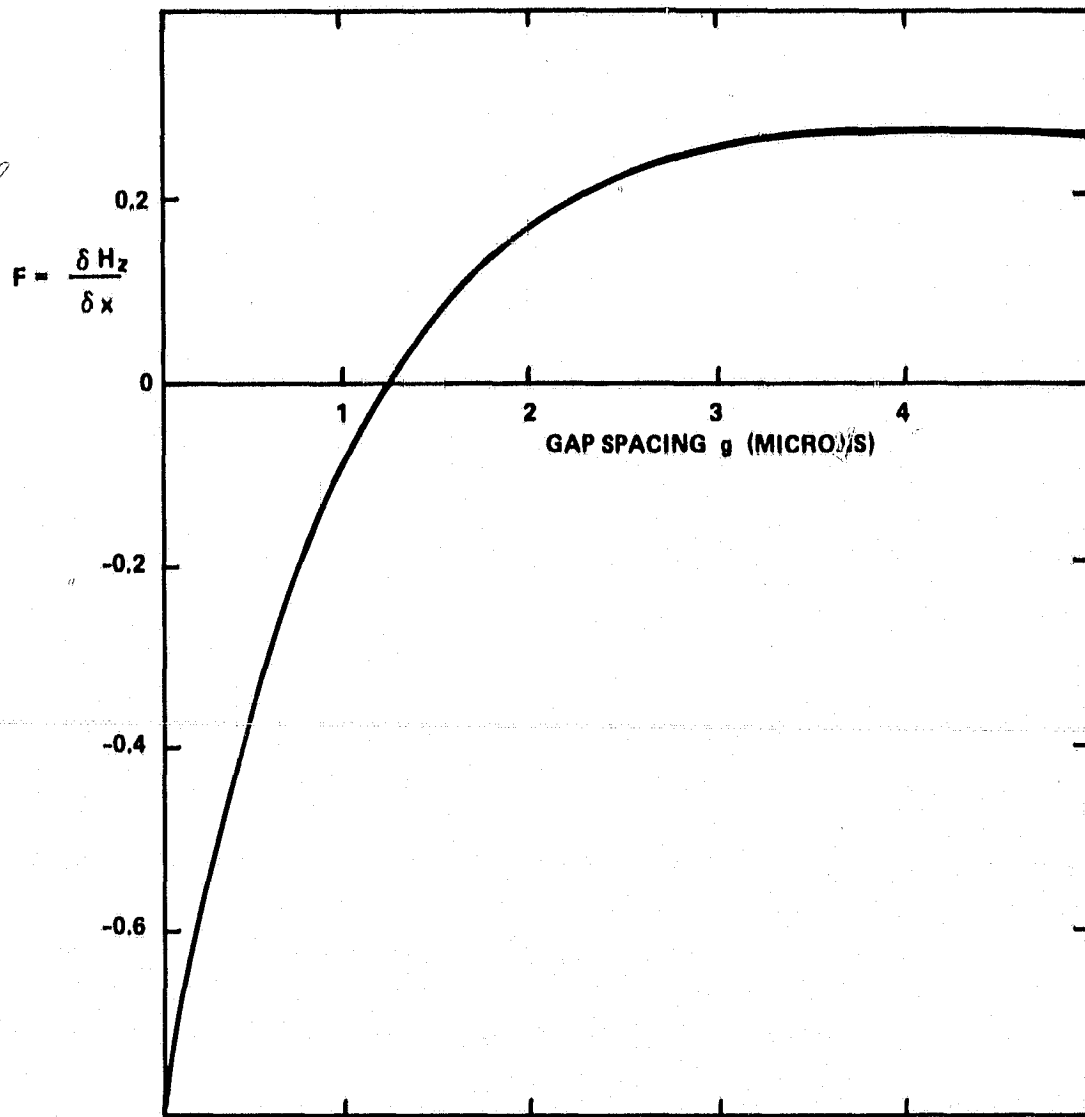


Figure 3.32 Force on a Stripe Domain Below a 2 μ m Wide Slot in a 18 μ m Wide Line Above a 5 μ m Thick Garnet.

Explicit expressions were derived for the change in run-out threshold due to changes in any of the following parameters: thickness, magnetization, characteristic length, anisotropy field, and exchange constant. It was shown that these parameters can be adjusted so that there are large carrier bubbles in one layer magnetostatically coupled to small data bubbles in another, such that both layers have the same run-out threshold.

A particularly important result is the discovery that stripes can be placed in tension when their ends are pinned and when the stripes are biased above the run-out threshold. The stripes can then be propagated by propagating the stripe ends. The stripe curvature was calculated and the maximum track width was found to be more than a millimeter. The pinning force between magnetic features and stripe ends was also calculated, as was the propagating force on stripes due to various current accessed propagation structures.

The theoretical work indicates that a self-structured multi-layer device with a carrier layer containing stripes or stripes and carrier bubbles magnetostatically coupled to data bubbles in a second layer is a very attractive configuration.

4. Experimental Investigations

4.1 Objectives

Conventional bubble memories require the presence of at least one propagation feature for each bubble domain. As a result, the entire memory area is populated with propagation features, which have a strong influence on device yield. It is an object of the following experimental investigations to reduce the number of propagation features, and to ultimately remove all such features from the memory area. This will allow for higher bubble densities, and higher device yields due to the reduced number of propagation features. A multiplicity of bubbles must, therefore, be moved with each propagation feature, and the experimental investigations reported herein are directed toward this goal. The designs must be compatible with current access techniques, whose advantages over field access methods have been discussed in section 2.3.

4.2 Experimental Equipment and Methods

Equipment employed for the experimental observation of garnet materials and propagation circuits includes a Reichert microscope and a 200 watt mercury arc light source. The light beam is polarized and applied at normal incidence to the sample, where the Faraday and/or the Kerr effect provide for visual observation. A television camera and monitor are utilized for ease of observation. The microscope stage is fitted with several coils to generate magnetic fields; normal dc fields up to 120 Oe, in-plane dc and rotating fields up to 150 Oe, and normal rf fields up to 10 Oe. One Oersted equals $1000/4\pi$ ampere turns per meter. Pulse generators with one amp output and 10 nanosecond risetime are available for testing current accessed circuits. A video tape recorder and a microscope camera are used for visual records of circuit performance and garnet material behavior.

Processing steps in the preparation of experimental circuits on garnet substrates include the thermal evaporation in vacuum of silicon monoxide as an insulating layer, aluminum-copper alloy or gold as a conducting layer, nickel-iron alloy as a magnetic feature layer, and sputtered silicon dioxide also as an insulating layer. Standard photoresist techniques are employed with chrome-on-glass artwork for circuit definition, and selective removal of material is accomplished with argon ion milling. Garnet dicing, mounting, and wire bonding follow standard integrated circuit procedures.

4.3 Experimental Circuits

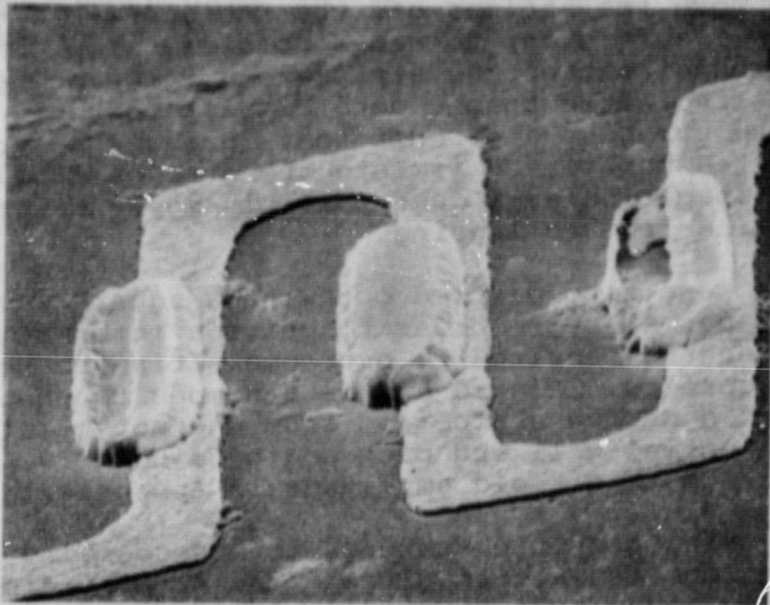
4.3.1 Early Current Accessed Circuits

The first current access circuit to be evaluated for propagation of stripe domains is shown in figure 4.1. This is a scanning electron micrograph of a serpentine pattern of the type successful in propagating bubbles. Because this has the appearance of a square wave on an oscilloscope, this serpentine structure is also called a square wave conductor. The permalloy bars are located to move the stripes off the regions where the field gradient is insufficient to cause domain motion, and also to determine which direction the stripes are to be propagated. The experiments indicated that a more complete circuit is required to propagate stripes, a circuit that includes a stripe generator, annihilator, a barrier to isolate the stripes from domains outside the propagation area, and possibly means to prevent the stripe domains from collapsing.

Experiments were also carried out with a square wave circuit without the permalloy in order to provide information about the current strengths required to overcome stripe coercivity in typical stripe garnets. Figure 4.2 is a composite photograph of the switching of a narrow stripe end from one potential well to an adjacent potential well and back again using a 10 μ sec bipolar current pulse with a field amplitude of approximately 100 Oe.

Instead of using magnetic features to move domains from low field gradient regions, an alternative method of providing the offset is to push by generating an excess of stripes on one end. The stripes repel each other with magnetostatic force, so when a new stripe is generated, it pushes on its nearest neighbors, which in turn push on their neighbors. The stripes are pushed by a generator and pulled at the stripe ends by square wave serpentine circuits. An invention disclosure has been filed on this concept.

Figure 4.3 shows an experimental version of the circuit known as an asymmetric sine wave. This circuit was fabricated from gold and permalloy on glass substrates, and tested on both high and low Q garnets. Some preference of stripe ends was found for the widest part of the pattern, provided the garnet is biased for very narrow stripes. A stripe end will slide along the circuit toward the wide part but moves only about one micron per current pulse. Hence, many pulses are required to move the stripe end along a quarter period of the circuit. It was not found possible to observe stripe motion past the wide part with currents that the circuit could safely support.



3.6 KX 65°

Figure 4.1. Scanning Electron Micrograph of a Serpentine Circuit with Permalloy Bars.

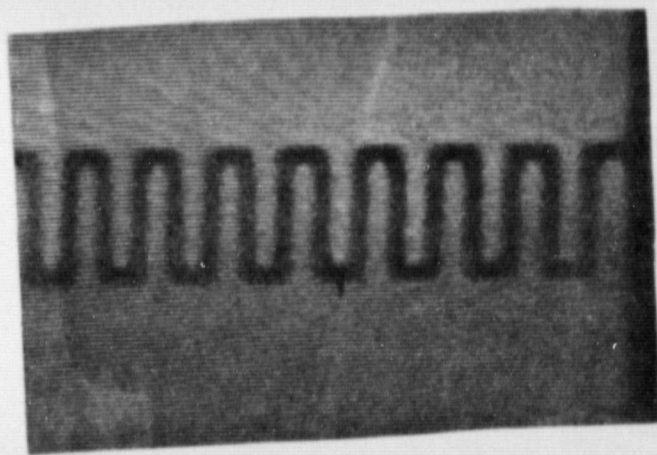
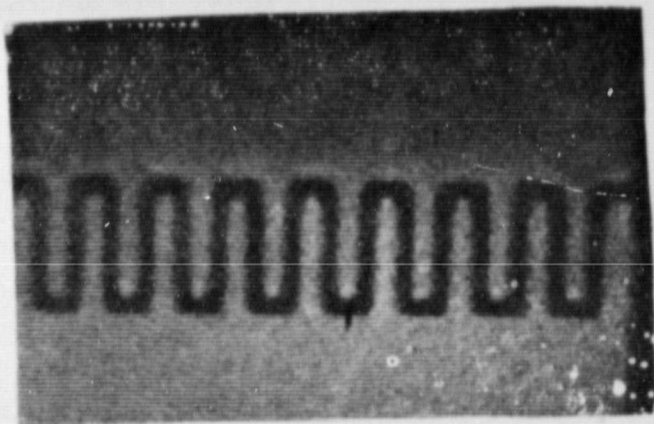


Figure 4.2. Micrographs of Stripe End Switching from One Potential Well to Another and Back Again.

ORIGINAL PAGE IS
OF POOR QUALITY

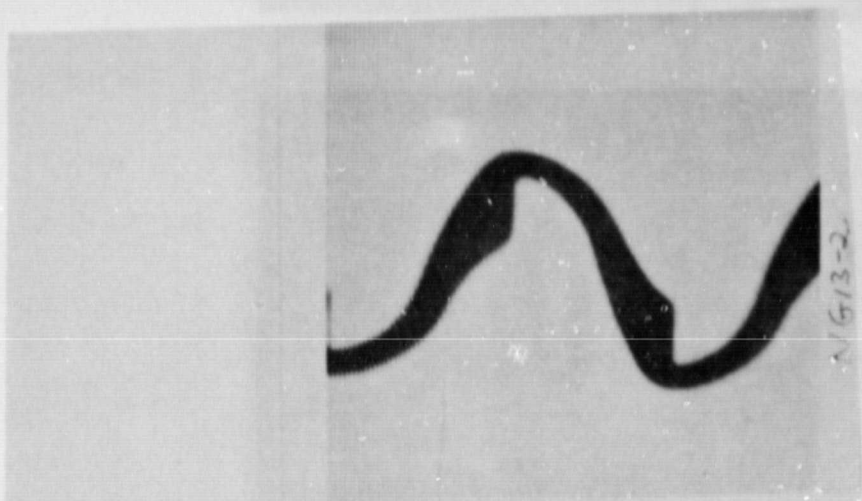


Figure 4.3 Asymmetric Sine Wave Circuit.

Stripes can be moved by long straight striplines parallel to the stripes. An array of such striplines can be used to propagate stripes, and such an array has been built and demonstrated. However, the first experiments were not conducted with such an array at all, but with a serpentine conductor. This conductor was rotated 90° from the usual orientation so that it ran parallel to the stripes, and the distance a pulse of given amplitude moved a stripe was measured. In this experiment, a high bias stripe was initially set so that it was $12.5\mu\text{m}$ from the conductor on one side and $62.5\mu\text{m}$ from an adjacent stripe on the other side. A current pulse was applied to the line and the distance the stripe moved recorded. Another current pulse was applied, and so on, until no further change in position could be observed. After reinitialization, the process was repeated at a different current amplitude. Figure 4.4 is a graph of the maximum distance a stripe moves with multiple pulses as a function of pulse amplitude. Also on the graph are the number of one μsec pulses at each current value required to maximize the distance. As the stripe moves, it eventually encounters the repulsion of the flanking stripe and a competition results. In all cases it was observed that the moving stripe would cause the adjacent stripe to move in the same direction. The photographs in figure 4.5 show this behavior for a current amplitude of 140 mA. This shows that pushing on one stripe in a lattice will push other stripes in the lattice.

A two layer conductor array was evaluated for stripe propagation. This is an array of long straight conductors in which the odd numbered conductors are pulsed first, then the even numbered conductors are pulsed, the odd numbered conductor again, and so on. The connections are made externally on this circuit, thus it can be used to study both two phase and three phase propagation.

The circuit was tested with biased stripes. It was found that the stripes could be propagated reliably and repeatedly both forwards and backwards with pulse currents of only 10 mA.

4.3.2 Offset Serpentine Array

A two phase single layer structure involving just a single evaporation is shown in figure 4.6. At one end of the structure is a set of conductors used for generating stripes and for pushing the stripes into the propagation region. Once in the region, the generated stripe is propagated by the offset serpentine structures, pulling on the ends of the stripe. There are four serpentine structures on each side, two of one phase and two oriented one quarter wavelength from that phase. The sets are pulsed alternately. Conductor numbers 1, 3, 5, and 7 are

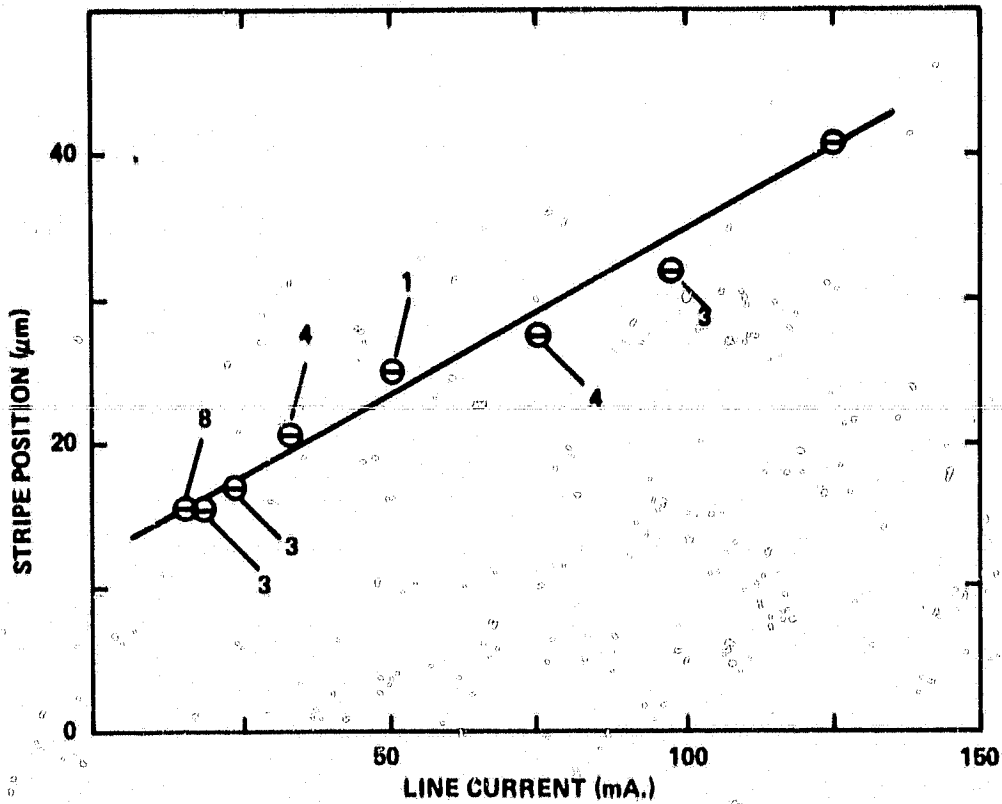


Figure 4.4 Stripe Domain Position Change due to a Conductor Field and an Adjacent Stripe; $H = 50$ Oe, and $4\pi M = 144$ Oe.

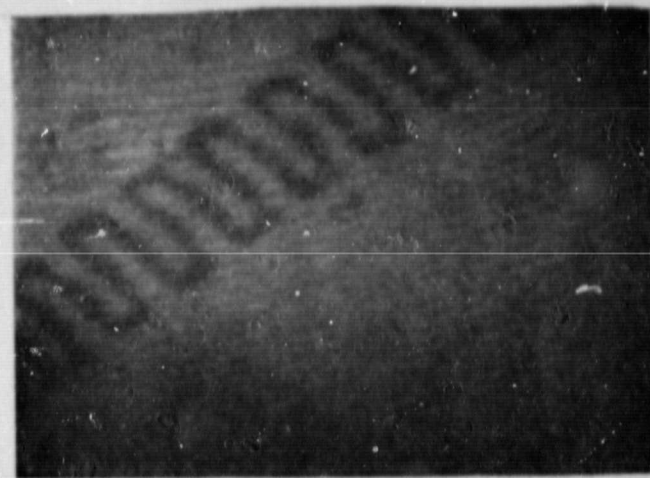


Figure 4.5 Micrographs of Stripe Being Pushed Away From Serpentine Circuit, Corresponding to the Graph of Figure 4.4.

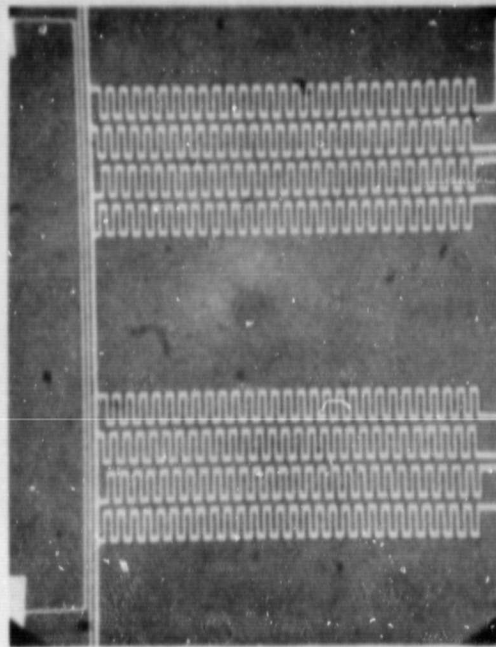


Figure 4.6 Micrograph of a Two Phase Single Layer Array Involving a Single Evaporation.

pulsed first; the polarity of the pulses on conductors 3 and 7 is opposite to the polarity of the pulses on conductors 1 and 5, because conductors 3 and 7 have been inverted to avoid current build-up on the bus line at the end. Next, the even numbered conductors are pulsed, and so on. Each pulse should move the stripe one quarter wavelength. To eliminate bowing of the wall, an rf tickle field is superposed on the external normal bias field.

This circuit was fabricated and exercised. The stripe generator at one end generated stripes, and the straight conductors expelled the stripes into the propagation region. The offset serpentine structure on the sides propagated those stripes even though an rf tickle field was not used. The circuit in its present form, however, has one important component missing, which created an unanticipated problem. A means for pinning the ends of the stripes was not included, and as the stripes were pushed into a neighborhood containing other domains, the stripes became shorter, contracting into dumbbells and bubbles. This circuit needs permalloy strips along the sides of the circuit to couple to the ends of the stripes and prevent them from contracting in length. A current conductor along the sides is an alternate method of accomplishing the same goal. A prime economical and practical advantage of this circuit is that only one conductor layer is required.

Figure 4.7 shows the test circuit with permalloy strips for the single level two phase serpentine stripe propagator. A single stripe is visible in figure 4.7. The stripe is pushed forward, or backward, one step at a time from alternate serpentine conductors. The ends of the stripe are pinned by permalloy strips at the side. The circuit must be operated at a normal bias field that is greater than the run-out threshold, which is necessary in order that the stripe be under tension and be relatively straight. The higher the bias field, the higher the tension, and the straighter the stripe.

The permalloy strips did an effective job of stripe pinning. The bias field could be raised not only above the run-out threshold, but approximately 10% above the bubble collapse threshold as well, without collapsing the stripe. The margin can be expected to increase as the number of stripes under the permalloy is increased to normal operating levels, and with further improvements in pinning bar design.

Stripe domains are easily and effectively nucleated by a set of three conductors shown at the bottom of figure 4.7. A single 50 nsec 900 mA pulse applied to the bottom conductor nucleates a complete stripe pinned at the permalloy bars, over the normal

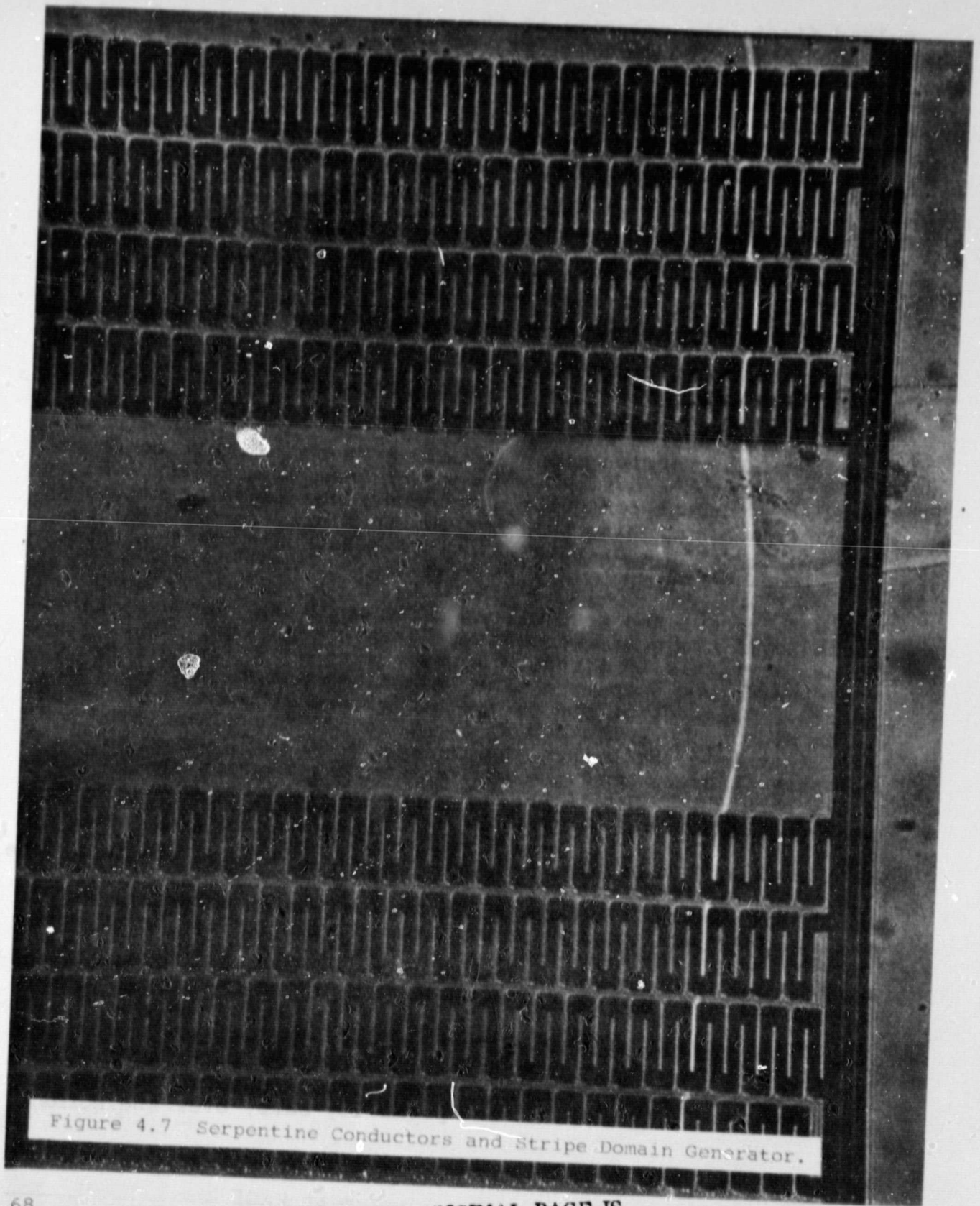


Figure 4.7 Serpentine Conductors and Stripe Domain Generator.

bias field range of 56-66 Oe. This can also be done with two complimentary pulses of lower amplitude on the two bottom conductors. Subsequent pulses on the upper two conductors translate stripes into the propagate test area.

Once into the propagate test area, the stripe is moved piecewise by the serpentine conductors. A current threshold of 5 to 10 mA is required in a serpentine circuit to reliably move a short segment of the stripe to a new equilibrium position. The amount of current required depends on the excess normal bias field above the run-out threshold. This is shown in the curve of figure 4.8. The reason for this behavior is that the higher the bias, the higher the tension in the stripe, and the greater the tendency for the adjacent segments to pull back the moved segment from the new position.

Figure 4.9 presents a four step sequence detailing the movement of a stripe end translating one half cycle under the left hand set of conductors. From the starting position shown in figure 4.9a, the required pulse sequence is $4^+ 2^- 3^+ 1^-$, which is shown in figure 4.9b through e, respectively. The second half cycle would follow with $4^- 2^+ 3^- 1^+$. Under normal operating conditions, conductors 4 and 2, as well as 3 and 1, are operated alternately in pairs, reducing the eight steps per cycle down to four. In addition, conductors 1 and 2 should be phase shifted one half cycle, allowing the pairs 4-2 and 3-1 to be activated with the same polarity pulses. A single pulse would therefore be sufficient to activate four of the conductors at the same time with a total of four pulses required to move the entire stripe one complete cycle.

The purpose of this study was to test a combination system which (1) generates stripes, (2) continuously pins the stripes on separate permalloy pinning strips over a range of bias fields, and (3) propagates the stripes along in a spatially separated stepwise fashion. The goal was to learn enough about such combinations to improve, redesign, and utilize them for future devices. A number of observations were noted:

- (1) The generator conductor is also the current return path for the serpentine conductors. This is undesirable, because when the stripe is near the generator, current in one of the serpentine conductors returns through a segment of the generator and causes a corresponding segment of the stripe to move the wrong way.
- (2) The magnetostriction of the garnet, coupled with the strain of the conductors on the garnet, sometimes causes the stripes to favor locating along the serpentine conductors even when the current is off.

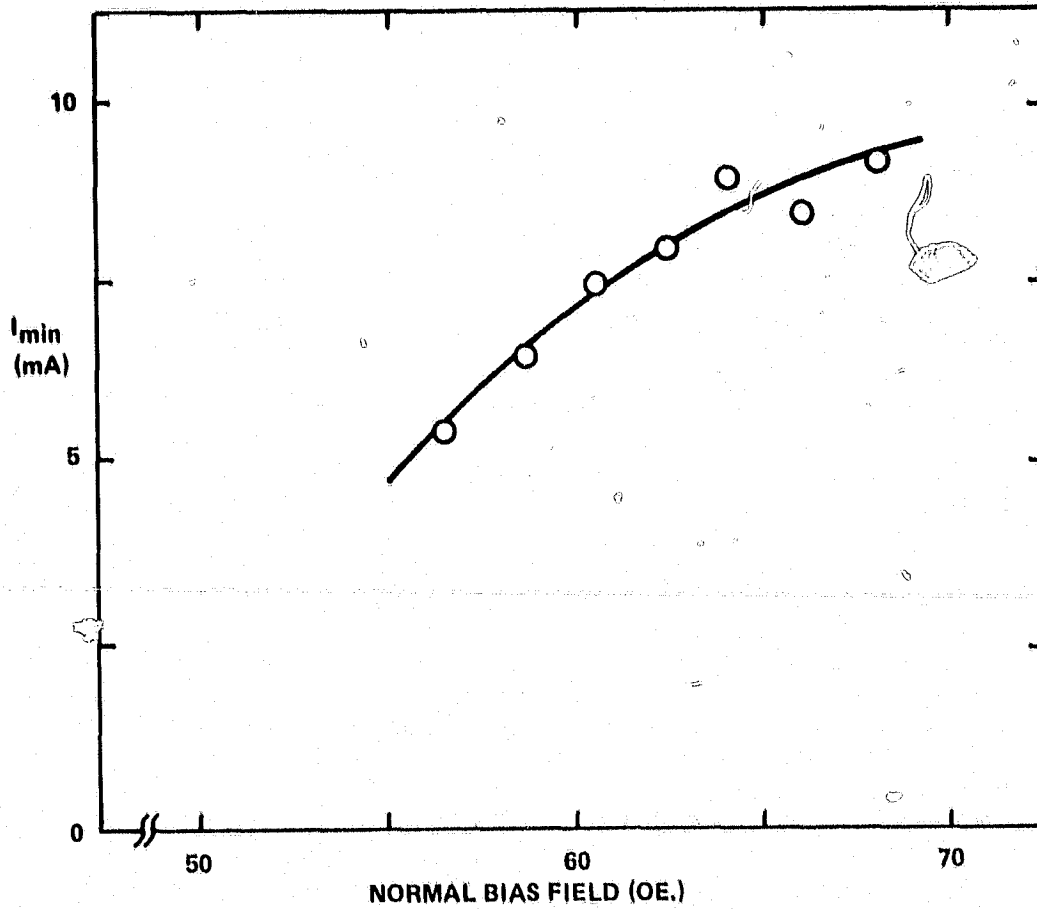


Figure 4.8 Minimum Drive Current Required to Move a Stripe Segment vs. the Normal Bias Field.

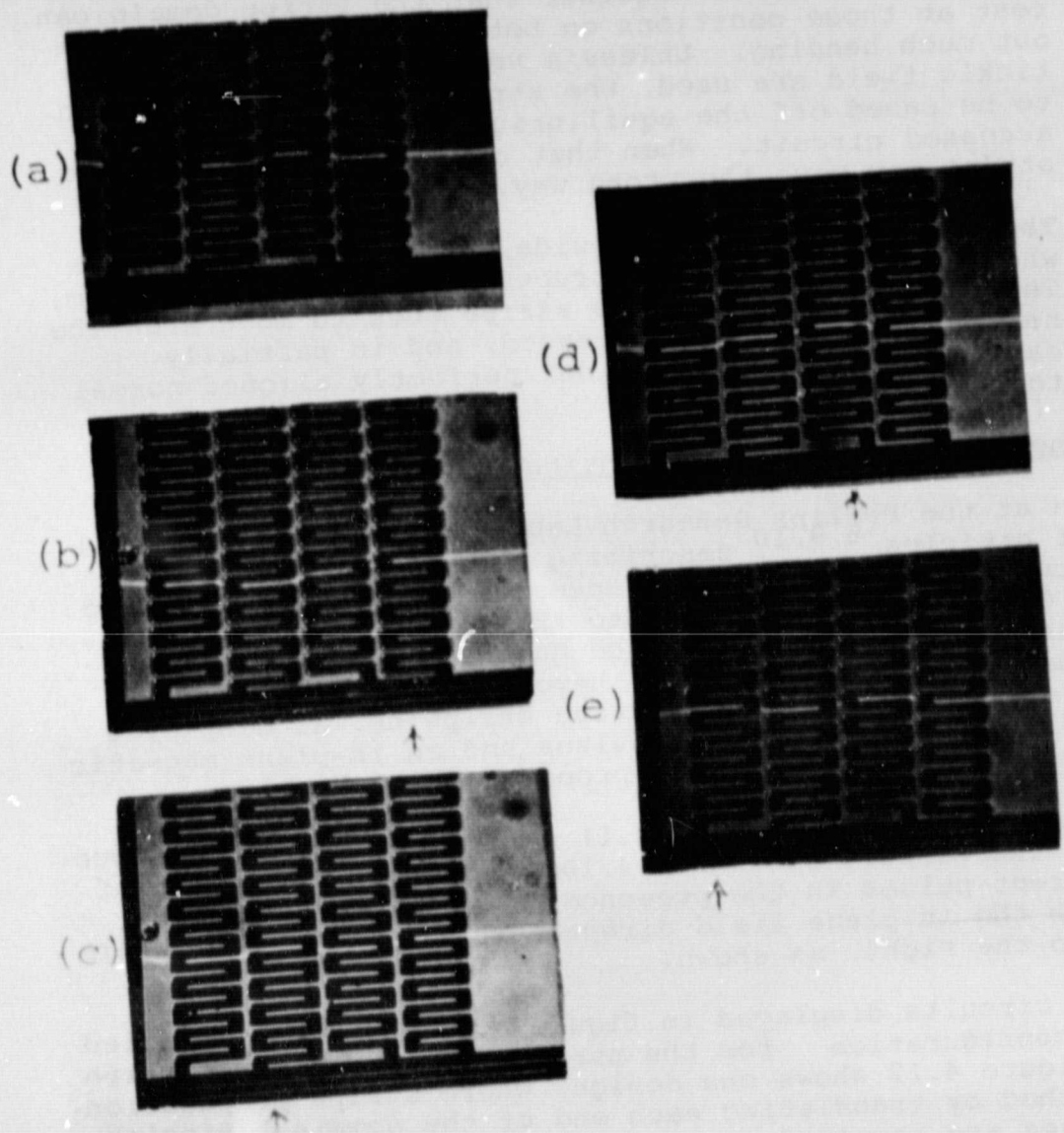


Figure 4.9 Piecewise Translation of One Stripe Domain
End for One-Half Cycle.

- (3) The equilibrium positions on the two serpentine circuits are so close together that the stripe domain can rest at those positions on both circuits at once without much bending. Unless a very high bias field and tickle field are used, the stripe is not stiff enough to be eased off the equilibrium position of the non-accessed circuit. When that circuit is accessed, the stripe may move the wrong way.
- (4) The pinning bars are too wide, generating a situation where a complex stripe structure can exist under them. This sometimes causes the stripe ends to move when the normal bias field is increased, and is partially caused by the bias field not perfectly aligned normal to the film.

4.3.3 Magnetically Assisted Serpentine Circuits

Researchers at the Philips Research Laboratories have published a series of articles ^{8,9,10} describing their investigations of bubble circuits having both field accessed and current accessed features. Of particular interest to this program are the magnetically assisted, current accessed bubble propagation and stretcher designs. These circuits have NiFe features that, in general, are located over a conductive stripline, as displayed in figure 4.10. Bipolar current pulses and an in-plane magnetic field are required for successful propagation of bubbles.

The series of drawings in figure 4.11 depict the motion of a bubble through the circuit of figure 4.10a with the application of bipolar current pulses in the presence of an in-plane magnetic field. With the in-plane field directed to the left, the bubble motion is to the right, as shown.

The Philips circuits displayed in figure 4.10 have been modified in design configuration for the purpose of propagating stripe domains. Figure 4.12 shows one design, where stripe propagation is accomplished by translating each end of the domain. Bipolar current pulses are required in each serpentine leg of the circuit, in addition to an in-plane magnetic field. Motion of the ends of the stripe domain is similar to that of a bubble domain depicted in figure 4.11. The long conductors at the top of the circuit are employed to generate stripe domains.

A second circuit design is presented in figure 4.13, where each magnetic bar of figure 4.12 has been replaced by a magnetic chevron. Although the period to gap ratio for the chevrons may not be optimized for field accessed propagation, the concept tendered

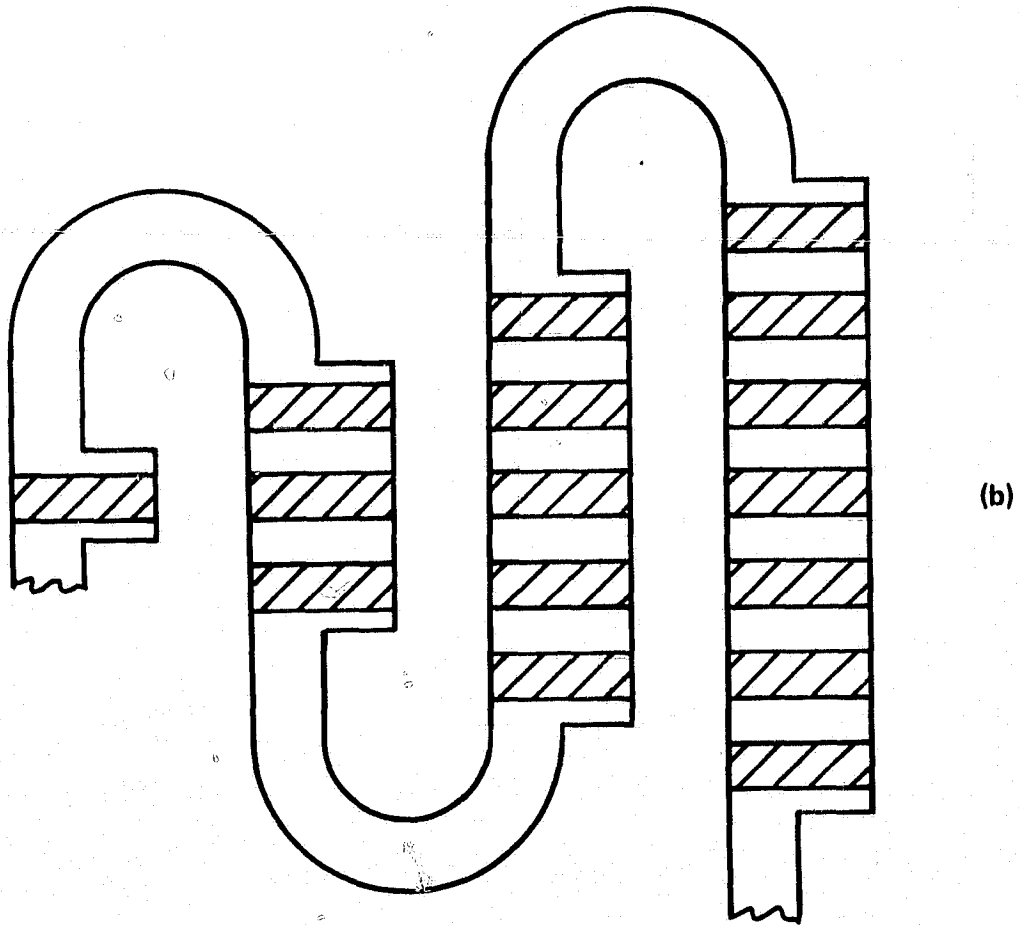
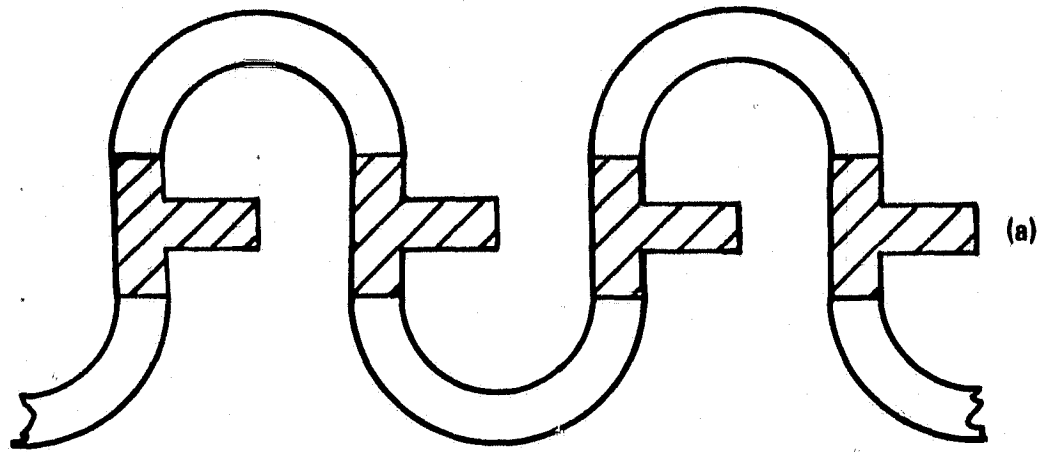


Figure 4.10 Magnetically Assisted Bubble Propagator (a) and Expander (b).

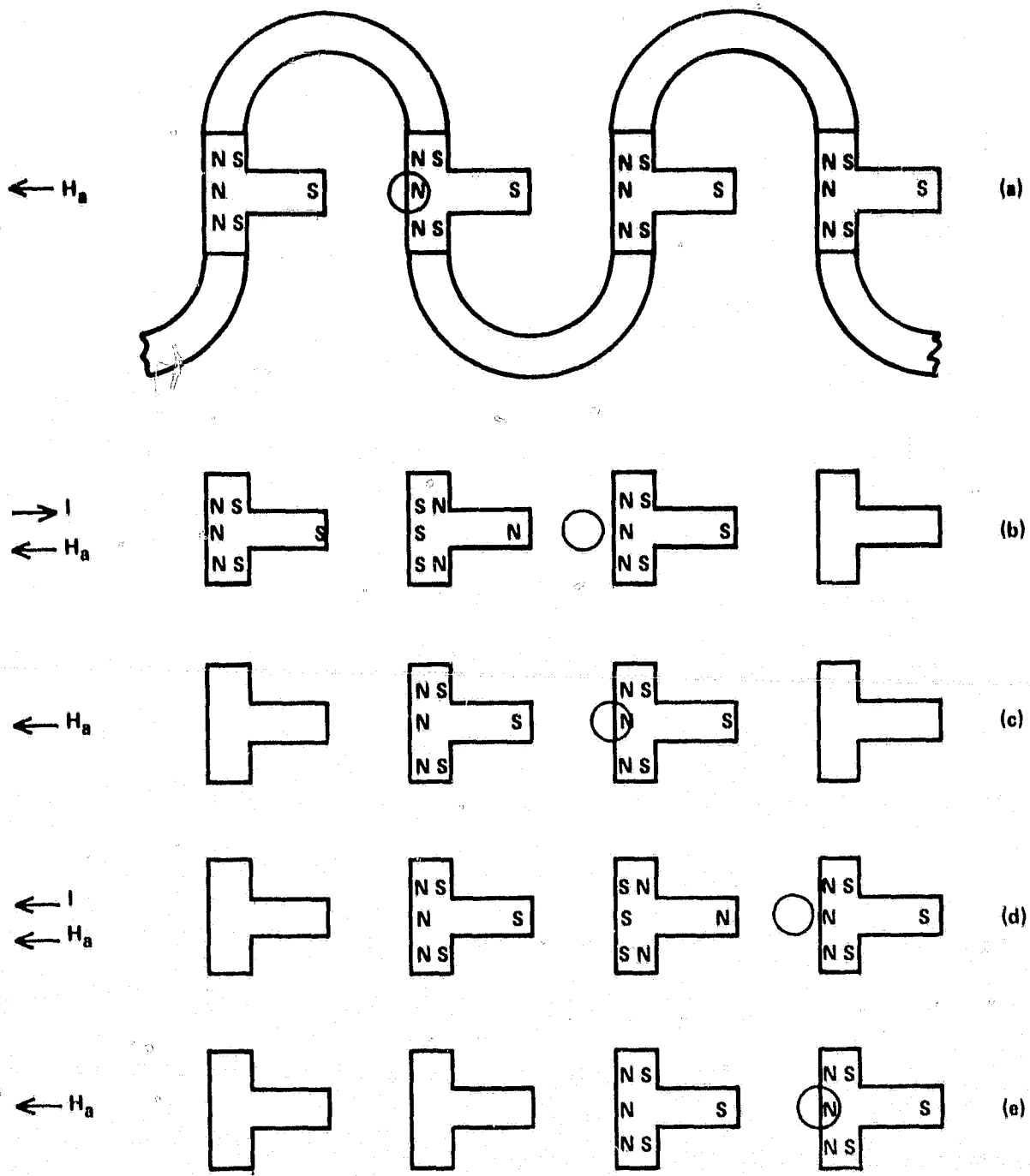


Figure 4.11 Propagation of a Bubble Domain with Applied Current I and Applied In-Plane Field H_a .

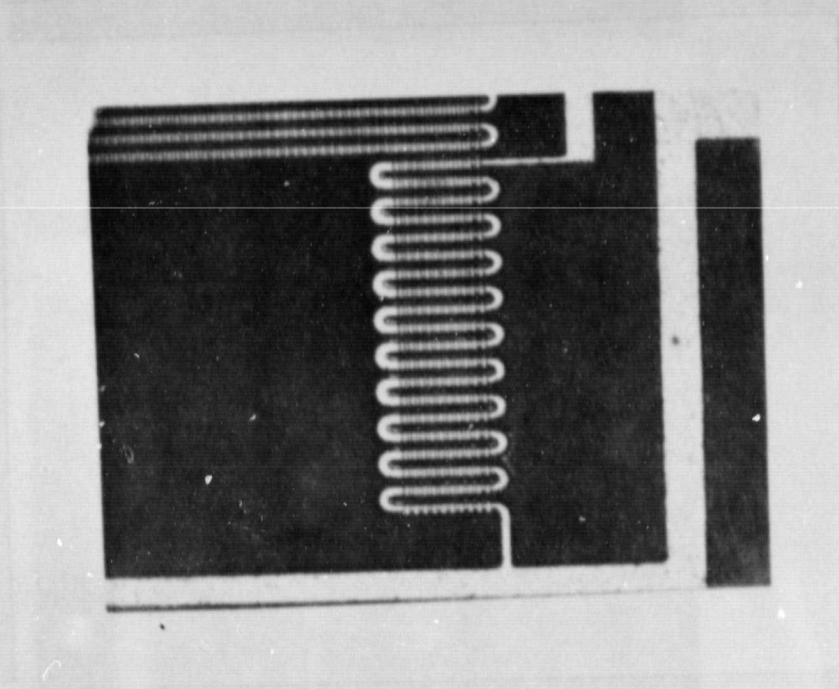
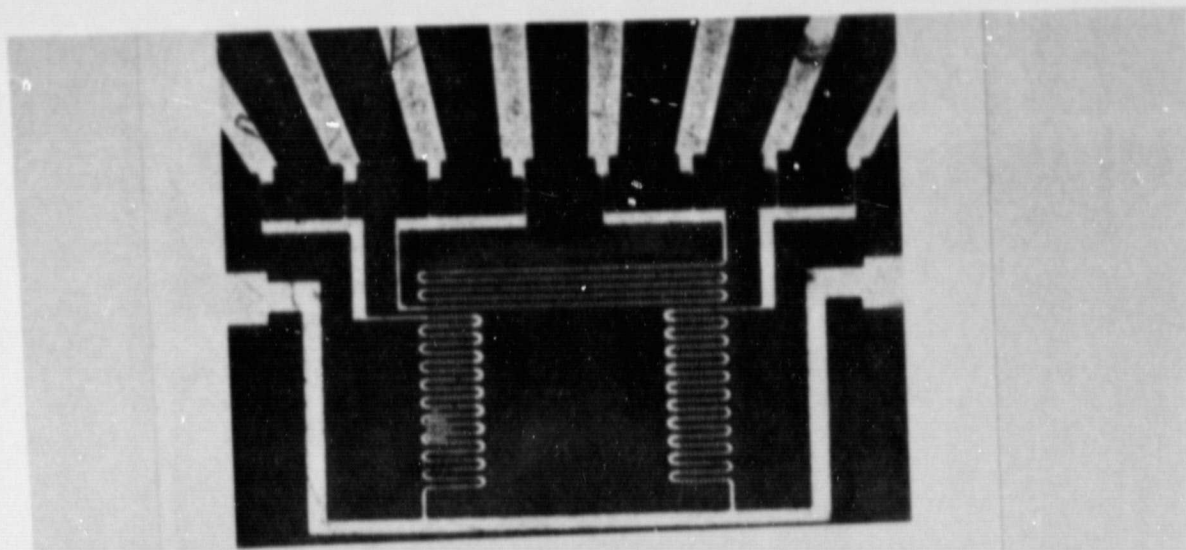


Figure 4.12 Stripe Domain Propagation Circuit with Magnetic Bars.

ORIGINAL PAGE IS
POOR QUALITY

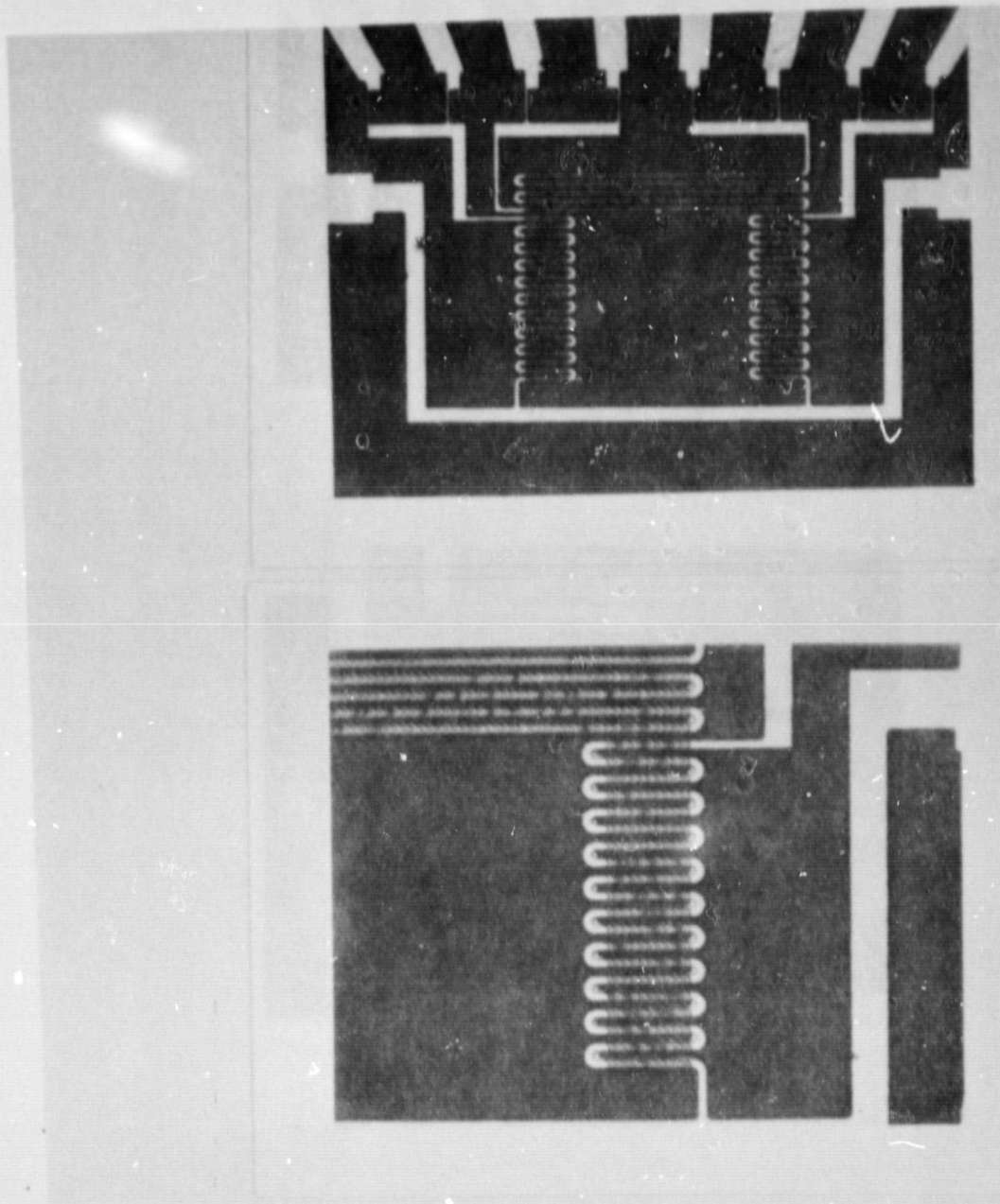


Figure 4.13 Stripe Domain Propagation Circuit with Magnetic Chevrons.

PHOTOCOPIED FROM THE
ORIGINAL FILED IN
SERIALS SECTION

is a circuit that may operate with either field accessed or current accessed techniques. Propagation of stripe domains through the use of chevrons and rotating fields have been demonstrated in the past. With current accessed conductors, these chevrons should propagate bubbles or stripe ends in the same manner as the bar circuit of figure 4.12.

One of the advantages in designing this type of circuit is to extend the time available for testing purposes. It is almost inevitable that the current accessed circuit will become an open circuit, either due to operator error or test equipment malfunction. This design will hopefully extend the useful test time, if the circuit becomes open, by employing field accessed techniques.

Testing the circuit with NiFe chevrons demonstrated that propagation of stripe domains can be accomplished with both field access and current access techniques. With a rotating field peak value of 60 Oe, and a normal bias field of 50 Oe, stripe domains were propagated along the chevron rows. The stripes showed considerable bowing at their center. Measuring the normal field value to collapse a free stripe, and also a NiFe pinned stripe, indicated that the magnetostatic coupling between the chevrons and the stripes was approximately 9 Oe. This coupling is relatively small, and explains the stripe curvature. If the chevrons were located between the conductor and the garnet, the coupling would be considerably greater. Reversing the direction of the in-plane field, approximately 15 Oe, caused the propagation direction to reverse.

Propagation of the ends of stripe domains was observed while employing current accessed techniques. With an in-plane field of approximately 15 Oe, a normal bias field of 52 Oe, and bipolar current pulses of + 20 mA and 1/3 μ sec duration, stripe propagation under and near the conductors was observed. Due to the weak NiFe to stripe coupling, propagation of the entire stripe domain was not accomplished. Generation and propagation of stripes in the long generator section of the circuit was successful. Under all circumstances of current access, there was no propagation when the in-plane field was removed.

4.3.4 Segmented Chevron Circuit

A third permalloy assisted current access circuit has been designed which does not employ serpentine conductors, and incorporates a new concept of segmented chevrons. Figure 4.14 displays this circuit, showing the segmented chevrons located above the conductors, and also showing three long rows of normal chevrons. The principal advantage of this design over the previous two is that the conductor is wide and straight and does not have to meander back and forth, and thus has much lower resistance, and

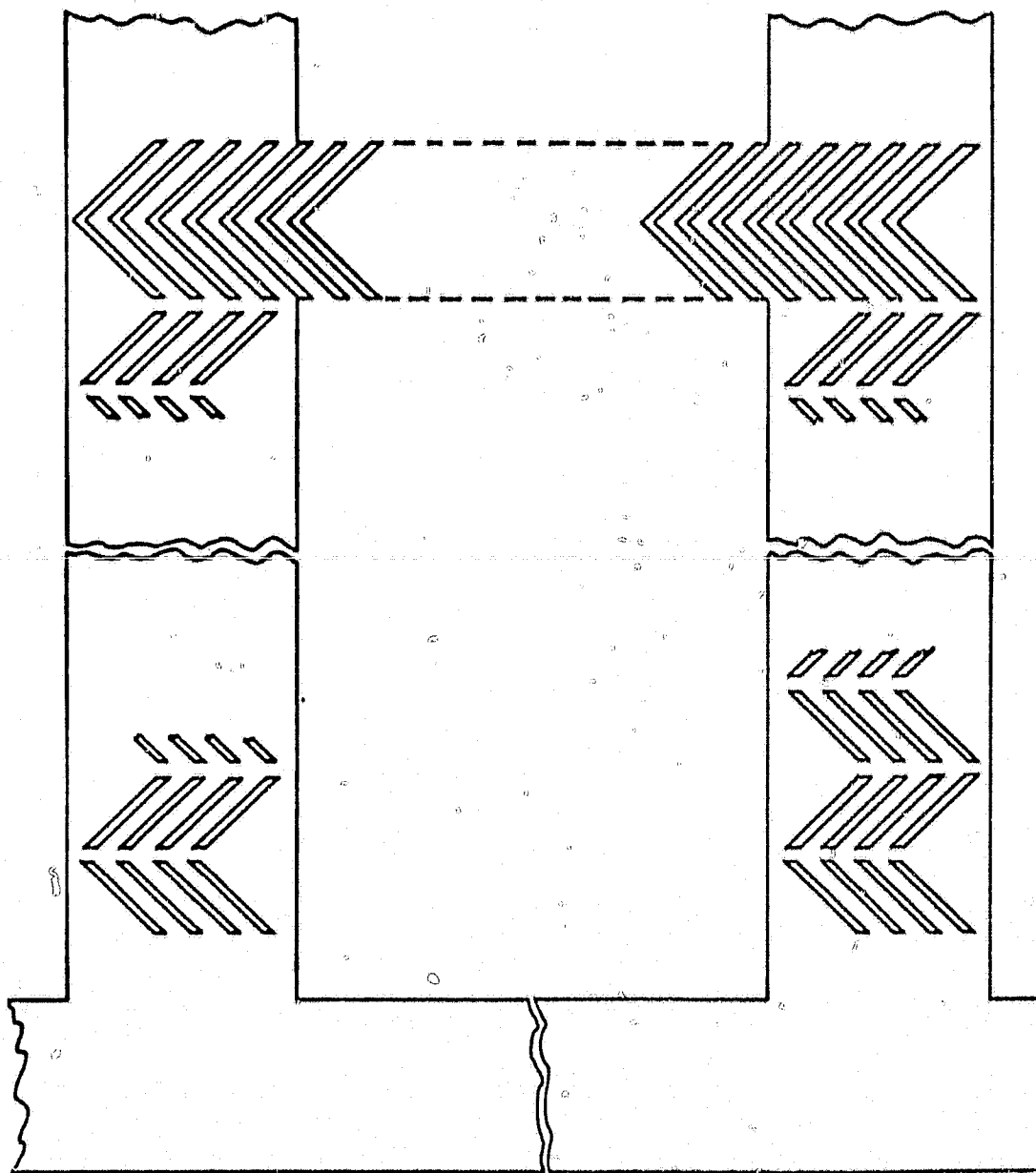


Figure 4.14 Segmented Chevron Circuit.

is easier to fabricate. This design also requires the presence of an in-plane field perpendicular to the stripe domains, in addition to bipolar current pulses. Figure 4.15 depicts the motion of a bubble along the segmented chevrons of figure 4.14 under magnetic field cycling.

Magnetization in one of the segmented chevron bars, parallel to the long edge, is shown in figure 4.16 as a function of the field from the strip line H_I , for an applied in-plane field H_a of 25 Oe. The chevrons shown in figure 4.14 have an interior angle of 90° between neighbors, which corresponds to the 45° curve of figure 4.16. This curve shows that a conductor generated field of 25 Oe will either saturate or demagnetize chevron A along its long dimension, depending on the polarity of the current pulse in the stripline. A bipolar current pulse which produces a field near + 75 Oe will be a good compromise for proper operation of both chevrons. For a line width of 28 microns, this corresponds to a current of ± 335 mA; or ± 190 mA for a 16 micron wide line.

The segmented chevron circuit can be operated either with current access or with field access. When the circuit is operated with field access, the external in-plane field does not rotate 360° around and around as is the case for normal chevrons, but rather rotates back and forth, through a total sweep of 180° . When operated in a current access mode, an alternating current in the conductor supplies an alternating in-plane field which, when combined with an external dc field, causes domains to be propagated in a direction opposite to the dc field. The direction of motion can be reversed by reversing the direction of the dc field. How the propagation works is illustrated in figure 4.15.

The advantages of the segmented chevrons for propagating domains are:

1. The conductor is straight and broad and can thus have low resistance. The conductor does not meander like the serpentine conductors required for the other permalloy aided circuits described in the previous section.
2. The conductor runs perpendicular to the stripes, so the field from the conductor exerts no force that would tend to move the stripe. The conductor can be placed above the permalloy or below the permalloy, in contrast to the other permalloy aided circuits described in the previous section. Those circuits require the conductor to be between the garnet and permalloy, seriously degrading the coupling between the permalloy and stripe.

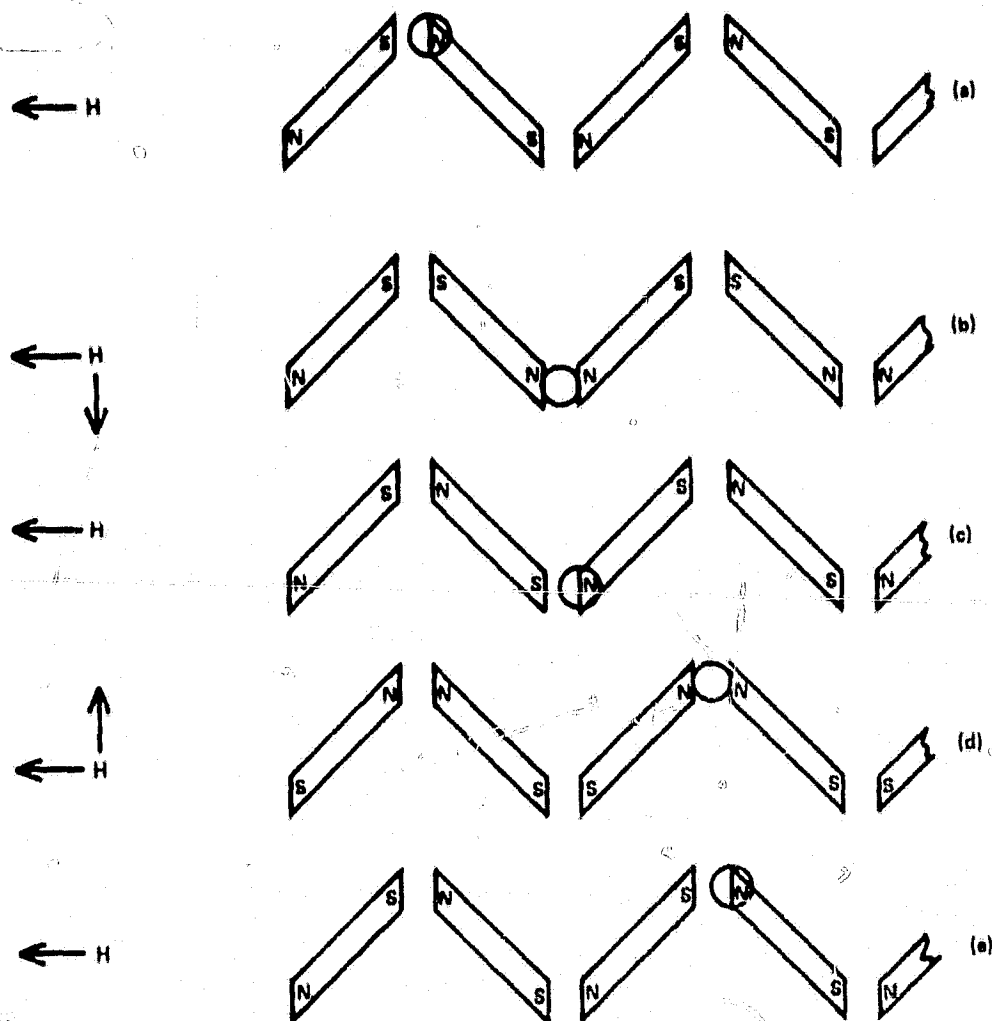


Figure 4.15 Bubble Propagation Through a Segmented Chevron Circuit, with Magnetic Fields from Conductor Current and External Application.

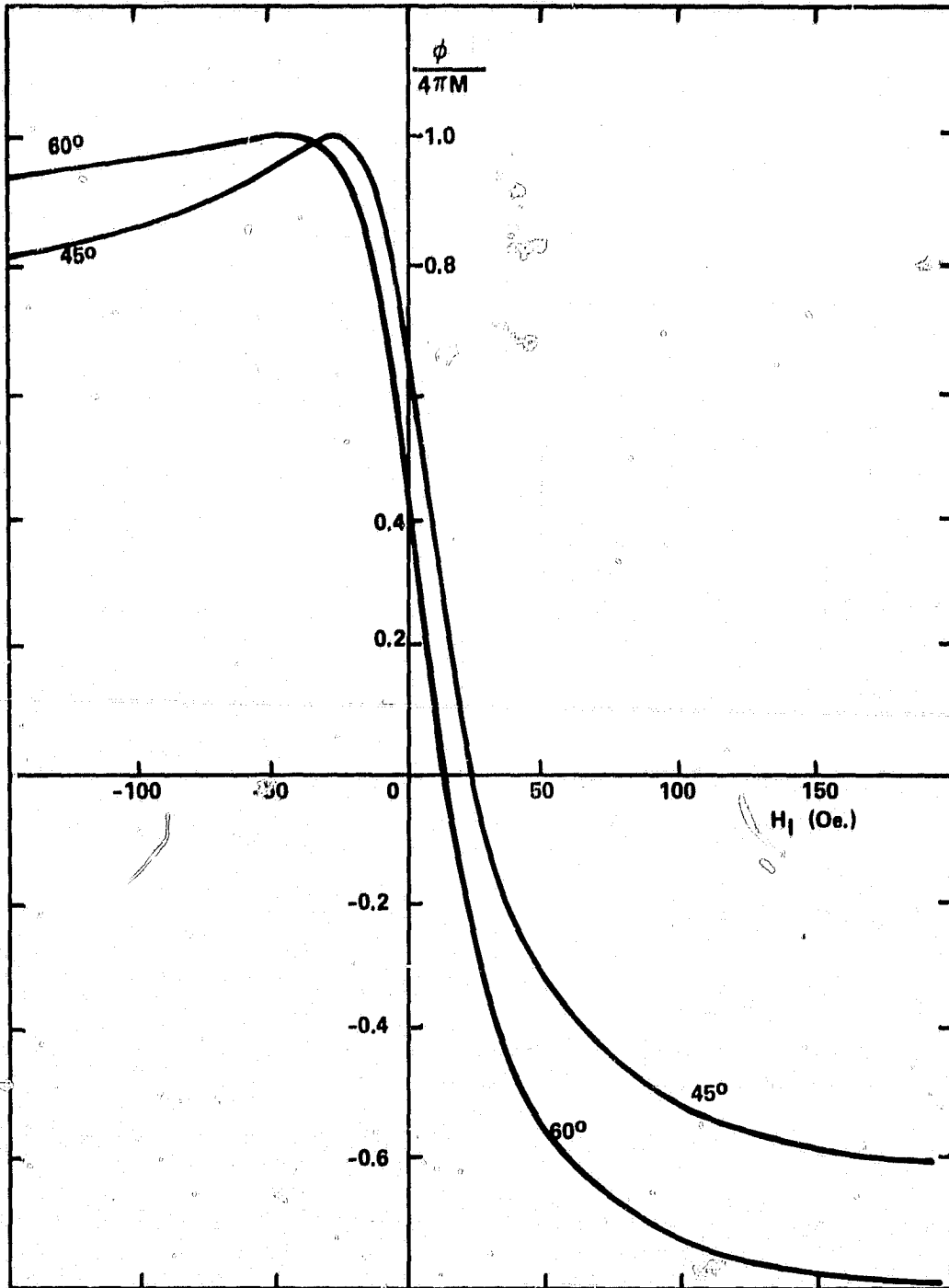


Figure 4.16 Magnetization Strength in a Chevron vs. the Magnetic Field from a Stripline Conductor, with $H_a = 25$ Oe.

3. Because the permalloy can be next to the garnet, the segmented chevron can be self-pinning, i.e., the chevrons can pin the ends of the stripes and prevent the stripes from contracting to bubbles even when the bias field is larger than the run-out threshold.
4. The segmented chevron can be used either in a field accessed mode or in a current accessed mode. This can be quite useful in experimentally analyzing the performance of an experimental device.
5. The dc in-plane field can be quite small, and is reversed only when the direction of propagation is to be reversed. Thus, the dc field does not impact the power or the speed of the device.

The disadvantages of this design are related to stripe cutting. There is a normal component of field from the conductor that is a maximum at the edge of the conductor. If this field is too large it can cut the stripe. The narrower the conductor and the farther away from the garnet, the smaller this effect. Propagation of stripes with this experimental device was possible without cutting the stripes.

Figure 4.14 displays the circuit that was tested. Segmented chevrons are used as propagating elements; full chevrons are used as stripe generators. The permalloy was placed on top of the conductor instead of between the stripline and the garnet, and resulted in weak coupling between the stripes and chevrons. The circuit was unfortunately fabricated on a garnet that has a long defect that runs diagonally across the circuit, which prevented full operation of the circuit.

The zero in-plane field coupling between stripes and segmented chevrons can be measured by measuring the difference in run-out threshold for stripes under the permalloy and stripes not under the permalloy. This was found to be only about 4 Oe for both normal chevrons and segmented chevrons. Operating bias is 65 Oe. This weak coupling is due to the large separation between the garnet and permalloy. Had the circuit been made with the permalloy next to the garnet, the coupling would have been much larger.

Propagation was tested in the leg of the circuit not blocked by the defect. Propagation was achieved both in the field access mode and the current access mode. A schmo plot was made of the region of propagation: a plot of the locus of the combination of in-plane bias field and stripline current amplitude that propagates stripes, which is shown in figure 4.17. Propagation is

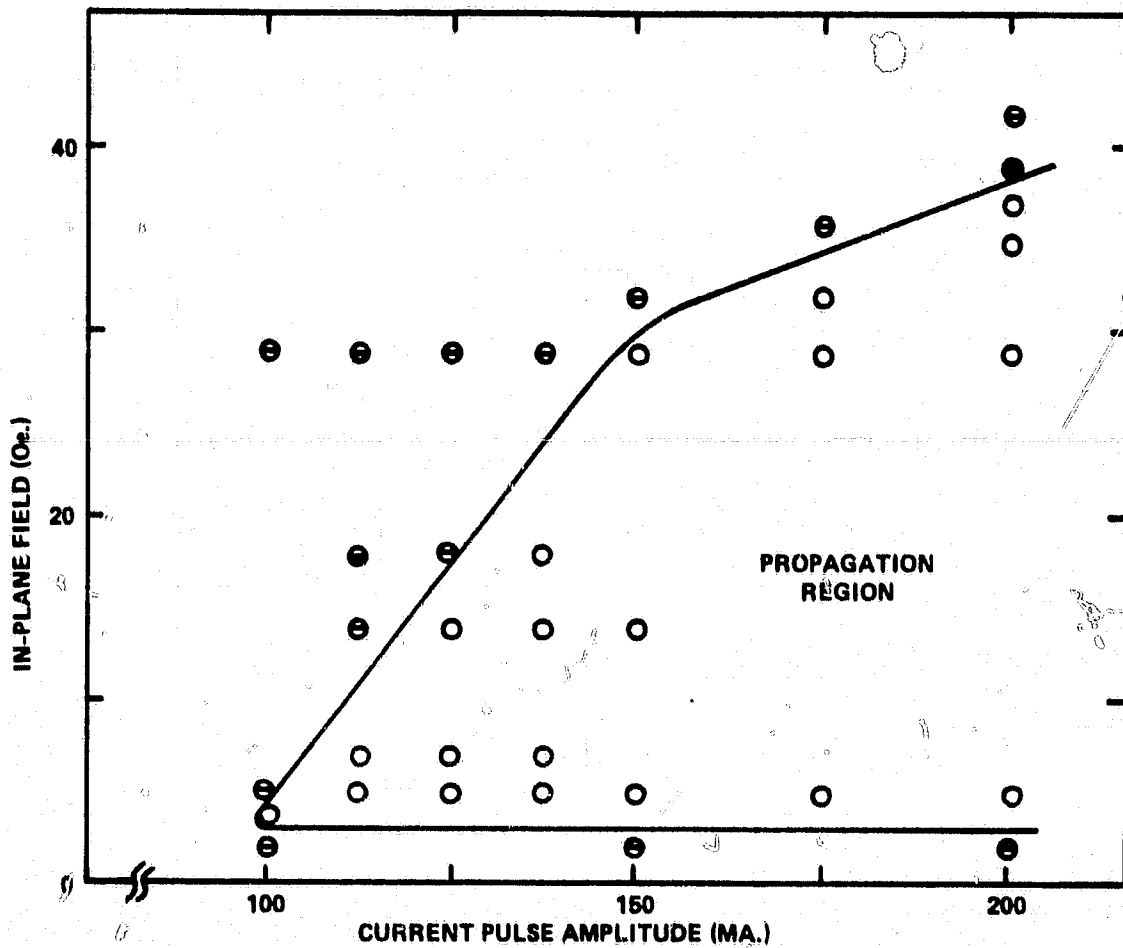


Figure 4.17 Propagation Region for the Segmented Chevron Circuit.
Normal Bias Field = 42 Oe.

achieved with an in-plane field as low as 3 Oe and a current pulse amplitude as low as 100 mA in each conductor. When the in-plane field is increased, the required pulse current amplitude, in general, is also increased. Propagation failed with current pulses shorter than one μsec . This corresponds to a domain velocity of 8m/sec, which is close to the limiting speed of domains in the garnet material.

The segmented chevron stripe propagator is extremely promising. It is the most attractive of the permalloy assisted current accessed propagators. It is self-pinning, fast, can be fabricated with the permalloy next to the substrate, has low registration specifications, requires low power, and can be operated as either a field accessed or current accessed device.

4.3.5 Stripe Domain Curvature

As an empirical verification of the theoretical calculations presented in section 3.4.6, two experiments have been performed. Both experiments involved the generation and propagation of isolated stripes in chevron devices similar to that shown in figure 3.19. Stripe domains were propagated back and forth along the track of the chevron device by reversing the direction of rotation of the drive field, being careful to preserve the phase sense at all time. At the end of each field application the amount of distortion, shown as z in figure 3.19, was measured. Two situations were considered. In the first, the stripe curvature was measured as a function of the rf tickle field, H_{rf} , while the bias and drive field amplitudes H and H_r remained constant. In the second, the bias field amplitude was varied while H_{rf} and H_r remained constant. Using equation 3.45, this data allowed for the calculation of the effective coercivity H_c .

Both experiments were performed on a three sided $12.7\mu\text{m}$ period chevron device fabricated on a YLaTmGaFeO garnet. The relevant garnet properties are: $h = 6.21\mu\text{m}$, $4\pi M = 115$ Oe, $H_K = 1060$ Oe, and $\lambda = 0.752$. The device employed was $185\mu\text{m}$ wide and about $1000\mu\text{m}$ long.

The results of the first experiment are shown in figure 4.18. Two calculations were performed. The coercivity H_c was first calculated using only the normal bias field H . In the second, the coercivity H_c^* was found using the value $H + H_{rf}$ as the effective bias field seen by the garnet, where H_{rf} is the peak value of rf bias tickle field. As expected, the effective coercivities are a strong function of the rf tickle field, showing a tendency to level out as H_{rf} reaches higher values. The effect was manifested in the stripe as an increase in the radius of curvature with increasing H_{rf} , i.e., the stripe was straighter at higher rf amplitudes.

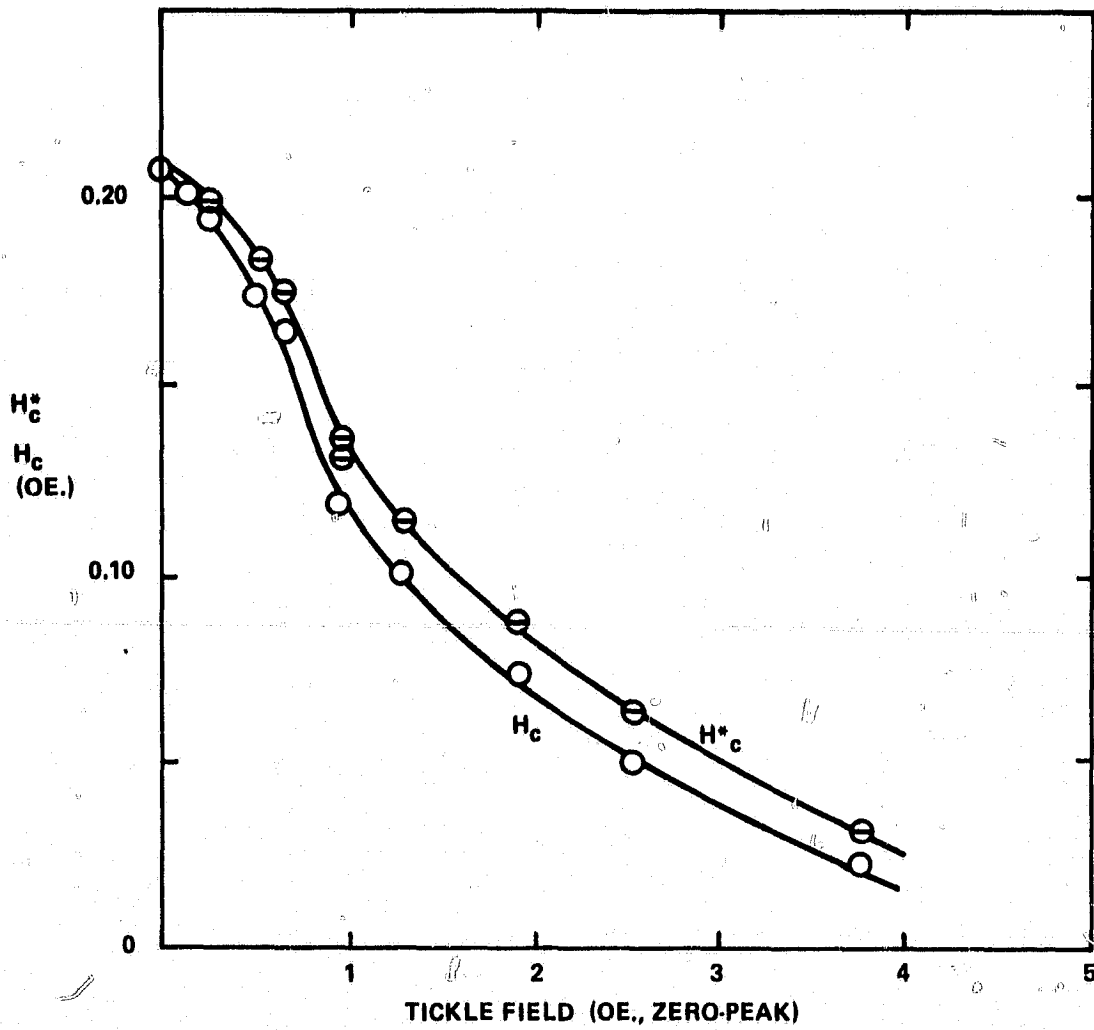


Figure 4.18 Garnet Coercivity vs. Tickle Field Amplitude.

In the second experiment the rf tickle field was held constant while the bias field was varied. The curvature was measured, and the coercivity was calculated from equation 3.46. As expected, the coercivity remained constant within experimental error. This lends confidence in the theory.

As a refinement to the theory, the data on curvature of the stripe was fitted to a catenary instead of an arc of a circle, but the difference was found to be negligible.

4.4 Magnetic Features and In-Plane Fields

During the initial testing of stripe propagation devices incorporating permalloy pinning bars, stripe ends were observed to creep along the permalloy bars as the bias field was increased. This phenomenon has been attributed to the domain pattern in the permalloy bars interacting with in-plane components of the bias field. As indicated schematically in figure 4.19, appropriate domains in the permalloy bars grow as the in-plane field component is increased, carrying the stripe ends along. In the extreme, this phenomenon can sweep the stripe domain completely off one end of the device. Although this phenomenon should not be a problem with a fully populated stripe array, it is a bothersome problem when testing devices populated with only a single stripe. To overcome this problem simply requires an alteration of the domain pattern in the permalloy bars. This can be easily accomplished by the use of a small in-plane field perpendicular to the NiFe pinning bars (i.e., parallel to the stripe) as illustrated in figure 4.20. Using 50 μ m wide bars and 5 to 11 Oe in-plane fields, it has been observed that pinned stripe domains are extremely stable as the bias field is varied through values from the run-out field H_{RO} up to 25% over the bubble collapse field, H_0 . The magnitude of this in-plane field is limited only by the value at which the pole strength at the inside edge of the pinning bar becomes strong enough to slice the stripe domain. Typical values for this threshold are 15 to 17 Oe, allowing ample margins for thorough testing of present devices.

The use of the perpendicular in-plane field provides improved stripe end pinning while at the same time reducing device sensitivity to a parallel in-plane field. This perpendicular field can also be supplied by the use of permanent magnet materials in the bars, as well as by a slight canting of the device with respect to the normal bias field.

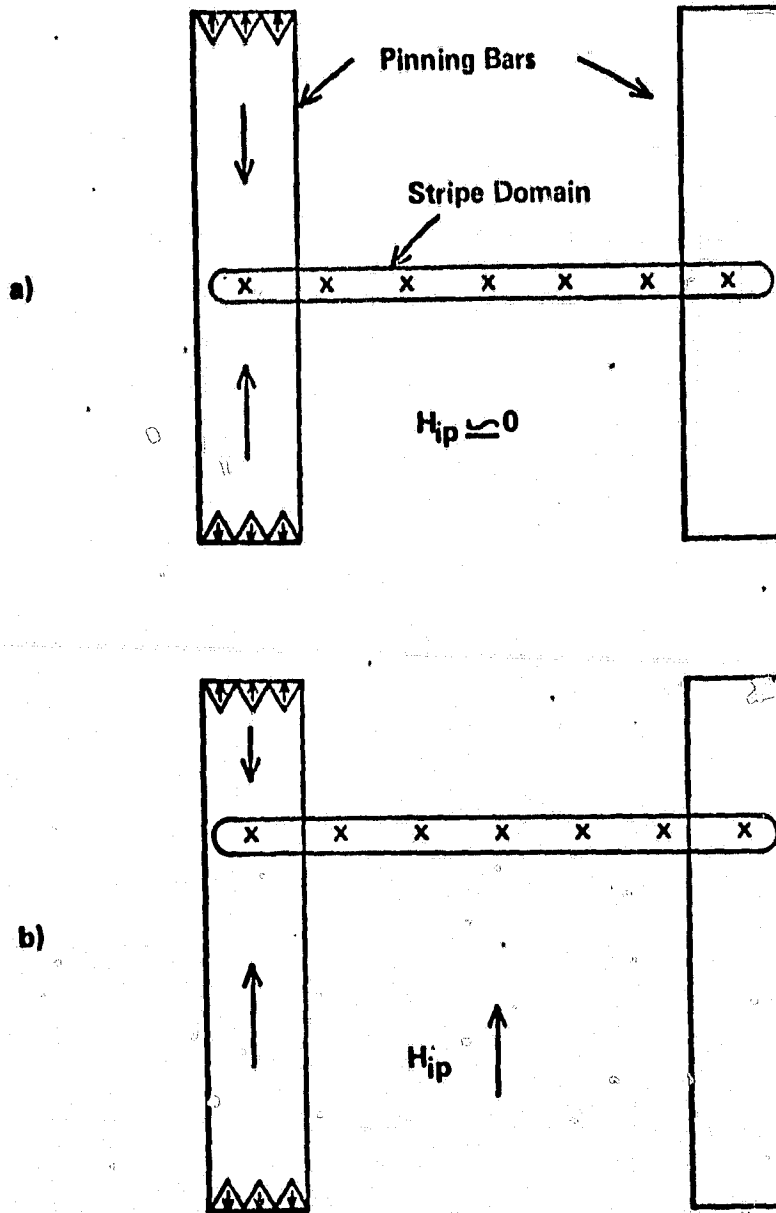


Figure 4.19 Simplified Representation of the Pinning Bar-Domain Interaction.

- a) Domain Configuration with No In-Plane Field
- b) Domain Configuration with an In-Plane Field Component Along the Length of the Pinning Bars.

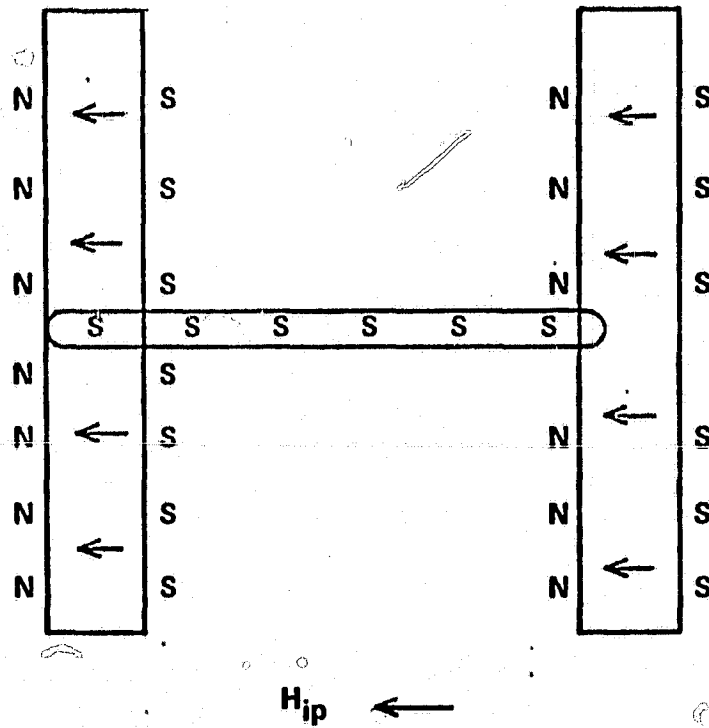


Figure 4.20 Simplified Domain Structure Using an In-Plane Field Perpendicular to the Pinning Bar

4.5 Garnet Materials

4.5.1 Objectives

Before device designs can be finalized, it is important to know the range of material parameters that are available in bubble supporting garnets. It is also very helpful to know the defect density in these materials, which will affect device yield, size, and required redundant circuitry. With multiple layer garnets, the coupling between layers must be known for material choice and layer thickness. It is the object of this section to determine the material parameters that are available, and how they influence the device design.

4.5.2 Garnet Survey

The two fundamental material parameters of bubble films are the saturation magnetization, M , and the characteristic length, λ . These are the two parameters independent of film thickness from which the other parameters important to bubble operation can be deduced.

A question important for multilayer bubble work is: "What combinations of $4\pi M$ and λ can be made?" Accordingly, a survey was made of garnet materials from Sperry Research Center and Univac Blue Bell, reported in two publications.^{11,12} The results are listed in Table 4.2.

When a graph is made of saturation magnetization, $4\pi M$, vs. characteristic length, λ , of these garnets, all the points fall on a single curve, as shown in figure 4.21. A mathematical relationship between the two parameters is found by plotting the natural logarithms of the two parameters, and the result is a straight line as shown in figure 4.22. The equation for that line is:

$$\ln 4\pi M = -.8125 \ln \lambda + 4.67$$

or

$$\lambda = \left(\frac{106.7}{4\pi M} \right)^{1.23} = \frac{313.8}{(4\pi M)^{1.23}} \quad (4.1)$$

Although no garnet films in the survey were found that did not fit that equation, this does not necessarily mean that such films cannot be made. The impact of the survey, however, is that garnets that do fit the equation can be made over the whole range of $4\pi M$ and λ .

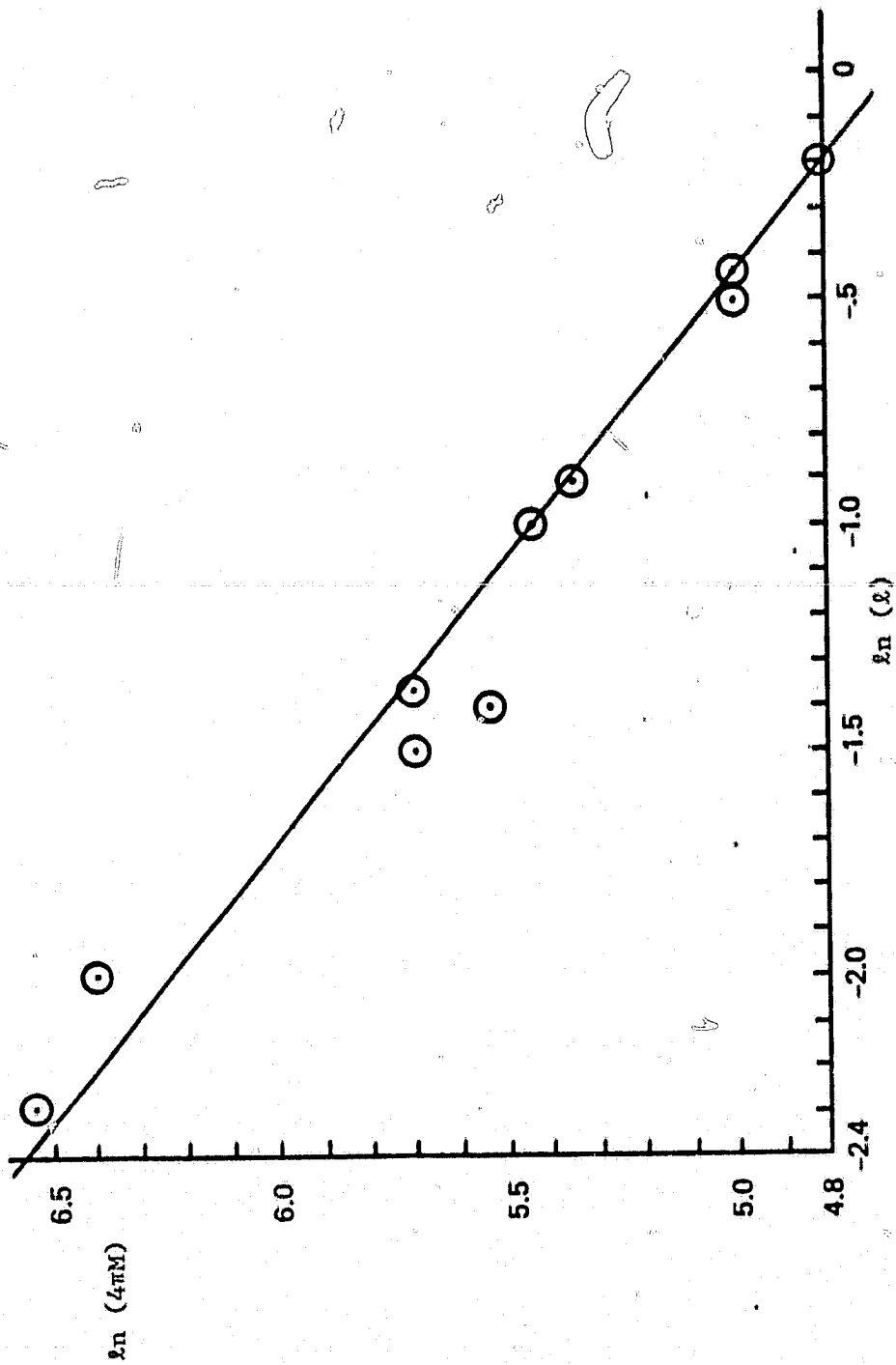


Figure 4.21 Magnetization vs. Characteristic Length of Typical Bubble Garnets

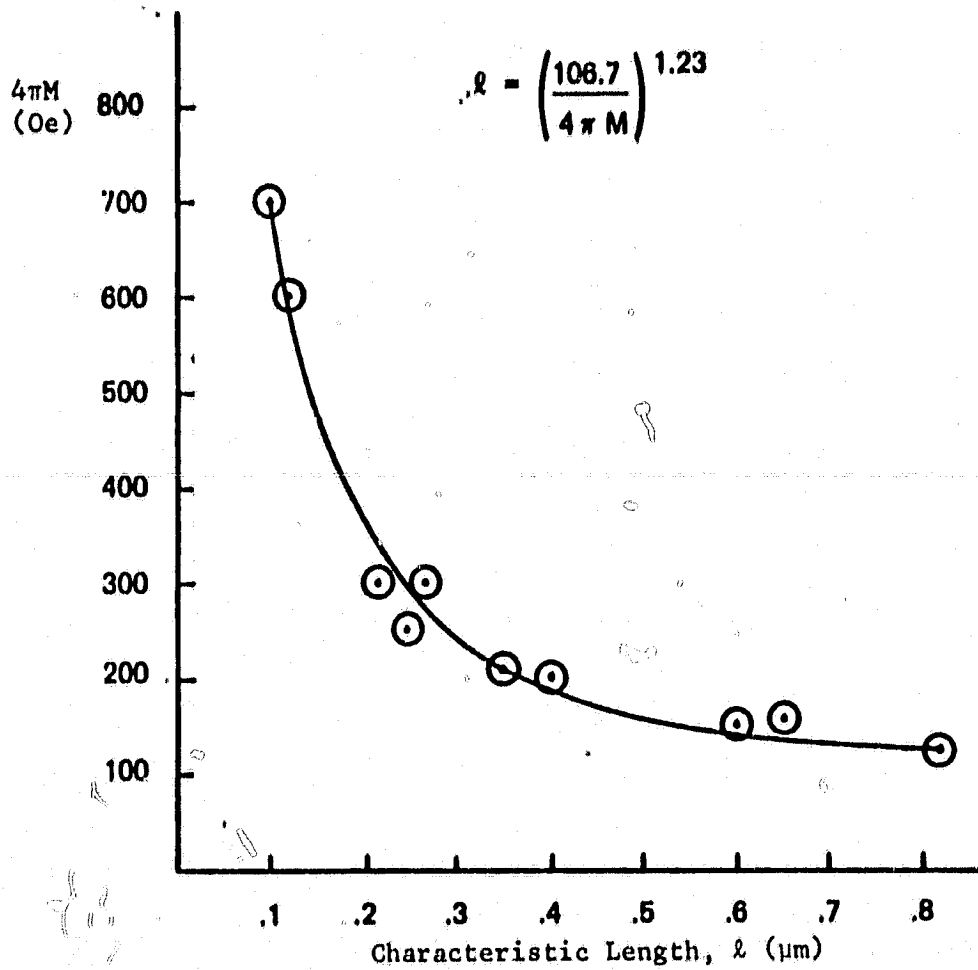


Figure 4.22 Magnetization vs. Characteristic Length of Typical Bubble Garnets.

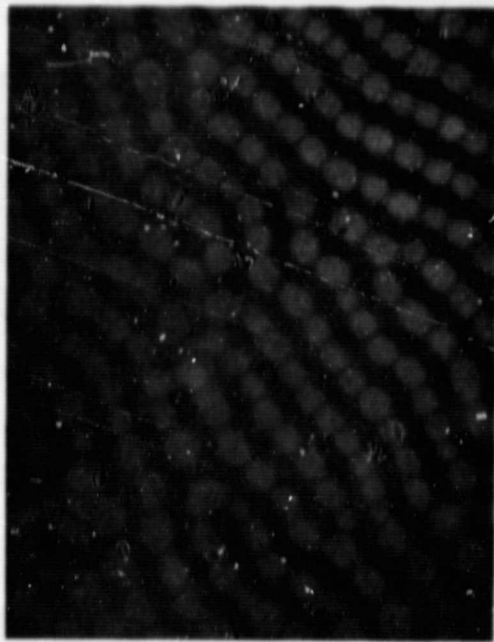
4.5.3 Multiple Layer Garnets

Three magnetostatically coupled, one inch diameter, triple layer garnet films were made by the Sperry Corporate Research Center. Each film is comprised of two $(Y\text{Sm})_3(\text{GaFe})_5\text{O}_{12}$ magnetic layers separated by a Gadolinium Gallium Garnet (GGG) layer. The samples were made with different separation layer thicknesses, holding the thicknesses of both top and bottom magnetic layers constant at as close to $6\mu\text{m}$ as possible. Samples #1, 2, and 3 have a GGG epi-layer thickness of $2.25\mu\text{m}$, $6.8\mu\text{m}$, and $13.75\mu\text{m}$, respectively.

TABLE 4.2

	4 M (Oe)	λ (μm)	H_K (Oe)	H_c (Oe)	Q	h (μm)
$(Y\text{SmLu})_3(\text{GaFe})_5\text{O}_{12}$	300	.26	1500	~ 200	5	
$(Y\text{SmLuCa})_3(\text{GeFe})_5\text{O}_{12}$	300	.22	1500	~ 200	5	
Ga	600	.13	1500	420	~ 2.4	
CaGe	700	.10	1100	~ 450	~ 1.8	
YLaTm 7/25/74C	124	.822				6.0
YLaTM 8/1/73C	253	.37		165		4.6
YLaTM 4/23/73B	232	.37		128		3.8
YLaTM 4/23/73A	213	.40		104		2.8
YLaTM E412B	154	.65		86		6.9
$Y_{2.0}\text{Sm}_{1.0}\text{Ca}_{.9}\text{Ge}_{.9}\text{Fe}_{4.1}\text{O}_{12}$	154	.61				

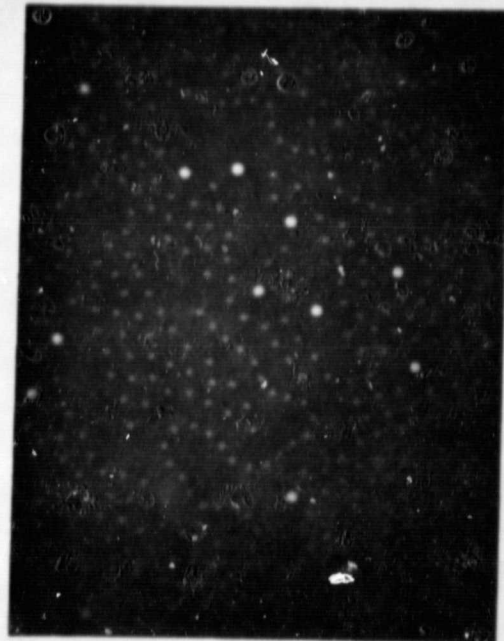
These films settled one very important question, whether or not defect-free multilayer films can be made. The high qualities of the triple layer films can be seen in figures 4.23 through 4.27. The only defects are in the photographs, such as the scratch in the emulsion of figure 4.25f. Similar dust-free furnace facilities are presently being installed in the Sperry Univac facility in St. Paul.



(a) $H = 0$



(c) $H = 38$ Oe



(d) $H = 40$ Oe

Figure 4.7: Domain Patterns in a Double Magnetic Layer Garnet, with GGG Thickness = 2.25 μ m.

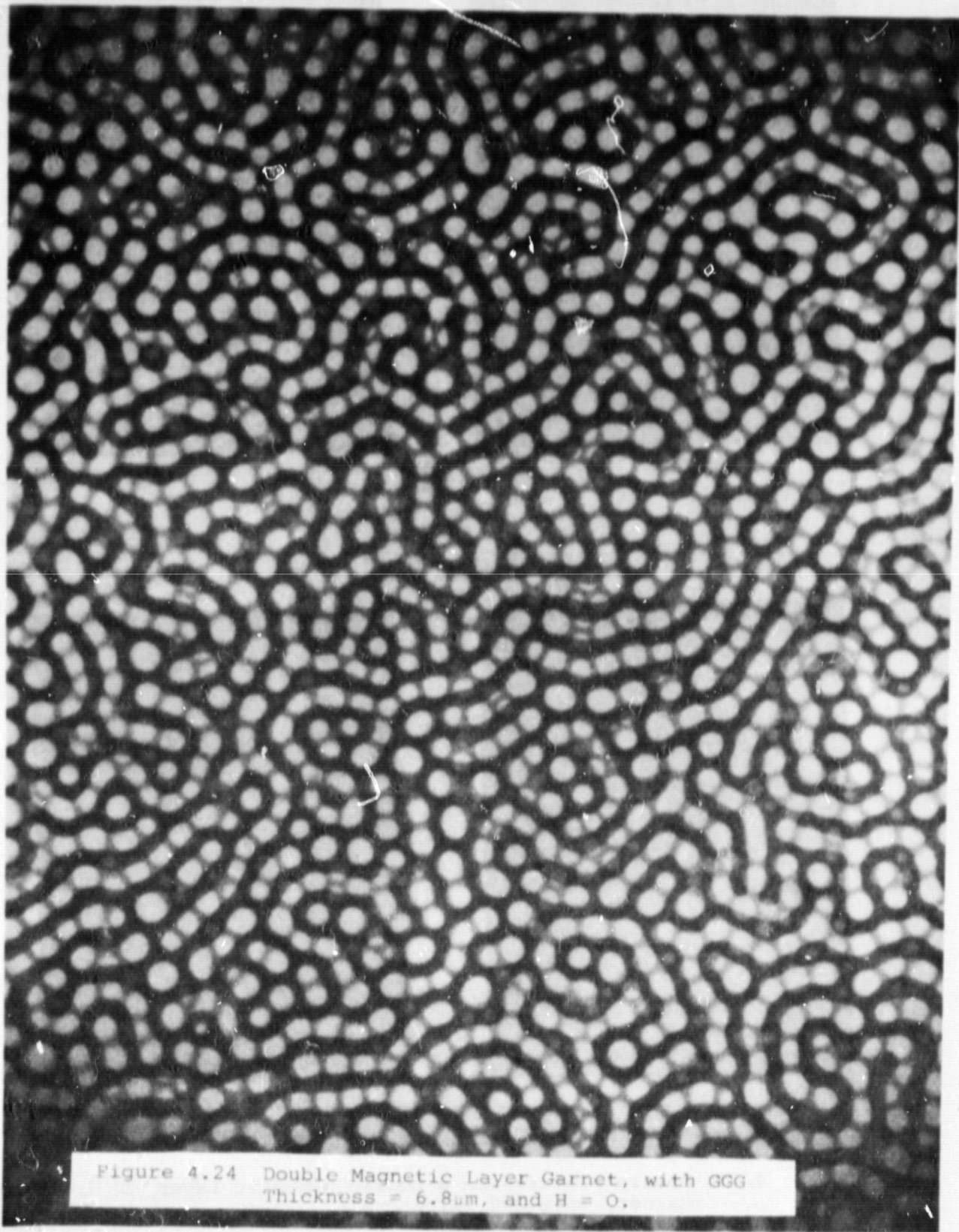
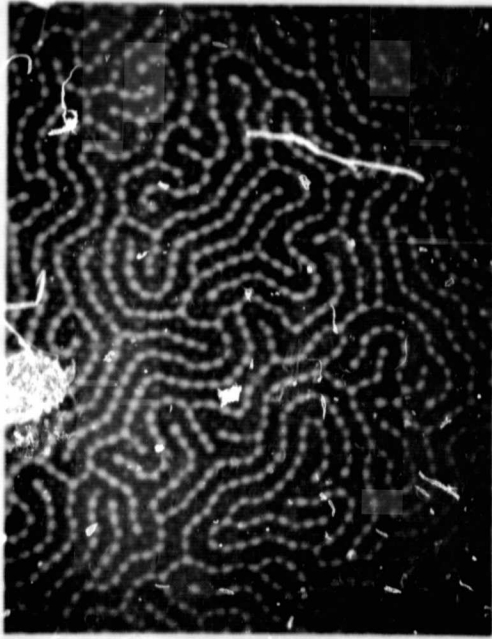


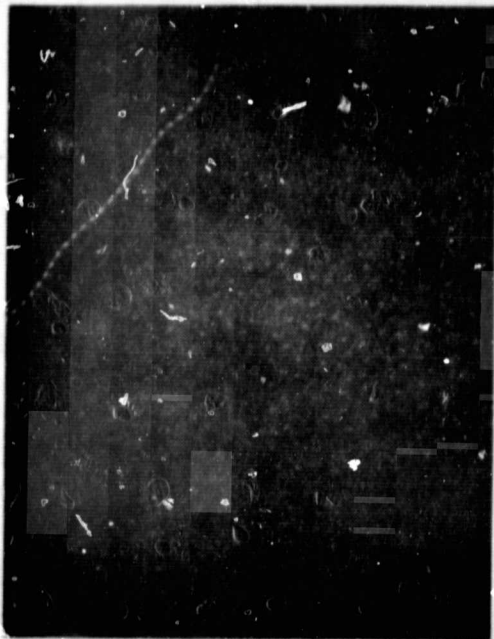
Figure 4.24 Double Magnetic Layer Garnet, with GGG
Thickness = 6.8 μ m, and H = 0.



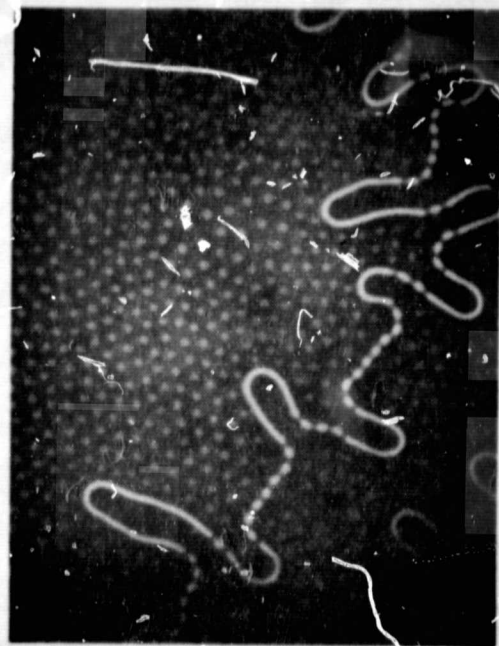
(a) $H = 28.5$ Oe



(b) $H = 41.8$ Oe



(c) $H = 62.7$ Oe



(d) $H = 40.8$ Oe

Figure 4.25. Domain Patterns in a Double Magnetic Layer Garnet, with GGG Thickness = $6.8\mu\text{m}$.

ORIGINAL PAGE IS
OF POOR QUALITY

C-2

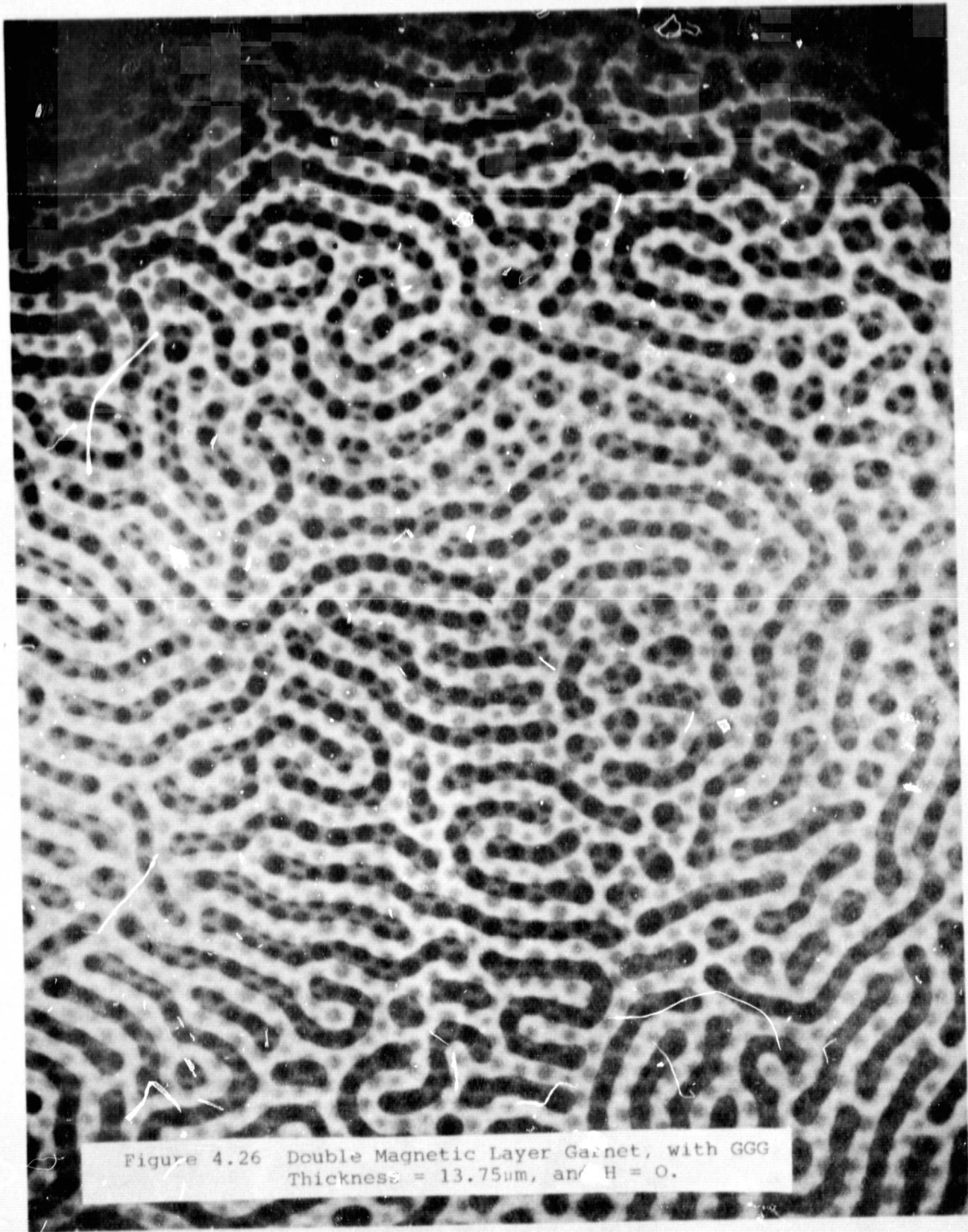
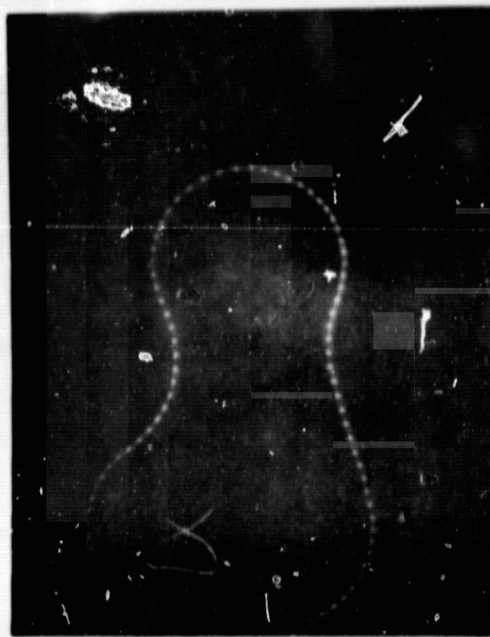


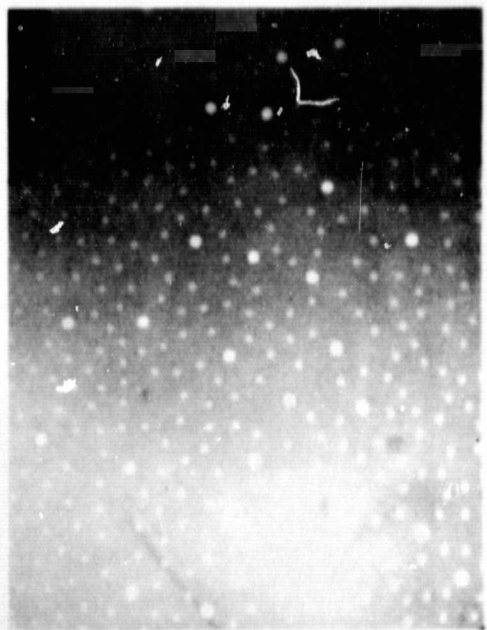
Figure 4.26 Double Magnetic Layer Garnet, with GGG
Thickness = 13.75 μ m, and $H = 0$.



(e) $H = 57 \text{ Oe}$



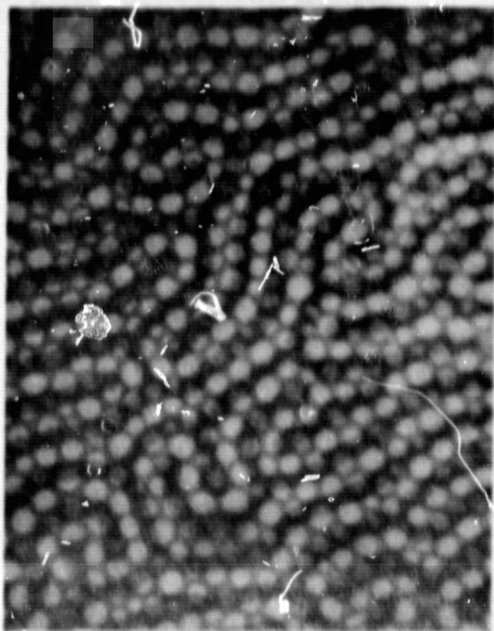
(f) $H = 66.5 \text{ Oe}$



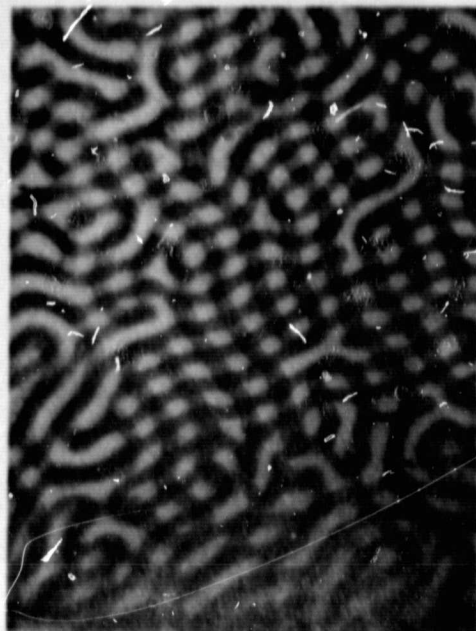
(g) $H = 49.4 \text{ Oe}$



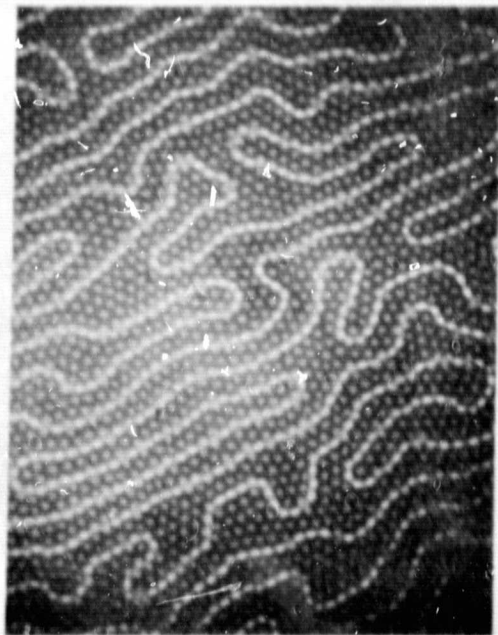
(h) $H = 59.8 \text{ Oe}$



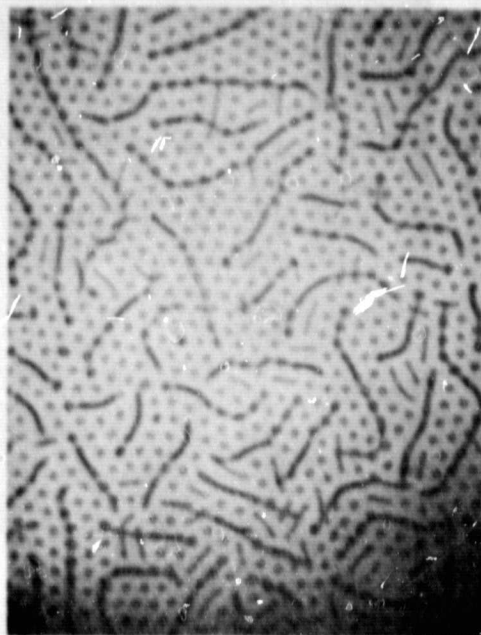
(a) $H = 0$



(b) $H = 0$, different area



(c) $H = 28.5$ Oe



(d) $H = 30.4$ Oe

Figure 4.27 Domain Patterns in a Double Magnetic Layer Garnet, with GGG Thickness = 13.75 μ m.

The magnetostatic coupling between the two magnetic layers varies from sample to sample, being greatest for the smallest GGG epilayer, and weakest for the largest. Figure 4.23 shows hubbles and stripes in the most strongly coupled triple layer film, sample #1 with 2.25 μ m GGG separation. Figure 4.23a is 219 μ m wide, while figures b, c and d are 438 μ m wide. Figure 23a shows bubbles strongly coupled to stripes at zero applied field.

Figure 4.23b shows the stripes collapsing when the normal applied field H is 28.5 Oe. When the stripes contract, they do so in jerks, ejecting a bubble each time. Bubbles are left behind by the receding stripes. Note that the uncoupled bubbles are smaller in diameter than the coupled bubbles. This is because the coupling field from the stripe is opposite to the normal applied field and tends to enlarge the bubble. Figure 4.23c, H = 38 Oe, shows some of the stripes have lost all but one of their bubbles and have collapsed to become double bubbles. These appear in the micrograph to be much brighter and larger than the single bubbles. They are brighter because the polarized light is going through two bubbles instead of one, and are larger because of the stray field of each bubble enlarges the other. Figure 4.23d, H = 40 Oe, shows all the stripes have collapsed, leaving only coupled and uncoupled bubbles.

Figure 4.24 shows coupled bubbles and stripes at zero bias field for sample #2, a triple-layer film with a 6.8 μ m thick GGG epilayer. Note the many different coupled bubble configurations. The coupling is not as strong for this structure as for sample #1. Figure 4.25a shows this same sample with an applied normal field of 28.5 Oe, and figure 4.25b at an applied bias of 41.8 Oe. The stripes are contracting, disgorging their bubbles as they do so. This contraction is jerky, but not as jerky as for the sample of figure 4.23b. This is because the magnetostatic coupling between stripes and bubbles is not as strong for the structure with the 6.8 μ m GGG epilayer as for the 2.25 μ m epilayer. Figure 4.25c is at 62.7 Oe; some of the bubbles are beginning to collapse. The bias field was then lowered to 40.8 Oe, which is below the run-out threshold for the coupled stripes, and is shown in figure 4.25d. The stripes expand via the kink instability, pushing the uncoupled bubbles out of their way. Figure 4.25e shows the domain pattern after the bias is raised to 57 Oe; this is the run-out threshold for the bubbles coupled to the stripes. Figure 4.25f has H = 66.5 Oe, and the non-coupled bubbles have collapsed, leaving only the coupled stripes and bubbles. The scratch on the micrograph is on the photograph, not on the sample. Figures 4.25g and h show bubbles coupled to other bubbles (double bubbles) and free bubbles. From the difference in diameter between coupled and free bubbles, the coupling field can be calculated. All the micrographs in figure 4.25 are 438 μ m wide.

Figure 4.26 shows triple layer sample #3, having a GGG epi-layer thickness of 13.75 μ m, resulting in the two magnetic layers being relatively uncoupled. The micrograph is 438 μ m wide. Figures 4.27a and b are 219 μ m wide, and show different film areas at zero bias. Figure 4.27c is 438 μ m wide and has H = 28.5 Oe. The stripes here move with only a small coupling to the bubble lattice. Somewhat greater coupling is exhibited in figure 4.27d, in which the applied normal field is 30.4 Oe. The probable cause for this increased coupling is that the bubble lattice is less dense in figure 4.27d than in figure 4.27c.

4.5.4 Magnetostatic Coupling in Multilayer Garnets

To characterize a triple layer garnet it is necessary to quantitatively evaluate it to determine the magnetic parameters of each layer, and especially to determine experimentally the magnetostatic coupling between domains in one layer and those in the other. This section describes how this can be done, and presents the measurements for the garnet layers whose micrographs are shown in the previous section.

The thickness of single layer garnets are usually measured from optical interference patterns. However, the pattern from a substrate with three layers on each side is prohibitively complex. The most accurate method of direct measurement is with a scanning electron microscope. An indirect method of thickness measurement of the magnetic layers can be made by measuring the bubble collapse and run-out thresholds, measuring the bubble diameter, and the magnetostatic coupling can also be calculated from these thresholds and bubble diameters with these formulae. The relevant definitions and formulae have been presented in section 3.2.2.

Suppose that the thickness of each layer is known. The radius of the bubbles at the collapse threshold is measured by using a comparator on a micrograph, and this yields X_0 . Equation 3.5 is inverted to give:

$$\lambda = \frac{3}{(3/2 + 1/X_0)^2}$$

and generates both λ and l . For example, for the top layer of film #2, $X_0 = 0.35$, $\lambda = 0.158$, and $l = .95\mu$ m. Next, equation 3.4 yields $H_0 = H_c/4\pi M$. In the case of the top layer of the film #2 this is $H_0 = 0.43$, so $4\pi M = 146$ Oe. An alternative method which does not require a direct thickness measurement is to measure the ratio of the collapse threshold to the run-out threshold, and

find λ from the graph of figure 4.28, which is calculated from equations 3.4 and 3.7. Then equation 3.3 or equation 3.5 is used to find $X = r/h$ at a given field, and use the measured value of the bubble radius r to find the film thickness h .

Equation 3.3 gives the normalized radius of a bubble as a function of normalized applied field. This is shown in figure 4.29 for $\lambda = 0.158$. By using the graph of figure 4.29, the field applied to a bubble is determined merely by measuring the radius of the bubble. Notice in the micrographs of figure 4.25 that the coupled bubbles are larger than the uncoupled bubbles. By measuring the radius of each, and using figure 4.29, one can calculate the coupling field. For example, the coupled bubbles in figure 4.25h have a normalized radius of $X = 0.5$ while the uncoupled bubbles have a normalized radius of $X = 0.35$. These correspond to $H = 0.41$ and 0.43 , respectively, in figure 4.29, and thus the difference in bias field is $4\pi M \cdot (0.43 - 0.41)$ or 2.9 Oe. The coupling field between carrier bubbles and data bubbles depends on the bubble size; the smaller the bubble diameter, the smaller the coupling field. Since the bubble size decreases with increasing bias field, the coupling field also decreases with increasing bias field. This is shown in figure 4.30 for sample #2 (thickness of GGG spacer is $6.8\mu\text{m}$).

When a thinner GGG spacer is used, the coupling strength is increased. For example, the bubbles in figure 4.23d (sample #1 with $2.25\mu\text{m}$ GGG layer) have a coupling strength of 11.7 Oe.

The coupling field of stripes to bubbles is expected to be larger than that of bubbles to bubbles. For example, the coupling field from a stripe to a bubble in figure 4.23b is 16 Oe.

The principal conclusions drawn from the two preceding sections are: (1) High quality triple epi-layer garnet films can indeed be grown, provided the proper equipment is employed; (2) All the relevant parameters of these triple layer films can be measured, including the coupling field of one domain to the other; (3) This coupling field decreases as the bias field increases; (4) The coupling field depends on the GGG epi-layer spacer thickness; (5) Bubbles can be uncoupled from stripes by raising the bias field past the stripe run-out threshold; and (6) The collapse threshold of coupled bubbles is larger than that of uncoupled bubbles by the value of the coupling field. This property may be useful in detecting bubbles in a data layer buried next to the substrate.

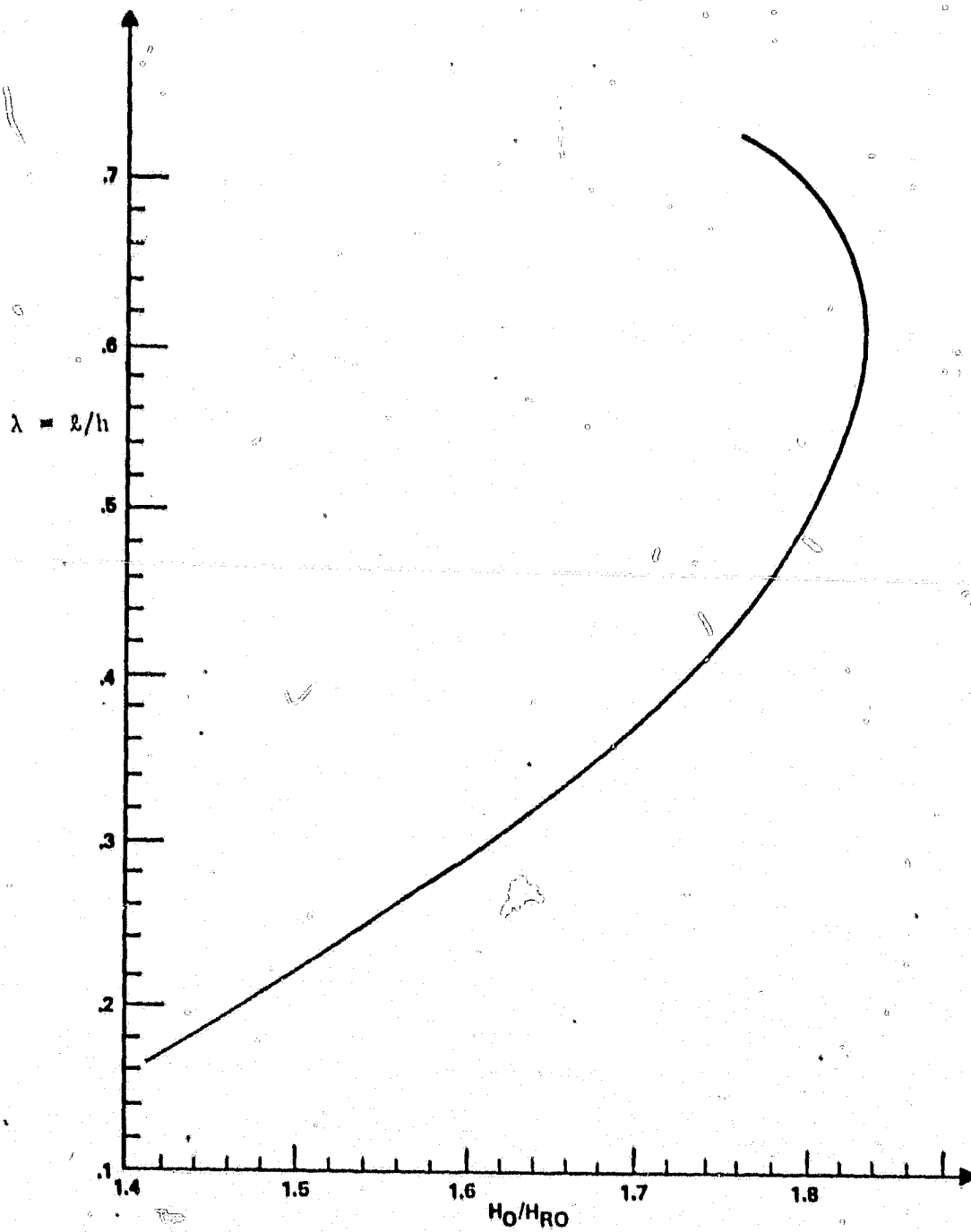


Figure 4.28 Characteristic Length vs. Ratio of Collapse to Run-Out Threshold

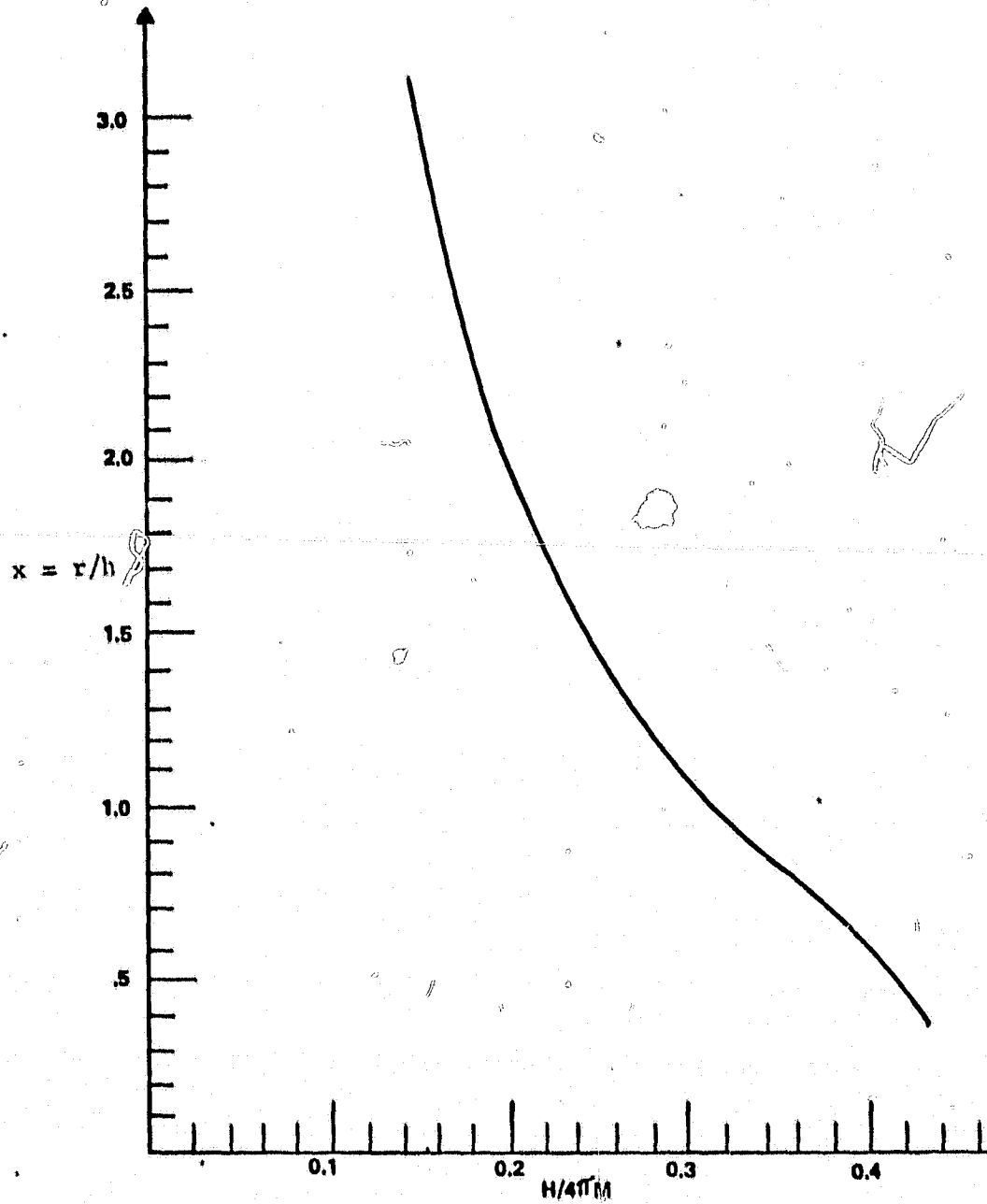


Figure 4.29 Bubble Radius vs. Applied Field for $\lambda = 0.158$.

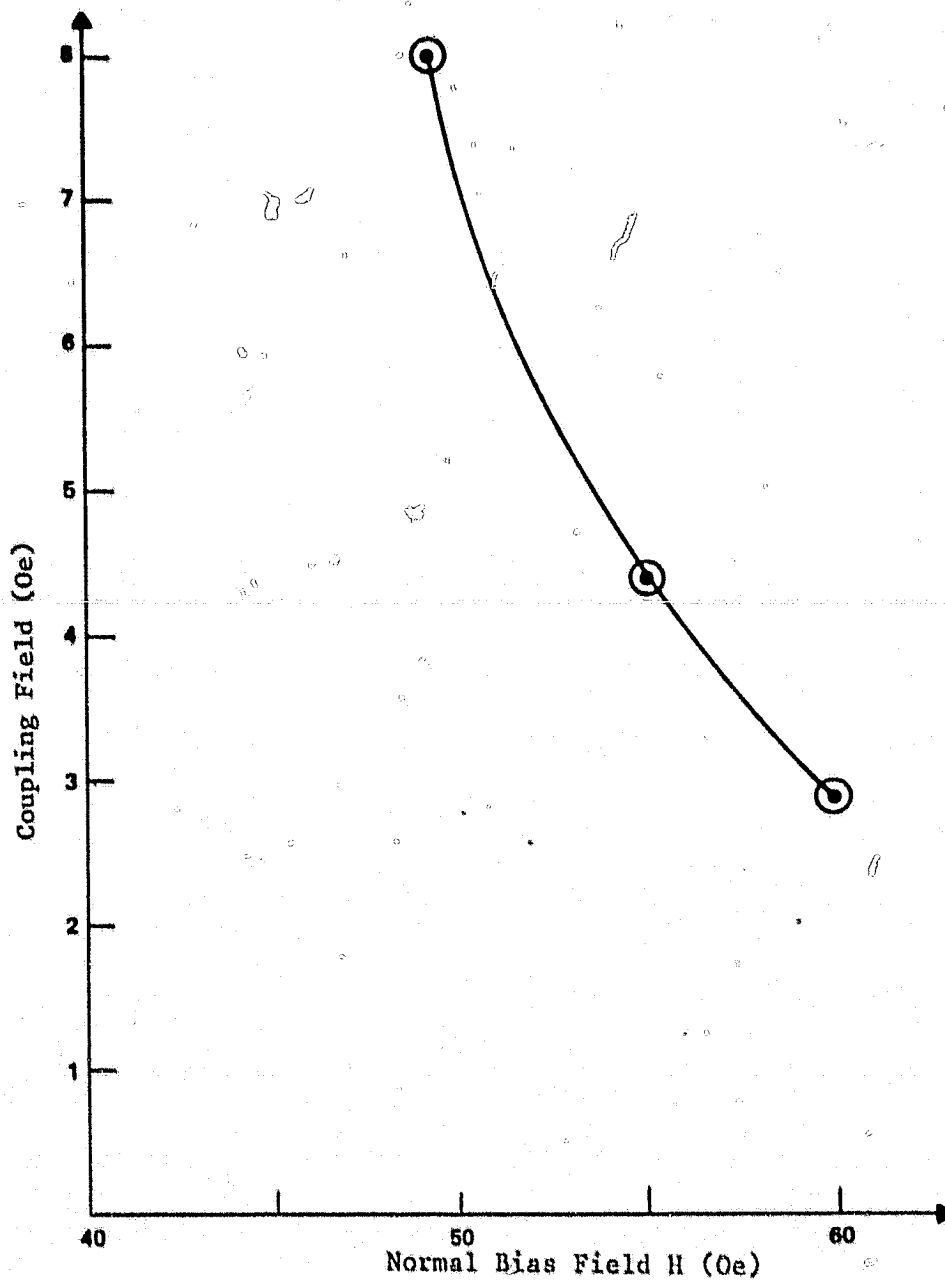


Figure 4.30. Coupling Field between Bubbles vs. Normal Bias Field Field for Sample No. 2.

5. Test Vehicles

5.1 Introduction

Various test vehicle circuits have been designed with the intent of propagating rows of stripe and bubble domains. Each circuit contains current accessed generators for stripe domains and bubble domains, in addition to current accessed circuitry for propagating stripe domains by translating the ends of each stripe domain. A general representation of the device design is illustrated in Figure 5.1.

Stripe domain generators consist of a set of long, narrow conductors, which are also employed to push and pull the newly formed stripe domain into the storage area. Bubble domain generators are of the hairpin design, and generally are connected in series for this series of test circuits. Several bubbles are generated at the same time with this arrangement, and does not represent the design which will be eventually utilized to insert data in the storage area.

Stripe domain propagation circuits have many designs, which include magnetically assisted circuits, double layer serpentine circuits, and various circuits with magnetic bias for stripe domain end pinning. Test results of several test vehicles are presented in the following paragraphs.

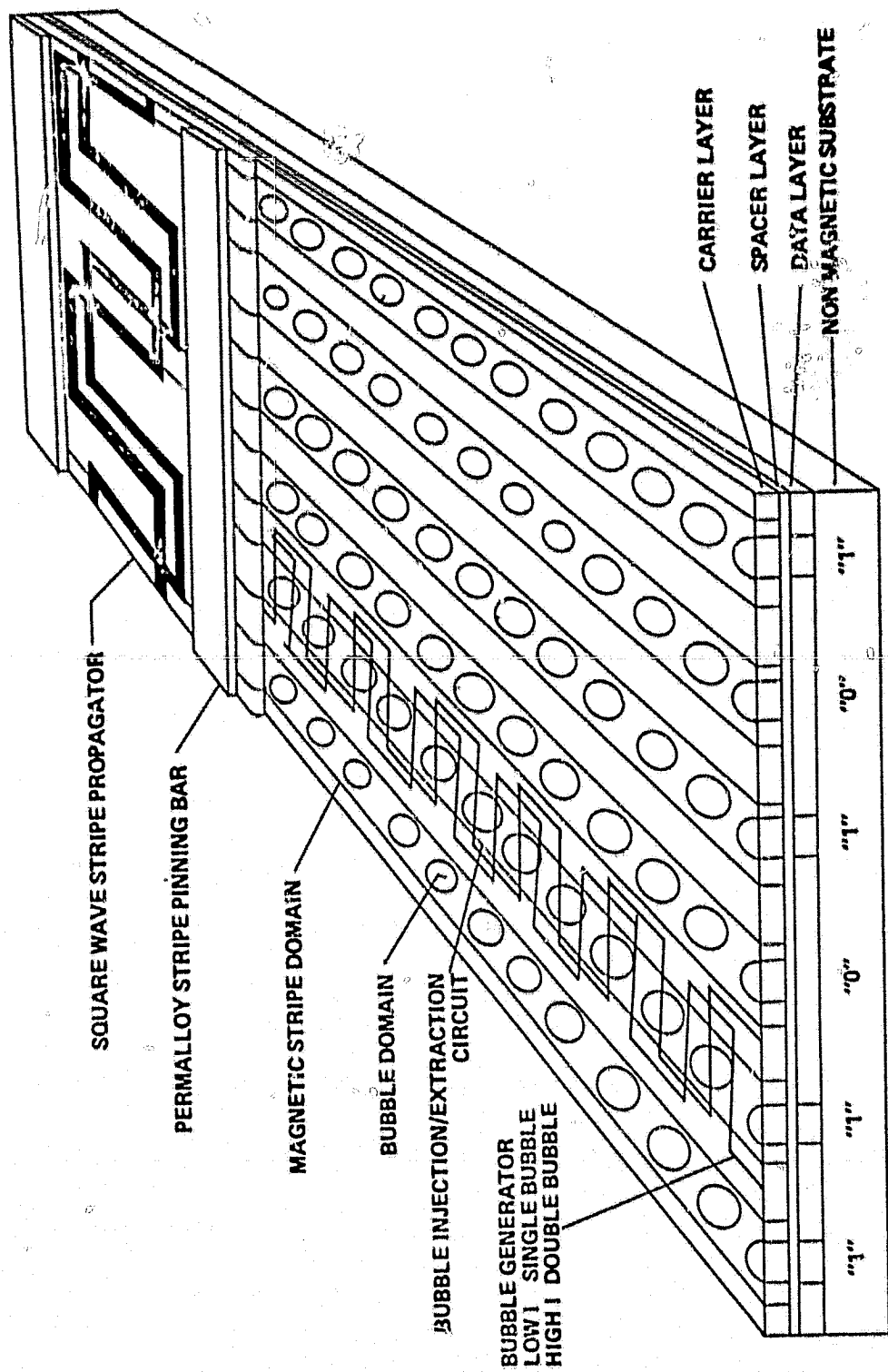


Figure 5.1 Schematic representation of a multilayer, self-structured memory.

5.2 Test Vehicle Evaluation

Four device designs were selected for the most recent test vehicle fabrication cycle. The devices are shown as:

Figure 5.2: Two layer, two phase square wave,

Figure 5.3: Permalloy assisted Philips' type square wave with side entry bubble generation,

Figure 5.4: Philips' square wave with series double bubble nucleation, and

Figure 5.5: Modified Philips' design with series single bubble nucleation.

These device designs were selected to allow at least one or more variations of each of the basic functions, including stripe nucleation, stripe end pinning, stripe transfer, stripe propagation, single and double bubble generation, bubble side entry, and bubble row transfer. Each of these functions will be discussed individually below.

Stripe domain nucleation has been demonstrated by two different methods: current pulses through an elongated hairpin loop and a single conductor stripline. In both cases a 500 μm stripe is produced pinned at both ends under the magnetic bars. The current required varies from ~100 to 600 mA x 0.2 μs , which is a function of garnet $4\pi\text{M}$ and the presence or absence of a "seed" domain beneath the magnetic pinning bar. Once generated and pinned, the stripe domains are stable in bias fields in excess of the bubble collapse field by up to 25% or more.

Pinned stripe domains can be transferred between the conductors in the generate region by 20 to 50 mA pulses 0.5 to 1.0 μs long.

A major obstacle was encountered in most Philips' type devices when it was attempted to hand off the stripes from the generate region to the propagation lines of the main storage area. The stripe domains were acted on by a variety of gradient producing conditions which attempted to push, pull, or flip the domains into the control of the propagation circuitry. However, the stripe domains consistently were severed at one or both ends, causing the stripe domains to collapse to bubbles when performed at bias fields greater than H_{RO} .

The reason for this behavior became readily apparent after a scanning Electron Microscope (SEM) study of two of the devices. Due to the nature of the ion milling process used for conductor line etching, a trench was ion milled into the garnet film surface near the edge of many of the AlCu conductors. As shown in Figure 5.6, the conductor edges susceptible to trenching effects are those which are exposed to an open area of more than 2 μm from the stripline edge. Stripline gaps of 2 μm

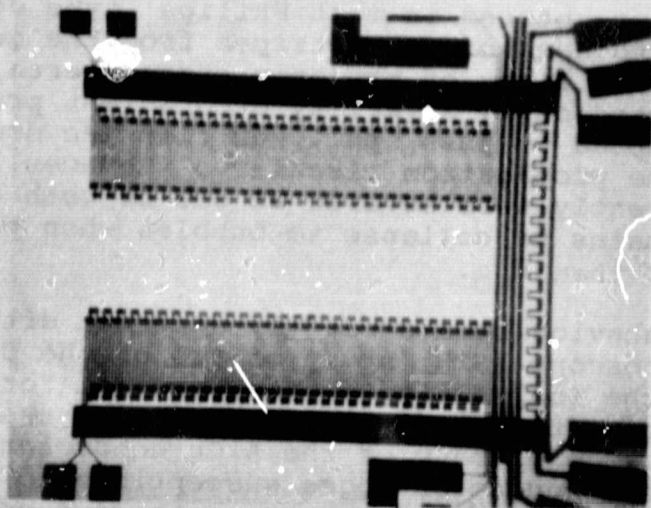


Fig. 5.1 2-layer, 2-phase square wave series single bubble nucleation

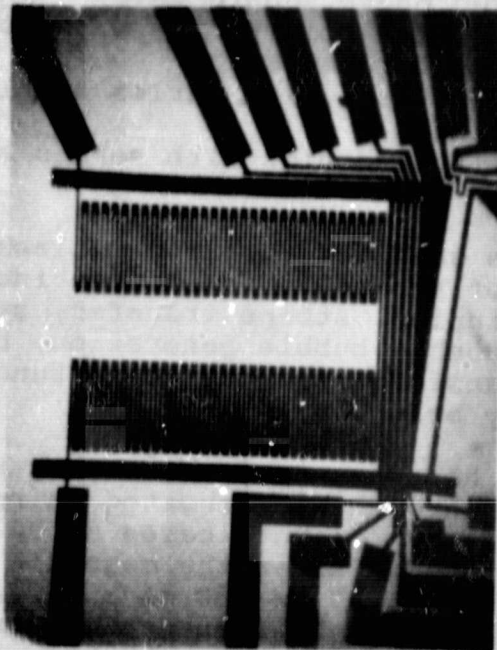


Fig. 5.2 Philips' type square wave with side entry bubble row generation.

ORIGINAL PAGE IS
OF POOR QUALITY

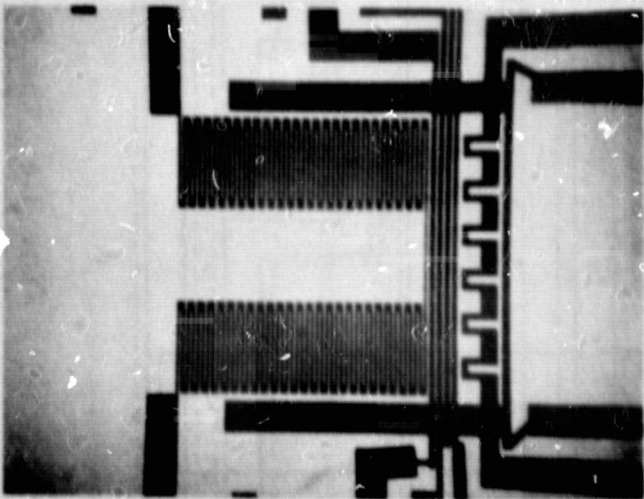


Fig. 5.3

Philips' type square wave
with double bubble nucleator

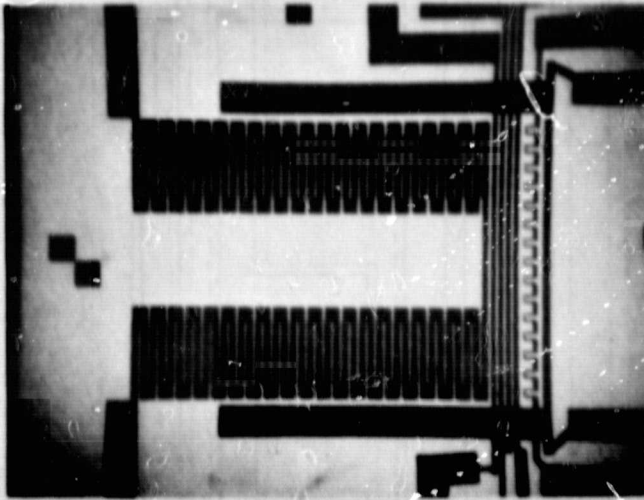


Fig. 5.4

Modified Philips' square wave
with single bubble nucleator

ORIGINAL PAGE IS
OF POOR QUALITY

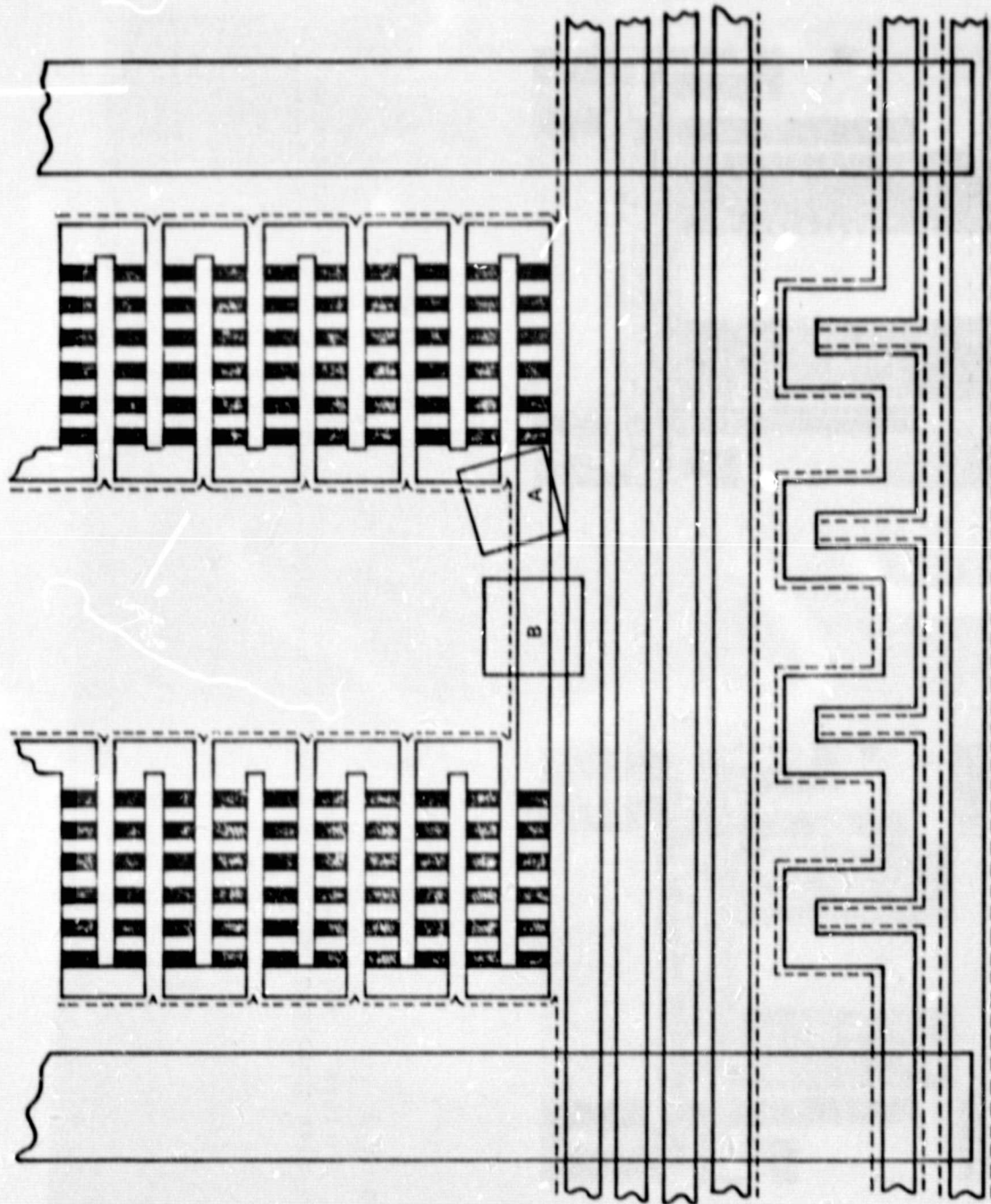


Fig. 5.6 The dashed line indicates device areas affected by the ion mill trenching effect. Blocks A and B refer to fig. 5.7a and 5.7b, respectively.

or less experience a less severe trenching effect which does not penetrate the 4500 Å SiO₂ spacer layer between the AlCu and garnet films. In general, the spacing between adjacent lines is 2µm, except between the lower three lines illustrated in the device of Figure 5.6, thus explaining the trench pattern shown.

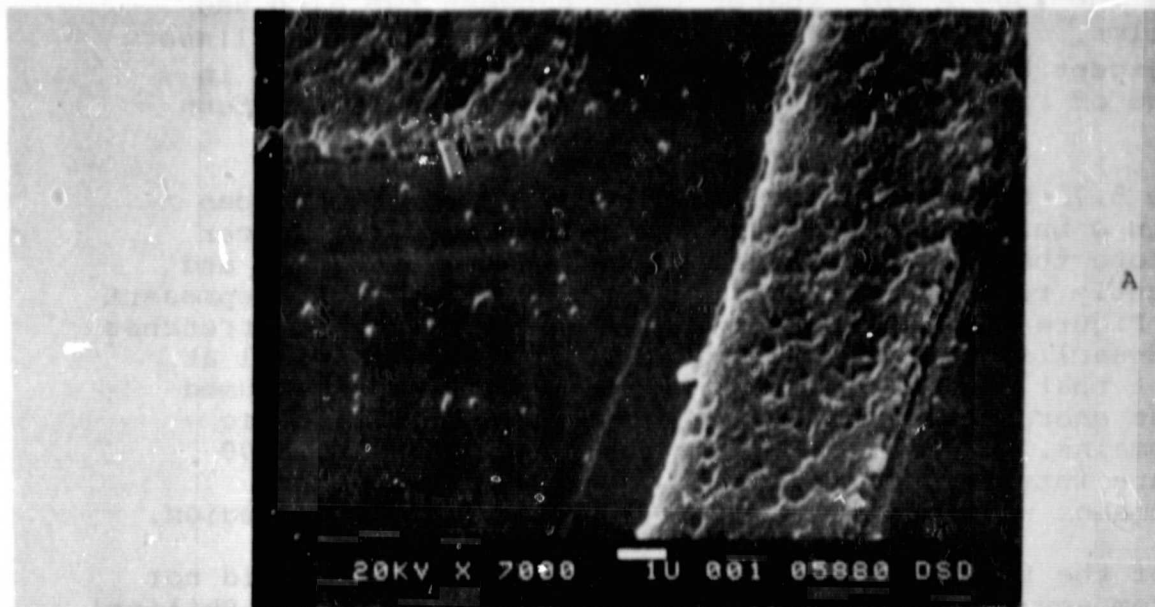
In Figure 5.7, SEM photographs show a device which has been etched in a buffered HF solution to remove the SiO₂ spacer layer. Note that the AlCu lines have also been attacked and significantly reduced in width. Figures 5.7A and 5.7B represent areas of Figure 5.3 labeled A and B, respectively. The trenches described earlier are clearly evident. One should recall at this point that ion milled channels and mesas are often used to provide energy barriers for the confinement of magnetic garnet domains. In this case, trenches of 2000 to 5000 Å depth are interfering with the movement of stripe and bubble domains within and out of the generate-transfer region.

Devices of the two layer two phase square wave variety did not suffer from any of the trenching effects observed in the Philips' variety. However, as shown in the SEM photo of figure 5.8, the SiO₂ step coverage over the AlCu conductors was incomplete due to processing steps which followed that SiO₂ deposition. As a result, magnetic pinning bars provided a continuous shorting bar for the entire length of the device, effectively disabling all current accessed functions.

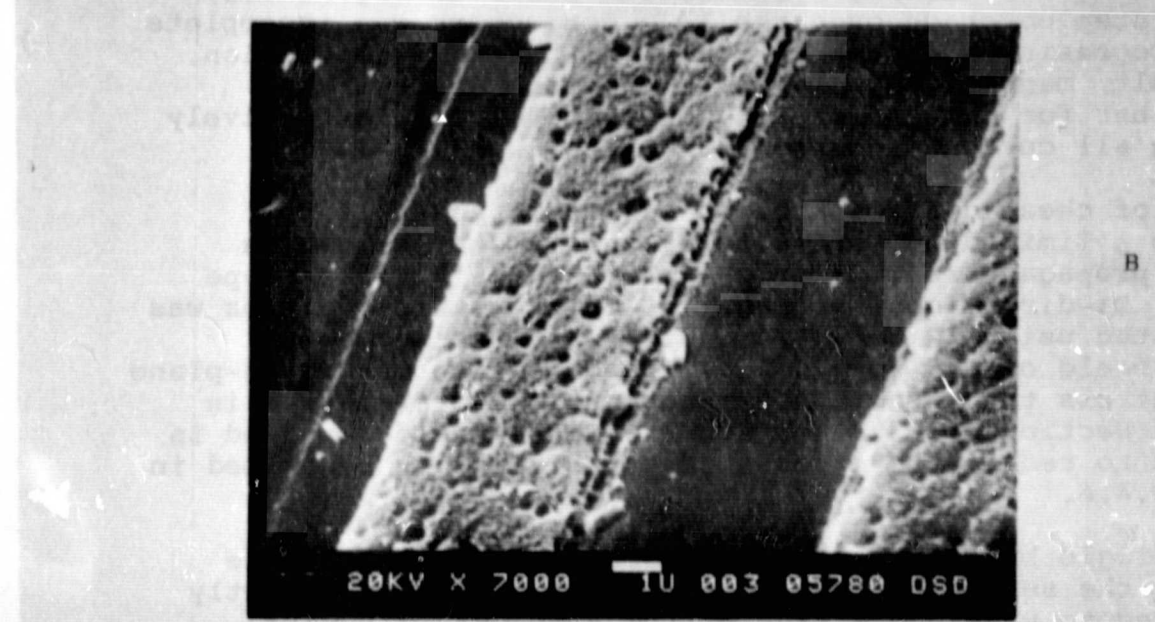
In spite of these difficulties it was still possible to introduce a limited number of fully pinned stripe domains into the propagate regions of a number of the Philips' type devices. Bi-directional propagation of the stripe domains was demonstrated using 12 to 15 mA x 0.5 µs pulses and a DC in-plane field of ± 5 to +20 Oe. The direction of the in-plane field controls the direction of propagation as explained in detail in Section 4.3.3. A 1 MHz rf tickle field was used in all cases to reduce the effects of coercivity, as described in Section 3.4.6.

Rows of single bubbles were easily generated with multiple pulses in the series hairpin loop conductor and subsequently transferred to within one line of the propagation region.

At this point, the ion milled trenches presented at least as great a barrier to the bubbles as to the stripes. It was, therefore, not possible to enter a bubble row into the propagation region to produce the desired "half-lattice" carrier array. However, both half and full lattice arrays were created with another circuit, as shown in figure 5.9.



A

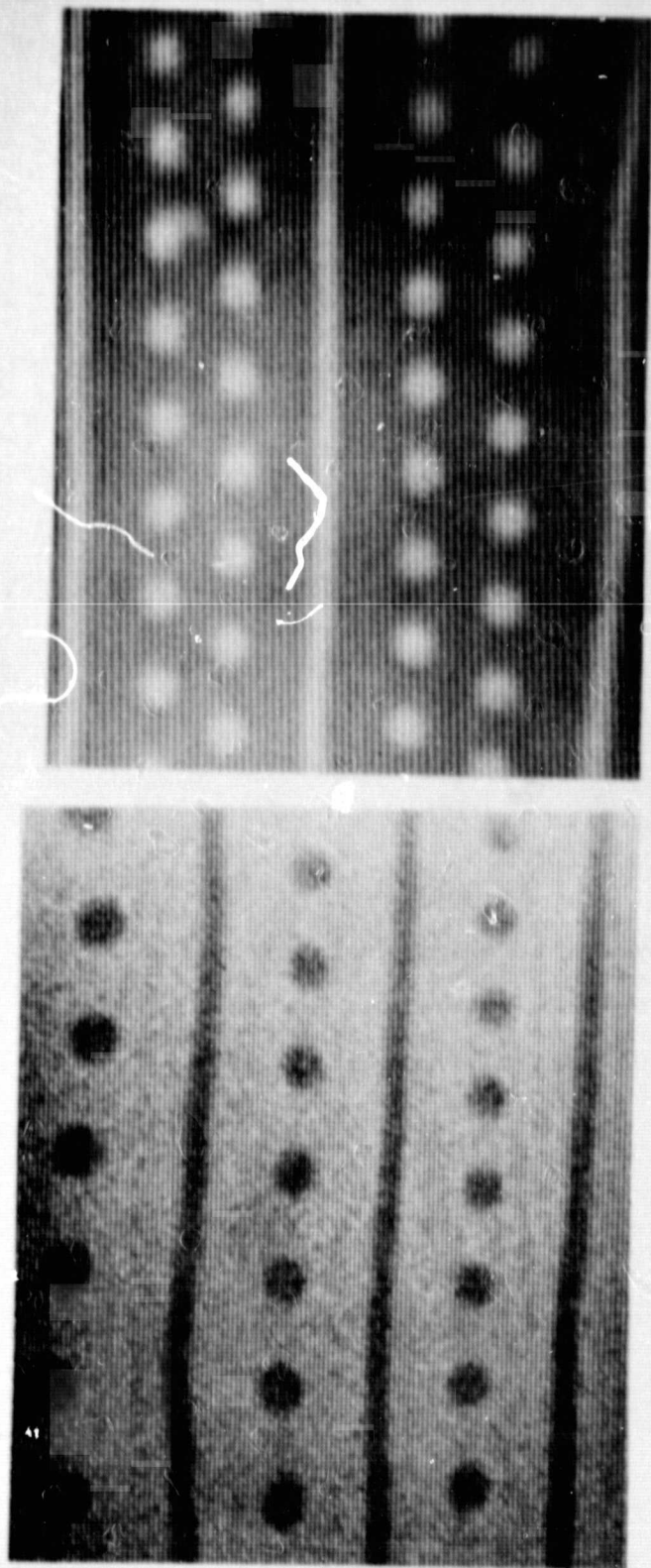


B

Fig. 5.6 SEM photos of garnet surface after HF removal of SiO_2 layers (AlCu striplines were also strongly etched). Note penetration of ion milled trench into the garnet film surface of this Philips' type device.



Fig. 5.7 SEM photo of 2-layer square wave device showing NiFe pinning bar shorting between two AlCu strip-lines. The SiO₂ to AlCu interfaces are clearly evident. The knife edge on the NiFe bar is also a result of the 10° ion milling angle used.



A

B

Fig. 5.8 Photographs of stripes and bubbles in A) "half-lattice" and B) "full-lattice" configurations.

Bubble row nucleation using the side entry technique of figure 5.3 has been judged unsuitable for use on present devices. The bias field gradient required to move bubbles along the line cannot be produced within the margins available for stable bubbles on the low $4\pi M$ garnets presently being used. As the project progresses to smaller bubble, higher $4\pi M$ materials, the bias margins will increase to a point where this design may once again be considered.

Double bubbles have been created using a scaled variation of the standard hairpin single bubble nucleator. The currents required are undesirably high. Alternative methods of double bubble generation, such as stripe cutting with garnet property variations, will be investigated.

5.3 Test Vehicle Summary

All functions necessary to develop a multilayer self-structured bubble memory device have been demonstrated. Specifically, these functions include:

- stripe domain end pinning,
- current accessed propagation of stripe and bubble domains,
- generation of arrays of co-existing stripe and bubble domains in one garnet layer,
- different values of the strip-out field for single and double bubbles, indicating adequate margins for data detection, and
- generation of single and double bubbles.

All of these functions have not been demonstrated on a single device, but have shown operational behavior in individual experiments.

6. Recommended Memory Storage Area Configuration

The proposed multilayer magnetic bubble structure is shown in Figure 5.1. The design of the propagation, or carrier, layer includes current accessed stripe domain propagation conductors, long and short stripe domains, magnetic bias for stripe end pinning, carrier bubbles, stripe generators, double bubble generators, bubble extraction conductors, and bubble expanders and detector circuitry. The data layer includes only the data bubbles.

Data bubbles are located directly under the carrier bubbles, due to magnetostatic interaction, and follow the motion of the carrier bubbles during propagation. Binary data is coded by the presence and absence of data bubbles associated with each carrier bubble. Propagation of the ends of the long stripe domains causes the short stripes and bubbles to also propagate in an orderly fashion. Utilizing a long and short stripe domain design enables the stripe spacing to be smaller than the minimum feature size of the propagation circuit, thereby relaxing the photolithographic resolution requirements of the conductors.

The data layer is located below the carrier layer, which simplifies the fabrication of the device. An earlier design had the data layer on top, with this garnet layer smaller in area than the bottom carrier layer to accommodate stripe domain propagation circuitry for the carrier layer. The difference in the bubble nucleate field provides the basis to write data into the device. A low level current in a simple generator loop will nucleate a single bubble in the carrier layer, and a high level current will nucleate a double bubble -- one bubble in each layer. Detection is based on the difference in the run-out threshold. A carrier bubble is placed in the detector and is tested by a current pulse, which reduces the local normal field below the run-out threshold for a double bubble. A double bubble will strip out across the expander/detector, while a single bubble will not strip out and no signal will be detected.

Bubble and stripe domains can co-exist in the same garnet layer when biased above the run-out threshold, since the stripes are prevented from collapsing to bubble domains by the end pinning action of the magnetic bias illustrated in Figure 5.1. Carrier bubbles in this layer are located between pairs of stripe domains, and are evenly spaced due to mutual repulsion.

The basic advantage of the stripe and bubble design is that the stable bubble positions are defined by the input-output propagate structure until a block is fully loaded, and then it is transferred to the storage region which is self-structured. This procedure greatly simplifies initialization and operation of the device. A penalty is paid in the loss of density due to the stripe domains.

A bubble generator and a magnetoresistive detector in the carrier layer are combined with a current accessed circuit to shift a row of bubbles. Forward and backward bubble propagation can be accomplished, if necessary, with proper current phasing in the circuit. To improve the data rate and average access time, multiple generate/detect propagation circuits can be incorporated. The cost of these multiple circuits is relatively high, but a significant reduction in the area required for stripe and bubble propagation is realized.

To achieve an information density greater than 10^6 bits/cm² a bubble period of 7 μ m or less is required in one direction, and a stripe period of 14 μ m or less is required in the other direction. These dimensions are based on the design where one row of bubbles is located between neighboring stripe domains. Multiple rows of bubbles between stripes is an alternate design, but it is not being addressed at this time. To achieve 4×10^6 bits/cm², the periods change to 3.5 μ m and 7.0 μ m, respectively, with a resultant bubble diameter less than 2 μ m.

If the memory area containing actual data bubbles is 1cm², and if only one detector is incorporated in the design, then 2cm² are required for bubble propagation, as illustrated in Figure 6.1. With four detectors employed, then only 1.25cm² are required. The extra area is necessary for bubble propagation past the location of the propagation circuits leading to the detectors. The length of the total chip area varies as $1+1/N$, where N is the number of detectors.

Using four detectors, the data area is 1.25 cm long by 1.00 cm wide, and contains 4×10^6 bits. If 0.5 μ sec detector propagation pulses are used, with four pulse periods required to have a bubble one period, the data rate is 500 KHz for each detector, or 2 MHz maximum for four detectors. The access time is the sum of the average time required to move a row of bubbles to the position where it can be removed from the storage area, plus the time required to move the individual bubbles in the row to the detector. The former time is the time required to move 125 stripes forward or backward at a 2 MHz rate; which is 0.062 ms. Four 0.5 μ sec pulses are required to move the long stripes one propagation period, but three short stripes are also moved. Therefore, the propagation frequency for the rows of bubbles (or the short stripe domains) is the

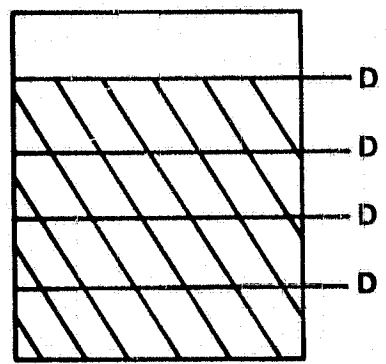
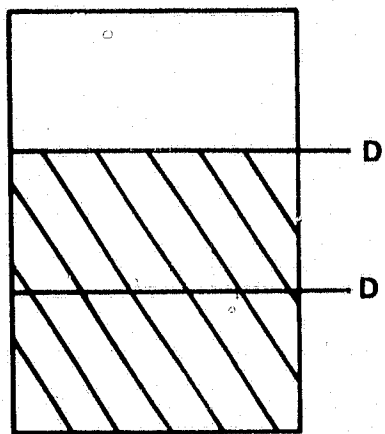
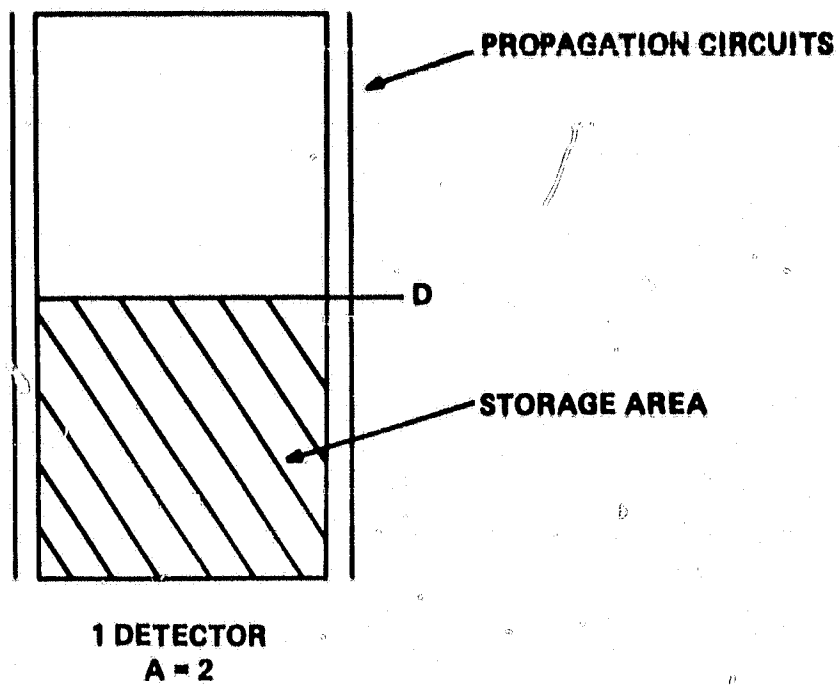


Figure 6.1 Total Area for a Memory Design vs. the Number of Detectors.

same as the driving pulses. This improvement in average access time is realized by employing propagation circuits which have feature sizes greater than the stripe spacing.

After the stripe domains are moved, the carrier and data bubbles are translated to the detector area. With the detectors on one side of the chip, 1000 pulses are required on each of two serpentine lines to move a row of 500 bubbles to the detector. Maximum propagation speeds are limited by the saturation velocity of the garnet material, which is near 10 meters per second. This corresponds to a time interval of $0.5\mu\text{sec}$ for a $5\mu\text{m}$ distance. Therefore, the minimum average access time is $125 \times 0.5\mu\text{sec} + 500 \times 0.5\mu\text{sec}$, or 0.32 msec, with a 8 MHz data rate. If eight detectors are also used instead of four, the average access time is reduced to 0.19 msec, and the data rate increases to 16 MHz.

The size of the garnet must be slightly larger than the data storage area, because of the stripe propagation circuitry. With four square wave conductors and two magnetic pinning bars on two sides, an extra 0.06 cm in width is required. Connection pads for the circuitry are required, and bubble expansion area is necessary for each magnetoresistive detector. With four detectors, the total area of the die is $1.3\text{ cm} \times 1.1\text{ cm}$, or 1.43 cm^2 , resulting in an effective density of 2.8×10^6 bits/cm².

The design presented herein requires stripe domains one centimeter long to be propagated by translating each end of the stripe. Experimental circuits have been constructed and tested with one millimeter stripe domains, with successful propagation results. The use of a rf tickle field is required to eliminate the bowing of the center of the stripe. It is not been demonstrated at this time if one centimeter stripes can be propagated with acceptable results. If additional pinning is required between the stripe end and the magnetic bar, a thicker and wider bar can be employed, or a magnetic material with a high saturation moment can replace the normally used permalloy, such as cobalt or iron, to prevent bar saturation.

If these techniques prove to be unsuccessful, then the total memory area must be divided into smaller modules, thereby requiring shorter stripe domains. With four modules on one die, current accessed propagation lines and pinning bars would be located along two edges and down the center. Detection circuits would be located along two edges, and possibly also in the center if access time is very important. The device bit density will be slightly lower with this modular design, due to the increased area required for additional propagation lines and detectors.

Three short stripe domains are included between neighboring long stripe domains in the designed test vehicle. The possibility exists that greater numbers of short stripes can successfully be propagated which leads to very high packing densities for propagation lines of nominal feature sizes. With seven short stripes, and with two phase propagation pulses and lines, a shift of two short stripe periods would occur for each quarter cycle, thereby requiring parallel detection schemes on two neighboring sets of carrier and data bubbles. The results are high bit density with high data rate. For adequate signal levels from the magnetoresistive detector, each bubble must be expanded several times to increase its area. Current accessed bubble expanders must be developed to accomplish this task.

Due to the large garnet area required for the total memory area, it is highly desirable that a defect free garnet need not be required. Therefore, either error correction schemes or redundant circuitry should be included in the total design. Either consideration will reduce the information density on the garnet, thereby requiring a larger garnet to achieve the desired memory capacity. Detectors may be placed on two opposite sides of the data area, and thereby reduce the average access time by a factor of two. Incorporating multiple readout and data generation stations will improve the data rate, access time, and area wasted for propagation run-over. These benefits must be weighed against increased cost, increased complexity, and decreased process yield.

7. Conclusions

As a result of the work performed under this contract, a multi-layer self-structured bubble memory appears to be very attractive. It has the advantages of higher data density and many fewer high resolution features than conventional bubble memories. Another advantage is current access, which saves weight and power, and is potentially much faster.

Of the large number of self structured configurations investigated, a three epi-layer configuration was found to be most advantageous. In this configuration, the layer next to the substrate contains data bubbles. The next layer is a non-magnetic G.G.G. spacer layer. The outer layer contains both stripe domains and carrier bubbles. The stripes are moved via current circuits at the stripe ends. The stripes move the carrier bubbles by magnetostatic repulsion. The carrier bubbles are magnetostatically coupled to data bubbles in the bottom layer.

A design was made of a memory with a single row of bubbles between stripes and having a density of 4×10^6 bits per square centimeter. The memory design has redundancy. All functions necessary to that memory have been demonstrated: Both the half lattice configuration (in which a single row of bubbles in the carrier layer exists between each pair of stripes in the carrier layer) and the full lattice configuration (in which multiple rows of bubbles exist between each pair of stripes) were demonstrated. These configurations, with both stripes and bubbles in the same magnetic layer were shown to be stable in the same bias field, provided that the stripe ends were pinned by permalloy features. It was demonstrated that the pinned stripes were stable even above the collapse field of the bubbles.

Current access stripe propagation was achieved by a variety of circuits. These were evaluated; the best was found to be a configuration in which the conductors are covered either with permalloy bars or chevrons. A curvature, or bowing of the propagating stripes was both calculated and measured as a function of bias field. The maximum track width is determined by that bowing, and for a typical film was found to be 1.5 mm. Propagation of bubbles was demonstrated by propagating stripes to which the bubbles were magnetostatically coupled. Triple epi-layer films were fabricated and found to have low defect density. Double bubbles and single bubbles were created in these films, using a current loop. The coupling between bubbles in different layers was both calculated and measured, as a function of applied bias field and thickness of the G.G.G. layer. This coupling was experimentally found to cause a difference in run-out threshold between double bubbles and single bubbles; this difference forms the basis of the readout method for detecting the presence or absence of a bubble in the buried data layer.

All the functions of the multilayer self structured memory have been demonstrated; however because of processing problems, the simultaneous operation of all functions on a single chip has not yet been demonstrated. This is planned for the next phase.

8. Acknowledgements

The authors wish to thank A.B. Smith and M. Kestigian of the Sperry Research Center in Sudbury, Mass. for their preparation of multi-layer epitaxial garnet materials, and S.J. Lins, R.J. Engfer, D.L. Fleming, J.A. Krawczak, D.S. Lo, R.E. Lund, C.J. Nelson, G.L. Nelson, and D.E. Sutliff for their technical assistance.

REFERENCES

1. Y.S. Lin, J. Appl. Phys. 45, 4084 ('74).
2. H. Callen and R. M. Josephs, J. Appl. Phys. 42, 1977 ('71).
3. T. H. O'Dell, Magnetic Bubbles, Halsted Press, New York, 1974, p. 52.
4. H. Uchishiba, H. Tominaga, and K. Asama, IEEE Trans. Mag. 11, 1079 ('75).
5. C. Kooy, and U. Eng, Philips Research Reports 15, 7 ('60).
6. T. H. O'Dell, op. cit., p. 35.
7. M. Kamin, J. A. Krawczak, S. J. Lins, E. J. Torok, and R. L. Sterner, J. Appl. Phys. 50, 2292 ('79).
8. E. H. L. J. Dekker, K.L.L. Van Mierloo, and R. DeWerd, IEEE Trans. Mag. 13, 126 ('77).
9. E.H.L.J. Dekker, K.L.L. Van Mierloo, and R. DeWerd, J. Appl. Phys. 49, 1927 ('78).
10. E.H.L.J. Dekker, N.J. Wiegman, K.L.L. Van Mierloo, and R. DeWerd, J. Appl. Phys. 50, 2277 ('79).
11. M. Kestigian, A. B. Smith, and W. R. Bekabrade, Sperry Research Report SCRC-RP-77-79, ('77).
12. A. B. Smith, Sperry Research Report SCRC-74-21, ('74).
13. R. E. Lee, J. Vac. Sci. Technol. 16, 164 ('79).
14. T. W. Collins and R. W. Cole, IBM J. Res. Develop. 20, 132 ('76).